DENSITY DEPENDENCE OF THE TERAHERTZ ABSORPTION SPECTRA IN OPTICALLY EXCITED SEMICONDUCTORS

Le Thi Hai Yen

March, 2015

Abstract

Topic of this doctoral thesis is the density dependence of terahertz (THz) absorption spectra in optically excited semiconductors. In particular, with analyzing the THz absorption spectra the exciton Mott transition can be studied.

Recent developments in THz techniques attract much interest because of its wide variety of potential applications ranging from the communication to biotechnologies. From the viewpoint of condensed matter physics, the THz spectroscopy is particularly useful because THz radiation can probe several interesting phenomena accompanied, for examples, by the low-energy excitations, carrier dynamics in electronic materials, collective vibrational and torsional modes in biomolecules, and rotational and vibrational transitions in molecules. Furthermore, since the ponderomotive energy of THz radiation for a given laser intensity is higher than that of visible light, we can apply strong electric fields ($\approx$ 1 MV cm^{-1}) using a single-cycle THz pulse. Therefore, THz techniques pave the new way for studying extreme nonlinear phenomena such as the impact ionization and the high-order harmonic generation in condensed matters, which cannot be analyzed with the perturbation theory.

In this thesis, I theoretically investigate the THz absorption spectra in optically excited direct bandgap bulk semiconductors for various $e-h$ pair densities with analyzing Coulomb interacting two-band $e-h$ systems. The analysis along this line has a distinctive advantage over approaches from the visible or near-infrared absorption because, with the THz absorption, exciton and $e-h$ pair plasma densities can experimentally be determined precisely.

In the present study, I investigate the THz absorption of excitons in low-density regime and that of $e-h$ plasmas in high-density regime on a same electron-hole basis. I derive the equations-of-motion of transverse dielectric functions, which determine the carrier distributions and interband polarization. In order to get a closed set of coupled differential equations, I introduce the time-dependent Hartree-Fock approximation (TD-HFA) to overcome the hierarchy problem. Taking into account the screening effect, I employ a longitudinal dielectric function given by the static single-plasmon-pole approximation (SPPA).

To theoretically investigate the exciton Mott transition (the density ionization) I analyze the THz absorption spectra based on the spectral and thermodynamical approaches.

In the spectral approach, the exciton Mott transition can clearly be studied because, above the critical density, the exciton structures originating from the intraexcitonic transitions disappear and only the Drude component is obtained. I also investigate the effects of state filling and screening on the carrier dynamics. The present theory predicts that the transition energy from $1s$ to $2p$ states is almost independent of density below the exciton Mott density.

In the thermodynamic approach, on the other hand, I also study the interplay between the density ionization of excitons and the abrupt increase in the ionization ratio and in the $e-h$ quasi-chemical potential owing to the quantum dissociation. I also show that the abrupt increase in these quantities take place at the density just below which the spectral components originating from the intraexciton transitions disappear in the THz absorption spectrum.

In conclusion, I have analyzed the density dependence of the THz absorption spectra in optically excited direct bandgap bulk semiconductors, and have shown that the exciton Mott transition can clearly be studied with analyzing the THz absorption spectra.

Acknowledgements

Foremost, I would like to express my deepest thanks to my supervisor, Professor Takeshi Inagaki. His patience, encouragement, and immense knowledge were key motivations throughout my PhD course. He carries out his research with an objective and principled approach to condensed matter physics science. He persuasively conveyed an interest in my work, and I am grateful for my inclusion in his project. I am truly thankful for his steadfast integrity, and dedication to both my personal and academic development. I cannot think of a better supervisor to have. I owe a great debt of gratitude to Prof. Inagaki.

Besides my supervisor, I would like to thank the rest of my PhD committee, Prof. K. Hattori, Prof. H. Daimon and Prof. J. Ohta, whose supervision and insightful comments have kept my research work on track, and on time.

I would like to express my thank to Prof. R. Shimano, from Tokyo University, for his interesting work and fruitful comments.

I would like to thank Nara Institute of Science and Technology for providing financial support so that I can finish my PhD study at Graduate School of Materials Science, NAIST.

I would like to thank my colleagues at Theoretical Condensed Matter Physics Laboratory, Graduate School of Materials Science and at Faculty of Physics, Hanoi University of Sciences, Vietnam National University for their collaboration and support.

I would also like to thank to my friends for their kind support and encouragement.

I want to express my special thanks to my parents and my younger sister who always understand, support and encourage me with their best wishes.

Last but not the least, my thanks go to my husband, Nguyen Anh Duong, and my son, Nguyen Ngoc Binh Minh, for their cheering me up and standing by me through out the good times and bad. Their support, encouragement, and companionship have turned my journey through graduate school into a pleasure. For all that, and for being everything I am not, they have my everlasting love.

Contents

List of Figures

List of Tables

Chapter 1

Introduction

Recent developments in terahertz (THz) techniques attract much interest because of a wide variety of potential applications ranging from the communication [1] to biotechnologies. [2] From the viewpoint of condensed matter physics, the THz spectroscopy is particularly useful because THz radiation can probe several interesting phenomena accompanied, for examples, by the low-energy excitations, [3] carrier dynamics in electronic materials, [4] collective vibrational and torsional modes in biomolecules, [5] and rotational and vibrational transitions in molecules. [6] Furthermore, since the ponderomotive energy of THz radiation for a given laser intensity is higher than that of visible light, we can apply strong electric fields ($\approx$ 1 MV cm^{-1}) using a single-cycle THz pulse. [7−9] Therefore, THz techniques pave the new way for studying extreme nonlinear phenomena such as the impact ionization [10] and the high-order harmonic generation [11] in condensed matters, which cannot be analyzed with the perturbation theory.

Because of the extraordinary long lifetime ($\simeq$ 1ms) originating from the parity-forbidden band structure and the pure spin singlet nature, 1s paraexcitons of the yellow series in Cu_2O have been studied to observe Bose-Einstein condensation (BEC) of excitons. [12,13] The phonon assisted photoluminescence (PL) spectra was fitted to the Bose-Einstein distribution function to estimate density and temperature. [14,15] However, the accuracy of this method has been questioned in Ref. 16, and the small radiative

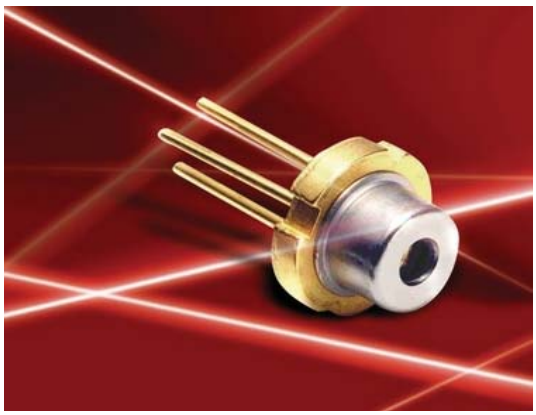

(a)

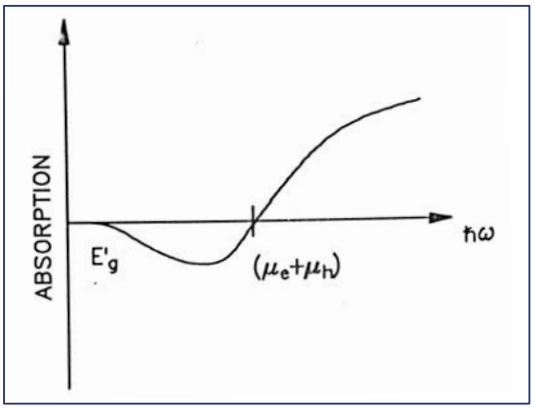

(b)

Figure 1.1: (a) Optoelectronic devices such as laser diode (LD). (b) The absorption-gain spectrum of the active region in electron-hole plasma that can experience gain if carrier density is sufficient high see Ref. [44].

efficiency makes it difficult to experimentally determine their effective mass and lifetime. In order to circumvent the difficulty, THz absorption accompanied by the intraexciton transition from $1s$ to $2p$ states is proposed to be observed. [17] This is the counterpart of the Lyman spectroscopy in atomic hydrogen, [18,19] and is particularly useful because intraexcitonic transitions induced by the THz absorption are independent of the selection rules of optical transitions. [20,21] Furthermore, they measure the coupling between $1s$ exciton ground state and higher relative momentum states, which independent of the center-of-mass momentum of excitons. On the other hand, exciton density evaluated with PL measurements is in general obscure because, due to the momentum conservation and small photon momentum, only excitons with vanishing center-of-mass momentum can take part in the radiative recombination. [22-24] Moreover, microscopic analysis based on the semiconductor luminescence equation revealed that not only excitons but also Coulomb correlated electron-hole plasmas contribute PL at the $1s$ exciton resonance. [25]

From the application viewpoint, highly photoexcited $e-h$ systems are very important to develop novel high-performance optoelectronic devices, such as laser diodes. The negative absorption, i.e., the optical gain may occur in the spectral region between the (renormalized) bandgap and the quasi-chemical potential if the carrier density in the

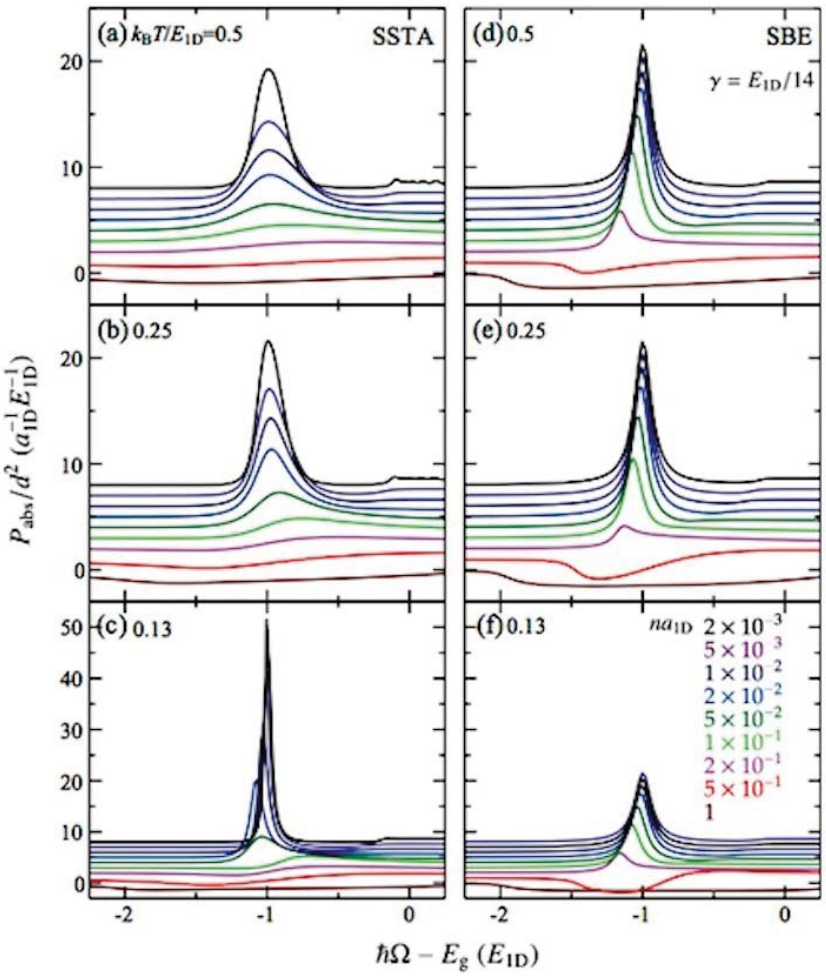

Figure 1.2: The absorption-gain spectra evaluated in quasi-one-dimensional $e-h$ system for various carrier densities from Ref. [30] with and without Coulomb correlation effects are taken into account on the left panel and right panel, respectively. Coulomb correlation significantly modifies the optical absorption spectra and notably the gain spectrum, the red line.

material is sufficiently high. Actually, laser devices use the radiative $e-h$ recombination in electron-hole plasma state for light emission. To design laser diode with low energy threshold, it is necessary to design laser diode that operates just above the critical carrier density of the stimulated emission. Around this density, it is well known that the excitonic structures in the absorption spectra disappear.

The exciton Mott transition is particularly important in this issue and has been studied for several decades. [26,27] Apart from its fundamental interests, understanding several physical properties around the exciton Mott transition point is particularly important to develop novel high-performance optoelectronic devices such as highly efficient

semiconductor laser diodes. This is because strong Coulomb correlations predominate around the transition point, which is a precursor for the optical gain by the $e-h$ plasma. In fact, it is shown both experimentally [28] and theoretically [29,30] (see Fig. 1.2) that the strong Coulomb correlation significantly modifies the optical absorption and gain spectra in quasi-one-dimensional semiconductors.

The motivation of this work is to clarify the nature of the $e-h$ system. In this thesis, I aim at theoretically investigating the exciton Mott transition (density ionization) in optically excited direct bandgap bulk semiconductors with analyzing THz absorption spectra for various $e-h$ pair densities.

1.1 Exciton and Exciton Mott Transition

In this section I will briefly discuss about the optical excitation in semiconductors accompanying the interband transition, the formation of excitons and the intraexcitonic transition, and the exciton Mott transition.

In a typical semiconductor, the gap between the valence and conduction bands corresponds to the energy $\hbar\omega$ of infrared or visible light. A photon with an energy $\hbar\omega > E_g$ can excite an electron from the valence band into the conduction band, leaving behind a hole in the valence band. This process is referred to as the interband transition between valence and conduction bands.

The photoexcited conduction-band electron and the valence-band hole carry opposite charges and interact via the mutually attractive Coulomb potential, and the electron tends to stay in the vicinity of the hole. Such a bound electron-hole pair is a neutral quasiparticle called exciton (see Fig. 1.3). This $e-h$ Coulomb interaction will naturally influence the optical spectrum of a semiconductor. Exciton can be conceived in one-electron and one-hole picture. It is no longer represents two quasi-particles, and its internal energy is lower than the bandgap energy E_g. The exciton is thus a quasi-particle representing the lowest electronic excitation in a semiconductor. Generally, there two

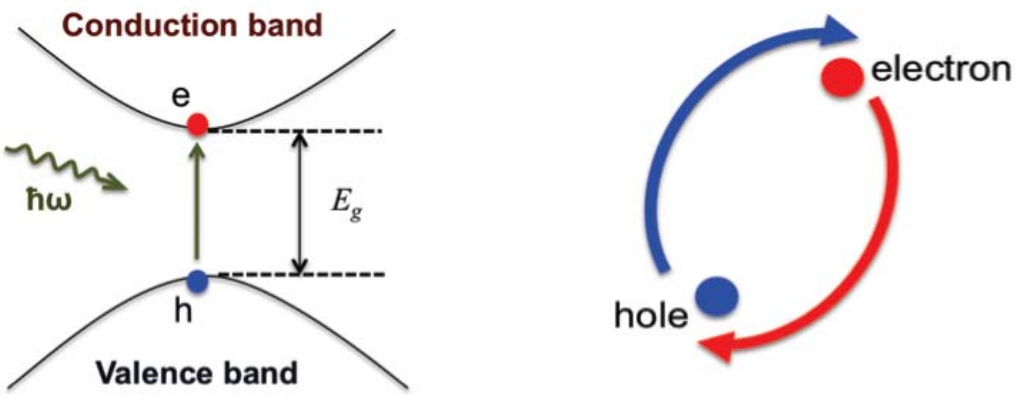

(a) **(b)**

Figure 1.3: An exciton is composed of an optically excited electron in conduction band and a positively charged hole in valence band by their attractive Coulomb interaction.

basic types of exciton are either Frenkel exciton or Wannier exciton. [31] Frenkel exciton is small-radius exciton, which is on the order of, or smaller than, an atomic unit cell. They exist in wide bandgap semiconductors/insulators and in some organic materials. Wannier exciton has a large radius in comparison to the length of the lattice unit cell. This condition is met in most II-VI, III-V, and column IV semiconductors. In this thesis, I am concerned with Wannier excitons (excitons).

The Wannier exciton as displayed in Fig. 1.4 can be conceived, to a first approximation, as a weakly bound electron-hole pair owing the attractive force results from the Coulomb potential,

$$U(r) = -\frac{e^2}{4\pi\varepsilon_0\varepsilon r} \tag{1.1}$$

where r is the electron-hole distance, and ε is the dielectric constant of the material. In such condition an exciton at which an electron circulates around a hole with radius, called exciton Bohr radius, defined by

$$a_B = \frac{\epsilon_0\hbar^2}{me^2} \tag{1.2}$$

where $1/m = 1/m_e + 1/m_h$, with m is the reduced mass of an electron-hole pair. The typical value of the ground state Wannier exciton radius a_B is $\sim$ 5 nm. The exciton

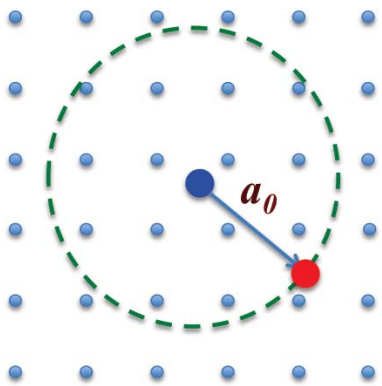

Figure 1.4: Systematic of the Wannier exciton in a two-dimensional crystal lattice, the wave function spread for several lattice unit cells.

Rydberg binding energy is given by

$$E_0 = \frac{\hbar^2}{2ma_0^2} = \frac{me^2}{2\hbar^2\epsilon_0^2} \tag{1.3}$$

and a typical value of E_0 is $\sim$ 13.6 meV. The Bohr radius of an exciton is much larger than that of a hydrogen atom (5×10^{-2} nm), while the binding energy of an exciton is much smaller that of a hydrogen atom (13.6 eV).

The Wannier exciton wave function has the form of product of four terms as

$$\psi(\mathbf{r}, \mathbf{R}) = u_{c0} u_{v0} \phi(\mathbf{r}) e^{i\mathbf{K}_c \cdot \mathbf{R}} \tag{1.4}$$

The first two terms, u_{c0} and u_{v0}, are Bloch wave functions that contain the character of the atomic orbitals forming the conduction and valence bands, respectively. Usually, in semiconductors because of the band structure, the highest valence band originates from p orbital, and the lowest conduction band from s orbital. Hence, the wave function of electron in conduction band is composed with s-like atomic character, and that of hole in valence band has p-like orbital. The symmetry of these functions determines the strength of the interband optical transition.

The third term, $\phi(r)$, is the exciton envelope function describing the relative motion of the electron and hole on a large scale, over many atomic sites. The final factor, $e^{i\mathbf{K}_c \cdot \mathbf{R}}$, expresses the translational symmetry of the crystal, giving the exciton its running wave

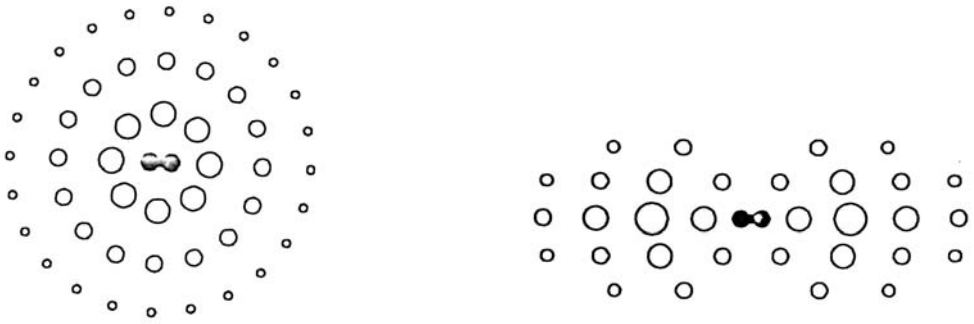

(a) **(b)**

Figure 1.5: (a) Representation of an s-like exciton with a p-like hole Bloch wave function, a s-like electron Bloch wave function, and an s-like envelope function. (b) Representation of a p-like exciton with p-like envelope function composed of electron wave function with s-like atomic character and a p-like hole Bloch wave function. The representation is in the hole reference frame, which sits at the center of each figure. The p-like character of the hole wave function is depicted by the ∞. The size of the circles represents the probability of the electron with s-like character. [44]

character. Figure 1.5 displays the schematic representation of excitons with s-like and p-like characters.

The Wannier exciton can be formed, to a good approximation, as a hydrogen-like series of states below the gap. The exciton dispersion relation (that is, exciton energy versus wave vector) is shown in Fig. 1.6.

$$E_n = E_g - E_0 \left(\frac{1}{n^2}\right) + \left(\frac{\hbar^2 K_c^2}{2M}\right) \tag{1.5}$$

with

$n = 1, 2, 3...$ principal quantum number,

$M = m_e + m_h$ total mass of $e - h$ pair,

K_c wave vector of exciton.

The upward arrows in Fig. 1.6(a) are depicted the transitions from the $|0\rangle$ state, the crystal ground state, i.e., the state of the crystal without excitons, to the $n = 1$ state (creation of the exciton in its ground state) and to the higher exciton levels $n = 1, 2, 3, \cdots$ In fact, the interband transitions are very distinctive absorption lines at certain discrete

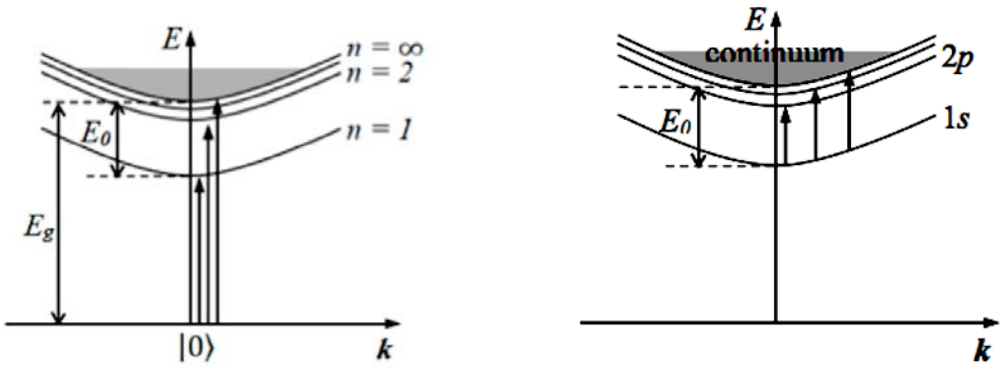

(a) (b)

Figure 1.6: The exciton dispersion relations E_n and optical absorption transitions (interband transitions) are also remarked as upward arrows in (a), intraexcitonic state transitions between the internal exciton states as remarked in (b).

energies $\hbar\omega < E_g$ observed experimentally at low temperatures. This is thus the characteristic and famous hydrogen-like series in the absorption spectra, comprising lines at energies

$$\hbar\omega = E_g - E_0\left(\frac{1}{n^2}\right), \quad n = 1, 2, 3, ...\infty \tag{1.6}$$

In which, the band-to-band absorption to the states labeled in Fig. 1.6(a) as $n = \infty$ begins by transitions to 'continuum' state.

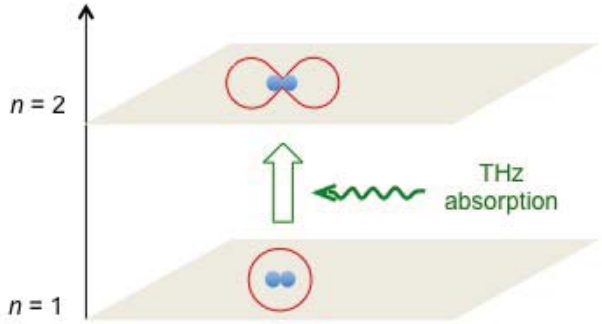

Figure 1.7: The schematic of the intraexcitonic transition from $1s$ to $2p$ state.

Aside from the interband transition between conduction and valence bands, there are the internal transitions between the eigenstates of exciton typically in the meV scales, the THz spectral range. These transitions are also known as excitonic intraband or intraexcitonic transitions. They are giving rise to dielectric response associated with

excitons absorption lines

$$\hbar\omega = \frac{E_0}{n_1^2} - \frac{E_0}{n_2^2}, \quad n_1, n_2 = 1, 2, 3, ...\infty \tag{1.7}$$

At low density limit, the THz absorption accompanied by excitonic structures originating from the intraexcitonic transition from 1s to np states as depicted in Fig. 1.6. (b) with the spectral position of the relevant lines as

$$\hbar\omega = E_0 - E_0\left(\frac{1}{n^2}\right), \quad n = 2, 3, ...\infty \tag{1.8}$$

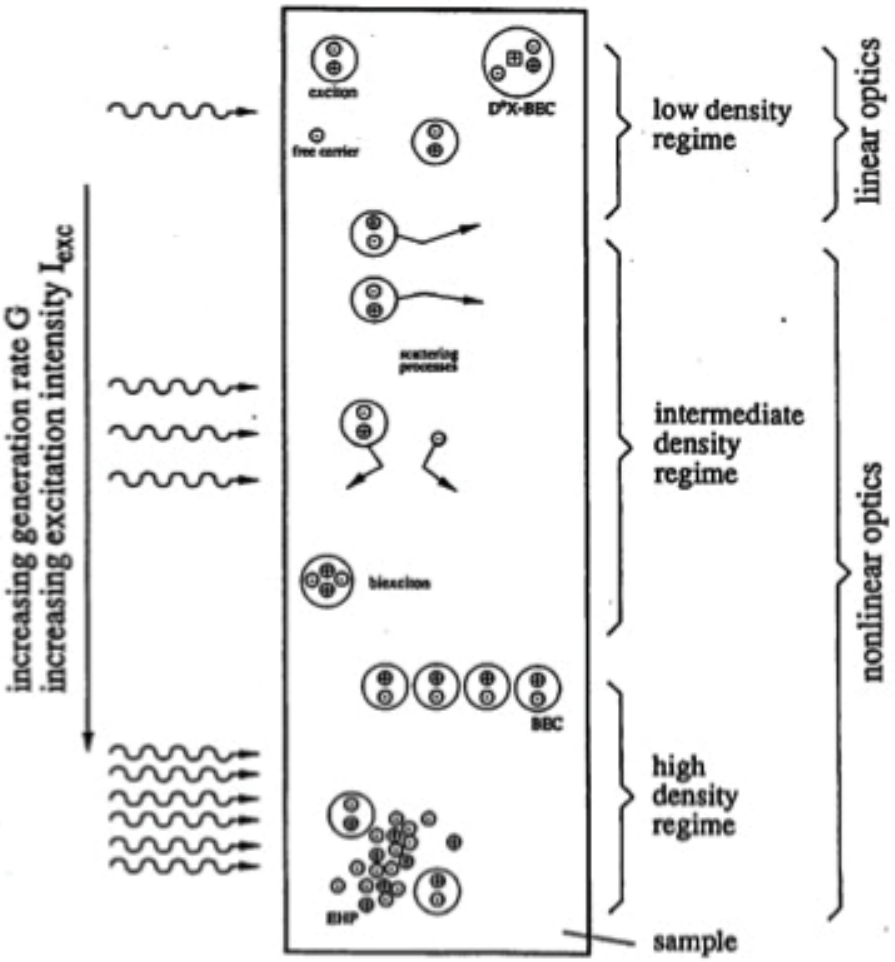

Figure 1.8: The general scenario for many-particle effects in semiconductors (see Ref. [34]) with D^0X-BEC: donor-bound exciton, biexciton: exciton molecule, BEC: Bose-Einstein Condensation, EHP: electron-hole plasma.

The schematic of the main intraexcitonic transition from 1s to 2p state is illustrated

in Fig. 1.7. The THz absorption is dealt in my present study in this thesis.

In optically excited semiconductors, many electronic states are known to be realized with controlling intensity and the frequency of the excitation light. Two extremes are clear and well understood: exciton gas in low density regime and $e-h$ plasma at high densities. A general scenario of the photoexcited $e-h$ system is schematically displayed in Fig. 1.7. At low excitation, i.e. low-density regime, excitons mainly determine the optical properties of the $e-h$ system. With further increasing the excitation intensity, the system arrives at the high-density regime. In this density regime, when the mean inter-distance between $e-h$ pairs is comparable or less than the exciton Bohr radius in which the screening effect is efficient, the bound $e-h$ pairs dissociate (a certain electron is no longer bound to a certain hole), i.e., excitons ionize, releasing free carriers. Excitons can no longer exist when the carrier density exceeds some critical density and the $e-h$ plasma is formed (see Fig. 1.9 for illustration of screening effect). The ***exciton Mott transition*** is referred to as a transition from insulating exciton gas to conducting $e-h$ plasma with increasing $e-h$ pair density. The optical gain is also considered the signature of exciton Mott transition.

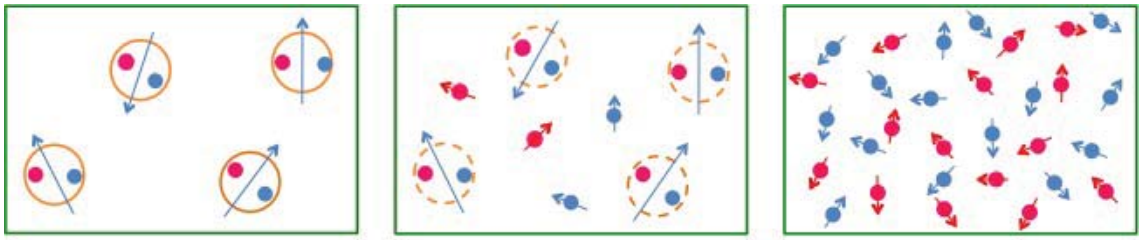

Figure 1.9: The schematic of screening effect in the $e-h$ system. From left to right, with the increasing of the carrier density, because of screening effect, the free carriers are released and exciton ionize forming the $e-h$ plasmas.

I believe that understanding several physical properties around the exciton Mott transition point is particularly important to develop novel high-performance optoelectronic devices such as highly efficient semiconductor laser diodes.

1.2 Optical spectroscopy

Optical spectroscopy is the most important method for gaining invaluable information [32] about a system based on measuring the interaction between matter and light radiation. It involves visible, ultraviolet, or infrared light, alone or in combination, to current-day ultrafast and terahertz spectroscopies, and is part of a larger group of spectroscopic techniques called electromagnetic spectroscopy. For solid state physics, it provides the information regarding the electronic bandwidth, semiconductor bandgap, phonons, plasma frequency and surface plasmons in addition to single-particle excitations.

The applied electric field induces a macroscopic electric dipole moment called polarization, $\mathbf{P}(\omega)$, which in general is a functional of the external field $\mathbf{E}(\omega)$ [11],

$$\mathbf{P}(\omega) = \mathcal{F}\left[\mathbf{E}(\omega)\right] \tag{1.9}$$

where ω is the angular frequency of the external field. In principle, all the information about the optical response of a system (absorption, refraction, reflection, diffusion,...) are associated with polarization $\mathbf{P}(\omega)$. In those processes the polarization oscillates at the same frequency as the incoming electric field.

For sufficiently low excitation intensities, the optical absorption and refraction do not depend on the intensity of the optical fields. For higher excitation intensities, the optical material properties may be modified, the response changes as the excitation density is varied. Therefore depending on the intensity of the excitation field, we have linear or nonlinear spectroscopy.

Linear spectroscopy is referred to regime where the external optical field is weak enough that the optical response is linearly proportional to the optical field. In the linear regime, the relation between polarization and external field is simply given by

$$\mathbf{P}(\omega) = \chi(\omega) \cdot \mathbf{E}(\omega) \tag{1.10}$$

where $\chi(\omega)$ is the optical susceptibility of the material.

In the linear spectroscopy, the absorption coefficient, $\alpha(\omega)$, which is proportional to the imaginary part of $\chi(\omega)$, is directly related to the energy eigenstates of the carriers in the system. Therefore, it is important to determine the ω in the linear spectroscopy to obtain the information of the electronic states.

When the electric field of the light is intense, the optical properties of basically all semiconductors exhibit nonlinear characteristics. The relation between $\mathbf{P}$ and $\mathbf{E}$ is nonlinear in this regime and thus the polarization can be expressed in a Taylor series of $\mathbf{E}$ [1,2]:

$$\mathbf{P}_i(\omega) = \sum_j \chi_{ij}^{(1)}(\omega)\mathbf{E}_j + \sum_{j,k} \chi_{ijk}^{(2)}(\omega)\mathbf{E}_j\mathbf{E}_k + \sum_{j,k,l} \chi_{ijkl}^{(3)}(\omega)\mathbf{E}_j\mathbf{E}_k\mathbf{E}_l + ... \tag{1.11}$$

where $\chi_{ij}^{(1)}$ is the linear optical susceptibility and corresponds to the susceptibility at low intensity; $\chi_{ijk}^{(2)}$ and $\chi_{ijkl}^{(3)}$ are the second and third-order nonlinear optical susceptibilities and are third and fourth rank tensors, respectively.

For many-particle systems, the optical nonlinearities originate from the many-body interactions between particles in the system, including band filling and Coulomb interactions. This nonlinearity has the consequence that the total response of the system is not a superposition of the response from each particle in the system. Therefore, finding the connection between many-body effects such as state-filling, band-gap renormalization, and plasma screening effects and their signature in optical spectroscopy is often an important task in this situation.

In this thesis, I deal with photo-excited semiconductor bulk materials. For such a system, linear optical response can be assumed if the excitation field is small enough such that the density of carriers in the system is low enough such that they are treated accurately noninteracting carriers (electrons, holes and excitons). However, a photo-excited semiconductor is essentially a many-body system. Many-body effects (state-filling, band-gap renormalization, and plasma screening effects) profoundly influence carrier dynamics

and the optical response of the system as a consequence. Thus in the theoretical treatment of these systems, it is important to include the key many-body effects particular to the system being investigated in the formalism employed, while remaining computationally tractable.

1.3 Overview of experimental studies on Exciton Mott Transition

Many different experimental techniques have been developed to investigate different aspects of these dynamical processes in semiconductors.

In conventional studies, the exciton Mott transition has been studied with the spectral and thermodynamical approaches [29]. In the spectral approach, one studies density dependence of the visible or near-infrared absorption spectra at the semiconductor band gap accompanied by the interband transition, and define the transition density at which the spectral component corresponding to the 1s exciton resonance merges with the band edge [30-32]. The photo-excitation generates in semiconductor the optical polarization induced by the interband transitions between valence and conduction bands. In the optical absorption spectrum, excitons may have signatures as discrete lines below the bandgap by their binding energy. Above the critical density the excitonic structure disappears and optical gain spectrum is observed. The optical absorption and/or photoluminescence (PL) measurements in Fig. 1.10 [28] give an example of exciton Mott transition. Although, this experimental result is in quasi-one dimensional $e-h$ system, it is a good illustration in terms of definition of exciton Mott transition.

In the thermodynamical approach, on the other hand, one studies density dependences of the ionization ratio and the quasi-chemical potential of $e-h$ pairs, and define the transition density at which these quantities increase abruptly with increasing the $e-h$ pair density [33−35].

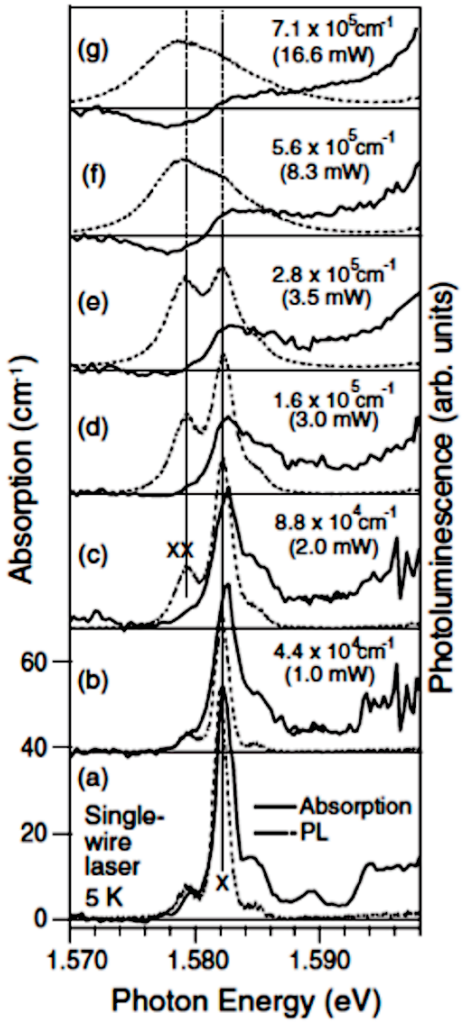

Figure 1.10: Absorption (solid curves) and photoluminescence (dashed curves) spectra from a GaAs quantum wire at 5K for various excitation densities (powers) from Ref. [28]. For carrier density $n > 7.1 \times 10^5$ cm^{-1}, the excitonic structure disappears and the optical gain spectra is observed. It shows that the exciton Mott transition occurs.

Despite the success of optical spectroscopy, because these optical methods measure the interband polarization based on the creation or destruction excitons which involves limitations. The absorption in this spectral range measure the generation of $e-h$ so providing the indirect information about $e-h$ pair population dynamics. In particular, because of momentum conservation photoluminescence can only observed from excitons with center-of-mass momentum close to zero. The dipole-forbidden interband transitions are not observable with visible or near-IR probes either. Additionally, the recent calculations and experiments [25,33] have shown that the unbound $e-h$ pairs can induce the excitonic resonances.

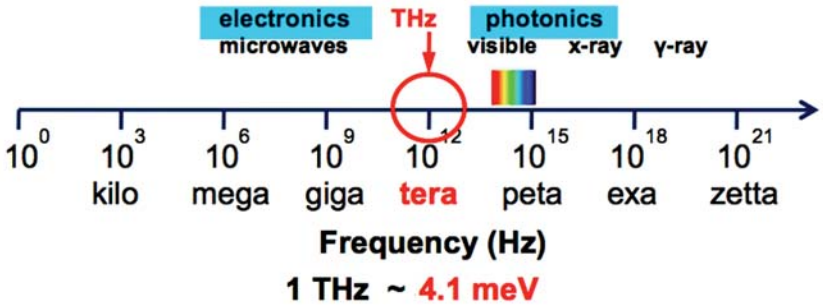

Figure 1.11: The terahertz (THz) region is the part of electromagnetic radiation spectrum.

Hence, the other methods, which can provide the supplementary information about the photoexcited $e-h$ systems in semiconductors, are expected. The developments in terahertz technology have rapidly extended the ability to study excitonic dynamics by investigating the transitions between quasi-particle states, i.e., the intraexcitonic transitions, in electronic materials. The Rydberg exciton binding energy is in the range of 1-100 meV (see Tab.1.1), and intraexcitonic transitions are typically a fraction of the binding energy [22,34,35]. THz radiation is electromagnetic radiation with frequencies from 0.3 to 3 THz (1 THz = 10^{12} Hz), wavelengths range of 1 mm to 0.1mm (or 100 μm), and corresponding to a photon energy of 4.2 meV at 1 THz. Therefore, THz radiation is sensitive to the response of charged carriers and elementary excitations, and described with distinctive types. Furthermore, since the ponderomotive energy of THz radiation for a given laser intensity is higher than that of visible light, we can apply strong electric fields ($\approx$ 1MVcm^{-1}) using a monocycle THz pulse. Therefore, THz techniques pave the new way for studying extreme nonlinear phenomena such as the impact ionization and the high-order harmonic generation in condensed matters, which cannot be analyzed with the perturbation theory.

Recently, Optical-Pump Terahertz-Probe Spectroscopy (OPTP), also known as time-resolved THz spectroscopy, has become a powerful tool to investigate exciton population dynamics as formation, and ionization of excitons. In the optical-pump THz-probe experiment, a short optical pump pulse excites in the sample, and then the THz pulse probes the photo-induced changes and evolution of charge carriers. The important advantage

is its detection scheme which enables the probing of induced polarizations with a time resolution in the subcycle regime. They probe the intraexcitonic transitions from the 1s exciton state to higher relative-momentum states. Therefore, THz transitions can determine densities of excitons and free carriers existing in the sample. In particular, the THz response of the charge carriers in conducting and insulating phases in semiconductors are strong and distinctive. Furthermore, because time-resolved THz spectroscopy measures both the real and the imaginary parts of the dielectric response over a wide range of frequencies.

Table 1.1: Exciton Rydberg energy of several typical semiconductors.

Semiconductor	Exciton binding energy E_0 (meV)
CuCl	190
GaN	28
CdS	30
GaAs	4.2
Si	14.7
Ge	4.15

The first experimental study on the dynamics of the formation and ionization of excitons was reported by Kaindl et al. (2003) on GaAs quantum wells [4]. An interesting study in excitation-dependent THz response was performed by Huber, Kaindl et al., 2005 [36] whereas they studied quasi-two-dimensional excitons in quantum wells. Later works by this group with a comprehensive experimental analysis, they have concluded that their dielectric function closely describes the THz absorption spectra of resonantly generated excitons at low density (Kaindl et al., 2009) [37]. For bulk semiconductor, for example Si, the formation of excitons and electron-hole droplet after photoexcitation was measured by using THz-TDS (Suzuki and Shimano, 2009) [38]. Furthermore, the THz spectroscopy provides a tool to observe several interesting phenomena, for examples, stimulated emission, quantum beats (Huber et al., 2006) [39], and Rabi cycling (Leinss

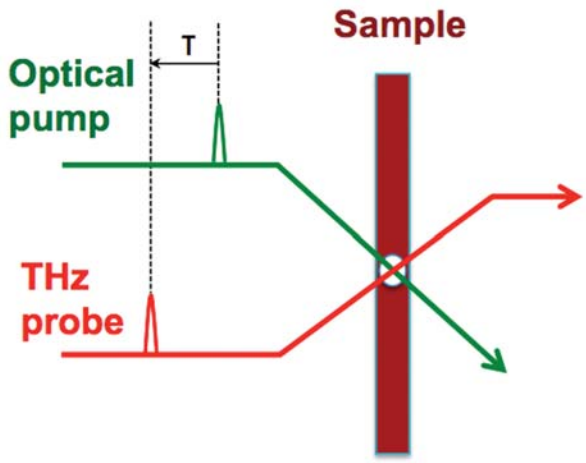

Figure 1.12: The schematic representation of Optical Pump Terahertz Probe Spectroscopy (OPTP).

et al., 2008) [40].

1.4 Theoretical Approaches Overview

Accompanying the experimental works, many theoretical approaches have been developed for investigating the dynamics of $e-h$ system in photoexcited semiconductor. The most commonly used methods are non-equilibrium Green's functions and equation-of-motion approaches [31]. The well-known semiconductor Bloch equations (SBEs) are based on the second approach [31], as are the dynamics controlled truncation (DCT) equations [21].

The formalism in the framework of nonequilibrium Green's functions, [41,42] where the interaction is described by a dynamical two-time-dependent propagator, yields a quite naturally method to determine the spectral and kinetic properties of a many-body system. This allows us to investigate, e.g., the dynamical build-up of screening after ultrafast carrier excitation. However, it has the disadvantage of being heavy computations.

On the other hands, based on equation-of-motion method, the deriving dynamical equations can determine the carrier distributions and polarization. Follow this approach one obtains, however, an infinite hierarchy of dynamical equations, which must be trun-

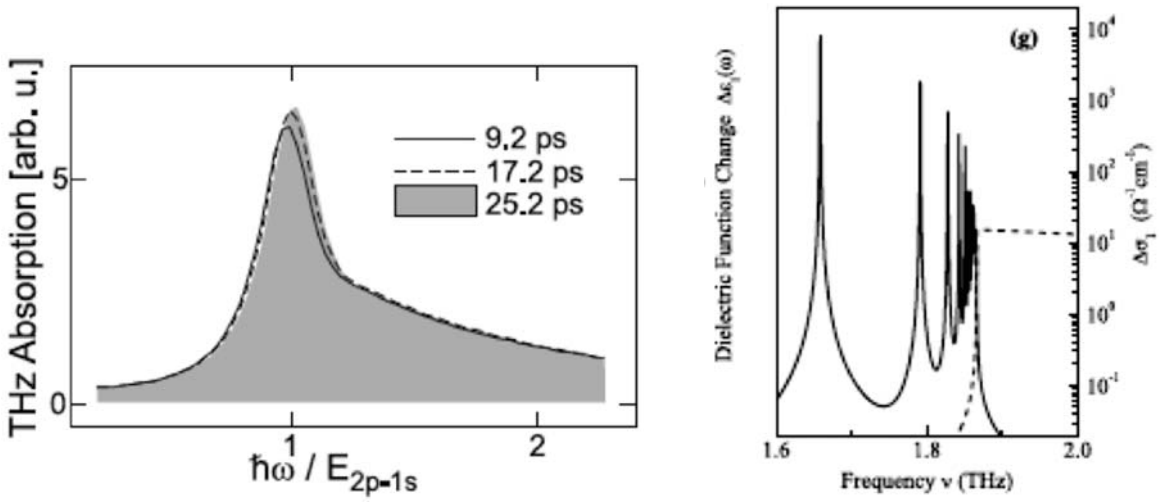

(a) **(b)**

Figure 1.13: (a) Terahertz spectra determined at different time moments after the resonant $1s$ excitation used in Kira et. al. work from Ref. [23]. (b) Kaindl et. al. calculate intraexcitonic model in GaAs quantum well structures in low density limit from Ref. [37].

cated at some stage in order to get a closed set of coupled differential equations by introducing some approximations. A well-controlled approximation is the perturbation theory performed in the optical field. [41] However, it cannot be used to examine effects such as density-dependent shifts of excitonic absorption peaks since it is limited to low densities. Alternatively, one makes factorization approximation splitting the four-operator expectation values into products of the relevant two-operator expectation values. This approximation scheme is often called random phase approximation (RPA), which yields the well-known semiconductor Bloch equations (SBEs). [31,41,42] The SBEs govern the dynamics of electrons, holes and the optical polarization in the spectral vicinity of the semiconductor band gap. More general truncation schemes, such as cluster expansions [43] can include the next higher level of correlations up to arbitrary order. In practice, however, this is often limited by the available computer resources.

Theoretically, THz absorption in exciton systems has been studied in seminal works by Hanken [18] and by Nikitine [19] based on the analogy between excitons and hydrogen atoms. Analysis along this line has been extended by Kaindl et al. [7]; using the wave functions and the energy eigenvalues of two-dimensional excitons, they have calculated

Table 1.2: The theoretical approaches to investigate the dynamics of $e-h$ system in photoexcited semiconductor.

Method	Advantage	Disadvantage
Non-equilibrium Green's function (as in work of Kwong et. al. [65])	systematically improving approximation by taking into account particular processes (represented in the form of Feynman diagrams)	being heavy in computations
Equation-of-motion (as in work of Kira et. al. [44-46] and this work)	describing the behaviour of a physical system in terms of its motion as a function of time	Infinite hierarchy of dynamic equation needs truncation by approximations

two-component THz dielectric function. With a comprehensive experimental analysis, they have concluded that their dielectric function closely describes the THz absorption spectra of resonantly generated excitons at low density. Based on the equation-of-motion approach combined with the cluster-expansion technique, [44-46] Kira et al. have developed a microscopic theory to study THz absorption in semiconductor quantum well structures, and they have successfully analyzed the formation dynamics of exciton resonantly as well as non-resonantly excited semiconductors. [47,48,22] This theory has suggested that $e-h$ system being composed of three components: a continuum of ionized excitons, intermediate exciton states, and a Coulomb-correlated $e-h$ plasma. Recently, the intraexciton 1s-2p transition energy and the 1s exciton creation energy in two- and three-dimensional systems have theoretically been studied in Refs. [49,50], based on the exciton picture where the quasi-Boson operator corresponding to excitons is introduced by the Usui transformation.

In this thesis, I propose a theory that is applicable for quasi-equilibrium case without heavy numerical computations, which offers a complementary viewpoint the previous

theories about THz absorption in semiconductors.

In the present study, I aim at investigating the THz absorption of excitons in low-density regime and that of $e-h$ plasmas in high-density regime on a same electron-hole basis. I derive the equations-of-motion of transverse dielectric functions which determine the carrier distributions and interband polarization. In order to get a closed set of coupled differential equations, I introduce the time-dependent Hartree-Fock approximation (TDHFA) to overcome the hierarchy problem. Taking into account the screening effect, I employ a longitudinal dielectric function given by the static single-plasmon-pole approximation (SPPA).

To theoretically investigate the exciton Mott transition (the density ionization), I study the exciton Mott transition based on the THz absorption that constitutes a fundamentally different approach from the visible or near-infrared absorption. Furthermore, I study the density dependence of the ionization ratio and the $e-h$ quasi-chemical potential with thermodynamical approach.

1.5 The contents and structure of this thesis

This thesis is organized as the follows. In Chap. 2, I construct the Hamiltonian for optically excited semiconductor with introducing BCS-like mean field approximation. It contains discussions on how many-body effects can be included in the formalism, and what types of many-body effects are treated in this thesis. The Chap. 3 is devoted to the derivation of equation-of-motion of the dielectric function, which is important to calculate the THz absorption spectra. In Chap. 4, I present the numerical results and examine the THz absorption spectra for various $e-h$ pair densities to investigate the exciton Mott transition based on the spectral and thermodynamical approaches. Finally, I present in Chap. 5 the conclusions and future directions in the study of THz response in optically excited semiconductors.

Chapter 2

Hamiltonian in Semiconductors

For the purpose of theoretically investigating exciton Mott transition with analyzing the THz absorption spectra in optically excited semiconductors, I consider the $e-h$ system in photo-excited semiconductor in a wide range of $e-h$ pair densities, from low to moderate exciton density, and high density of $e-h$ pairs. The construction of the Hamiltonian of the $e-h$ system in semiconductor is the focus of this chapter.

This chapter is organized as the follows. In Sec. 2.1, the Hamiltonian for optically excited semiconductors in the electron-hole basis is established. I introduce in Sec. 2.2 the BCS-like mean-field approximation. Taking into account the $e-h$ pair correlation (excitonic effects) the Bogoliubov transformation [51-53] is introduced in Sec. 2.3. The Bogoliubov parameters are determined using the BCS-like pairing theory [54-60,51-53] with deriving BCS-like gap equations in Sec. 2.4. Finally, I have a brief summary of this chapter in Sec. 2.5.

In this thesis, for simplicity, I consider a three-dimensional electron-hole system in a direct bandgap bulk semiconductor, which consists of an isotropic and non-degenerate parabolic conduction and valence bands with effective masses m_e and m_h, respectively.

The system is supposed to be in quasi-equilibrium state with carrier temperature T. In the optically excited semiconductor, the quasi-equilibrium state can be realized after relatively long time scales (typically several few femtoseconds) when the created electrons

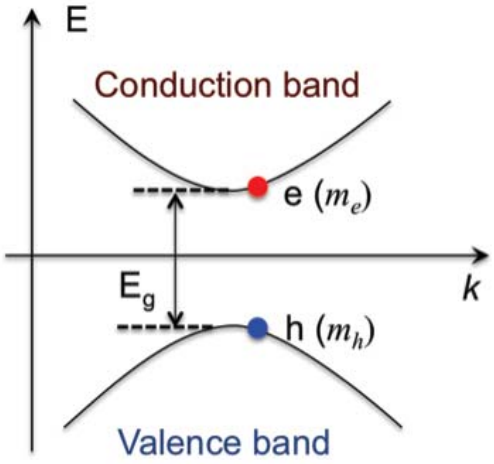

Figure 2.1: The model of the two-band $e-h$ system in bulk semiconductor consists of non-degenerate parabolic conduction ($a = 1$) and valence ($a = 2$) bands with effective masses m_e and m_h, respectively.

and holes have had sufficient time to interact among themselves and establish Fermi-Dirac distributions within each band. This means that after their creation, the carriers in the different bands have had sufficient time to interact and establish a plasma temperature and a chemical potential, which are the two thermodynamic quantities needed to define a Fermi distribution function for a given density. In this study, the electron and hole density are controlled by their quasi-chemical potentials μ_e and μ_h, respectively. This assumption is appropriate for the excitons with long lifetime, such as 1s paraexcitons in Cu_2O.

I also assume that the system is charge neutral. Furthermore, I focus on the THz absorption of excitons and that of $e-h$ plasmas on a same basis. I therefore neglect the spin degree of freedom, which plays an essential role when we study excitonic molecules; I also neglect phonon effects.

2.1 The interaction Hamiltonian

I first investigate the radiation-matter interaction Hamiltonian and the current operator. Introducing the electron-field operator $\Psi(\boldsymbol{x})$ and a lattice-periodic potential $U(\boldsymbol{x})$, the single-particle Hamiltonian H in the second quantization form describing an electron

system interacting with a classical electromagnetic field $\boldsymbol{A}(\boldsymbol{x},t)$ is expressed as

$$H(t) = H_0 + H_1(t) + H_2(t) \tag{2.1}$$

where

$$H_0 = \int d^3x \Psi^\dagger(\boldsymbol{x}) \left[-\frac{1}{2m_0} \bigtriangledown^2 + U(\boldsymbol{x}) \right] \Psi(\boldsymbol{x}) \tag{2.2}$$

$$H_1(t) = \int d^3x \Psi^\dagger(\boldsymbol{x}) \left[\frac{ie}{m_0} \boldsymbol{A}(\boldsymbol{x},t) \cdot \bigtriangledown \right] \Psi(\boldsymbol{x}) \tag{2.3}$$

$$H_2(t) = \int d^3x \Psi^\dagger(\boldsymbol{x}) \left[\frac{e^2}{2m_0} \boldsymbol{A}^2(\boldsymbol{x},t) \right] \Psi(\boldsymbol{x}) \tag{2.4}$$

Here m_0 and $-e$ are the free electron mass and the electron charge, respectively. The total Hamiltonian of the system is

$$H_{tot} = H(t) + H_{int} \tag{2.5}$$

where H_{int} is the Coulomb Hamiltonian between electrons. For the sake of simplicity, the spin degrees of freedom and the spin-orbit interaction is neglected. Throughout this calculation, I use the Coulomb gauge $\bigtriangledown \cdot \boldsymbol{A} = 0$.

Using the Bloch basis $e^{i\boldsymbol{k}\cdot\boldsymbol{x}} u_{\boldsymbol{k}a}(\boldsymbol{x}) / \sqrt{V}$ with band a ($a = 1, 2$) and lattice momentum $\boldsymbol{k}$, then $\Psi(\boldsymbol{x})$ is expanded as

$$\Psi(\boldsymbol{x}) = \frac{1}{\sqrt{V}} \sum_a \sum_{\boldsymbol{k}} e^{i\boldsymbol{k}\cdot\boldsymbol{x}} u_{\boldsymbol{k}a}(\boldsymbol{x}) c_{\boldsymbol{k}a} \tag{2.6}$$

where V, $c_{\boldsymbol{k}a}$, and $u_{\boldsymbol{k}a}(\boldsymbol{x})$ are the volume of the system, the annihilation operator of electrons, and the lattice periodic function, respectively. Substituting Eq. (2.6) into Eqs.

(2.2-2.4), the Hamiltonian H_j $(j = 0, 1, 2)$ are

$$H_0 = \sum_a \sum_{\boldsymbol{k}} E_{\boldsymbol{k}a} c^\dagger_{\boldsymbol{k}a} c_{\boldsymbol{k}a} \tag{2.7}$$

$$\begin{aligned} H_1(t) = &-\frac{e}{m_0} \sum_{ab} \sum_{\boldsymbol{k}} \boldsymbol{A}(t) \cdot \boldsymbol{P}_{ab}(\boldsymbol{k}) (1 - \delta_{ab}) c^\dagger_{\boldsymbol{k}a} c_{\boldsymbol{k}b} \\ &-\frac{e}{m_0} \sum_a \sum_{\boldsymbol{k}} [\boldsymbol{k} + \boldsymbol{P}_{aa}(\boldsymbol{k})] \cdot \boldsymbol{A}(t) c^\dagger_{\boldsymbol{k}a} c_{\boldsymbol{k}a} \end{aligned} \tag{2.8}$$

$$H_2(t) = \frac{e^2}{2m_0} \sum_{ab} \sum_{\boldsymbol{k}} \boldsymbol{A}^2(t) c^\dagger_{\boldsymbol{k}a} c_{\boldsymbol{k}a} \tag{2.9}$$

Here I have defined

$$\boldsymbol{P}_{ab}(\boldsymbol{k}) \equiv \frac{1}{V_0} \int_{V_0} d^3x u^*_{\boldsymbol{k}a}(\boldsymbol{x}) (-i\bigtriangledown) u_{\boldsymbol{k}b}(\boldsymbol{x}) \tag{2.10}$$

where V_0 is the volume of the unit cell. The first term on the right-hand side of H_1 describes the interband transition, while the second term and H_2 represent the intraband transition. In deriving Eq. (2.10) I have employed the long wavelength approximation in which the $\boldsymbol{x}$-dependence of the vector potential is neglected; this approximation is justified when we investigate the optical or THz response where the wavelength of the radiation field is sufficiently long comparing with the lattice constant of the semiconductor crystal (dipole approximation). Since the band energy $E_{a\boldsymbol{k}}$ is expressed as

$$E_{a\boldsymbol{k}} = \frac{1}{V_0} \int_{V_0} d^3x u^*_{\boldsymbol{k}a} \left[-\frac{1}{2m_0} (\bigtriangledown + i\boldsymbol{k})^2 + V(\boldsymbol{x}) \right] u_{\boldsymbol{k}b}(\boldsymbol{x}) \tag{2.11}$$

$[\boldsymbol{k} + \boldsymbol{P}_{aa}(\boldsymbol{k})]/m_0 = \partial E_{\boldsymbol{k}a}/\partial \boldsymbol{k}$; this quantity is approximated by $\boldsymbol{k}/m_a$, where m_a is the effective mass of the band a, if I assume an isotropic band dispersion. From Eq. (2.9), the current operator $\boldsymbol{J}(t)$ turns out to be

$$\boldsymbol{J}(t) = -\frac{e}{m_0} \sum_{ab} \sum_{\boldsymbol{k}} (1 - \delta_{ab}) c^\dagger_{\boldsymbol{k}a} c_{\boldsymbol{k}b} + e \sum_a \sum_{\boldsymbol{k}} \frac{\partial E_{\boldsymbol{k}a}}{\partial \boldsymbol{k}} c^\dagger_{\boldsymbol{k}a} c_{\boldsymbol{k}a} - \frac{e^2}{2m_0} \boldsymbol{A}(t) \sum_a \sum_{\boldsymbol{k}} c^\dagger_{\boldsymbol{k}a} c_{\boldsymbol{k}a} \tag{2.12}$$

For later convenience, I define

$$j_{\boldsymbol{q}}^{\lambda} \equiv e \sum_{\boldsymbol{k}} \sum_{a} \left(\boldsymbol{e}_{q}^{\lambda} \cdot \frac{\partial E_{\boldsymbol{k}a}}{\partial \boldsymbol{k}} \right) c_{\boldsymbol{k}a}^{\dagger} c_{\boldsymbol{k}a} \tag{2.13}$$

$$X_{\boldsymbol{q}}^{\lambda} \equiv \frac{e}{m_0} \sum_{\boldsymbol{k}} \sum_{ab} (1 - \delta_{ab}) \left[\boldsymbol{e}_{\boldsymbol{q}}^{\lambda} \cdot P_{ab}(\boldsymbol{k}) \right] c_{\boldsymbol{k}a}^{\dagger} c_{\boldsymbol{k}b} \tag{2.14}$$

where $\boldsymbol{e}_{\boldsymbol{q}}^{\lambda}$ ($\lambda = 1, 2$) is the polarization vector. In this study, the radiation field propagates along the q-direction, and the polarization vector is defined so that ($e_{\boldsymbol{q}}^{1}$, $e_{\boldsymbol{q}}^{2}$, $\boldsymbol{q}/|\boldsymbol{q}|$) forms a right-handed set of orthonormal vectors.

Hamiltonian of two-band system

In this study, I consider an $e-h$ system, which consists of conduction and valence bands. Hence, the Hamiltonian can be expressed in two-band approximation.

The electron part of the Hamiltonian in two-band approximation is written as,

$$\begin{aligned} H_{e-h} &= H_0 + H_{int} \\ &= \sum_{a} \sum_{\boldsymbol{k}} E_{\boldsymbol{k}a} c_{\boldsymbol{k}a}^{\dagger} c_{\boldsymbol{k}a} + \frac{1}{2} \sum_{ab} \sum_{\boldsymbol{kpq}} \mathcal{V}_{\boldsymbol{q}} c_{\boldsymbol{k}+\boldsymbol{q}a}^{\dagger} c_{\boldsymbol{p}-\boldsymbol{q}b}^{\dagger} c_{\boldsymbol{p}b} c_{\boldsymbol{k}a} \end{aligned} \tag{2.15}$$

where $a = 1$ and 2 are band indices corresponding to the conduction and valence bands, respectively.

The single-particle energies of electrons in the conduction band and holes in the valence bands are given by,

$$E_{\boldsymbol{k}1} = \frac{\boldsymbol{k}^2}{2m_e} + E_g - \mu_e; \quad E_{\boldsymbol{k}2} = \frac{\boldsymbol{k}^2}{2m_h} - \mu_h \tag{2.16}$$

where E_g is bandgap energy between conduction and valence bands, $m_e(m_h)$ is effective mass of electron (hole), respectively.

The bare Coulomb interaction is written as,

$$\mathcal{V}_{\boldsymbol{q}} = \frac{4\pi e^2}{\epsilon_0 \boldsymbol{q}^2 V} \tag{2.17}$$

where, ϵ_0 is the background dielectric constant of the unexcited crystal, and V is the volume of the system.

The Hamiltonian describes the interband dipole coupling to the light field is

$$H_1 = -\sum_{\boldsymbol{k}} \mathcal{E}(t) \left(c^{\dagger}_{\boldsymbol{k}1} c_{\boldsymbol{k}2} d_{cv} + h.c. \right) \tag{2.18}$$

where, d_{cv} is the interband dipole matrix element; $\mathcal{E}(t) = \mathcal{E} e^{-i\omega_0 t}$ is the light field.

When analyzing the matter that is driven by a coherent light, it is convenient to convert the matter Hamiltonian to the time-independent form in the so-called rotating frame. For this purpose, I use the unitary transformation given by the unitary time-evolution operator,

$$T(t) = exp\left[-\frac{i\omega_0 t}{2} \sum_{\boldsymbol{k}} \left(c^{\dagger}_{\boldsymbol{k}1} c_{\boldsymbol{k}1} + c^{\dagger}_{\boldsymbol{k}2} c_{\boldsymbol{k}2} \right) \right] \tag{2.19}$$

where, ω_0 is pump light frequency.

The transformed Hamiltonian is expressed as follows,

$$H_{e-h} = \sum_{\boldsymbol{k}} \mathcal{E}^{\mu}_{\boldsymbol{k}} c^{\dagger}_{\boldsymbol{k}a} \left(\tau^{\mu}\right)_{ab} c_{\boldsymbol{k}a} + \frac{1}{2} \sum_{ab} \sum_{\boldsymbol{kpq}} \mathcal{V}_{\boldsymbol{k}a} c^{\dagger}_{\boldsymbol{k+q}a} c^{\dagger}_{\boldsymbol{p\text{-}q}b} c_{\boldsymbol{p}b} c_{\boldsymbol{k}a} \tag{2.20}$$

where, $\mathcal{E}^{\mu}_{k}$ is written as follows:

$$\begin{aligned}
\mathcal{E}^0_{\boldsymbol{k}} &= \frac{1}{2}\left(E_{\boldsymbol{k}1} + E_{\boldsymbol{k}2}\right); \\
\mathcal{E}^1_{\boldsymbol{k}} &= -\frac{1}{2}\mathcal{E}\left(d + d^*\right); \\
\mathcal{E}^2_{\boldsymbol{k}} &= -\frac{i}{2}\mathcal{E}\left(d - d^*\right); \\
\mathcal{E}^3_{\boldsymbol{k}} &= \frac{1}{2}\left(E_{\boldsymbol{k}1} - E_{\boldsymbol{k}2} - \omega_0\right)
\end{aligned} \tag{2.21}$$

The resulting stationary state of the driven electron-hole system is controlled by the frequency of pump light ω_0.

Here for convenience, I use the 2×2 unit matrix τ^0 and the Pauli matrices τ^j $(j = 1, 2, 3)$

$$\tau^0 = \begin{pmatrix} 1 & 0 \\ 0 & 1 \end{pmatrix}; \quad \tau^1 = \begin{pmatrix} 0 & 1 \\ 1 & 0 \end{pmatrix};$$
$$\tau^2 = \begin{pmatrix} 0 & -i \\ i & 0 \end{pmatrix}; \quad \tau^3 = \begin{pmatrix} 1 & 0 \\ 0 & -1 \end{pmatrix} \tag{2.22}$$

In the following analysis, I use the summation convention with respect to indices μ and ν $(\mu, \nu = 0, 1, ..., 3)$, unless otherwise stated.

For the theoretical description of THz processes, the light-matter interaction discussed in this study is extended to include the coupling to intraband quantities. In this study, THz absorption is calculated semi-classically, it means that the THz field is not quantized. The THz field is given by the vector potential $\boldsymbol{A}_{\boldsymbol{q}}(t)$. With the Coulomb gauge condition $(\bigtriangledown \cdot \boldsymbol{A} = 0)$, the interaction Hamiltonian between carriers and THz field is

$$H_2 = -\frac{1}{V} \sum_{\boldsymbol{q},\lambda} (-1)^{\lambda-1} j^{\lambda}_{\boldsymbol{q}}(t) A^{\lambda}_{-\boldsymbol{q}}(t) \tag{2.23}$$

where $j^{\lambda}_{\boldsymbol{q}}(t) = \boldsymbol{e}^{\lambda}_{\boldsymbol{q}} \cdot \boldsymbol{J}_{\boldsymbol{q}}(t)$ and $A^{\lambda}_{-\boldsymbol{q}}(t) = \boldsymbol{e}^{\lambda}_{\boldsymbol{q}} \cdot \boldsymbol{A}_{\boldsymbol{q}}(t)$ are transverse components of the intraband current density operator and the vector potential, respectively. Using the electron-hole representation, the intraband current operator is expressed as follows,

$$j^{\lambda}_{\boldsymbol{q}}(t) = -\frac{e}{V} \sum_{\boldsymbol{p}} \left(\frac{1}{m}\right)^{\mu} \left(\boldsymbol{p} \cdot \boldsymbol{e}^{\lambda}_{\boldsymbol{q}}\right) \left(c^{\dagger}_{\boldsymbol{p}\text{-}\boldsymbol{q}a} \left(\tau^{\mu}\right)_{ab} c_{\boldsymbol{p}a}\right) \tag{2.24}$$

where

$$\left(\frac{1}{m}\right)^0 = \frac{1}{2}\left(\frac{1}{m_e} - \frac{1}{m_h}\right);$$
$$\left(\frac{1}{m}\right)^3 = \frac{1}{2}\left(\frac{1}{m_e} + \frac{1}{m_h}\right);$$
$$\left(\frac{1}{m}\right)^\mu = 0, \qquad \mu = 1, 2 \tag{2.25}$$

Discussion of the electron-hole Hamiltonian

For the discussion about Hamiltonian, it is convenience to write the Hamiltonian in the electron-hole representation. Inserting the definitions of creation operators of electron in conduction band ($a = 1$) and hole in valence band ($a = 2$),

$$c^\dagger_{\boldsymbol{k}} = c^\dagger_{\boldsymbol{k}1}$$
$$d^\dagger_{-\boldsymbol{k}} = c^\dagger_{\boldsymbol{k}2} \tag{2.26}$$

respectively, into the Hamiltonian (2.20) and restoring the normal ordering of the electron and hole operators, we obtain

$$\begin{aligned} H = &\sum_{\boldsymbol{k}} \left(\mathcal{E}^e_{\boldsymbol{k}} c^\dagger_{\boldsymbol{k}} c_{\boldsymbol{k}} + \mathcal{E}^h_{\boldsymbol{k}} d^\dagger_{-\boldsymbol{k}} d_{-\boldsymbol{k}}\right) \\ &+ \frac{1}{2}\sum_{\boldsymbol{kpq}} \mathcal{V}_{\boldsymbol{q}} \left(c^\dagger_{\boldsymbol{k+q}} c^\dagger_{\boldsymbol{p\text{-}q}} c_{\boldsymbol{p}} c_{\boldsymbol{k}} + d^\dagger_{\boldsymbol{k+q}} d^\dagger_{\boldsymbol{p\text{-}q}} d_{\boldsymbol{p}} d_{\boldsymbol{k}} - 2 c^\dagger_{\boldsymbol{k+q}} d^\dagger_{\boldsymbol{p\text{-}q}} d_{\boldsymbol{p}} c_{\boldsymbol{k}}\right) \\ &- \sum_{\boldsymbol{k}} \mathcal{E}(t) \left(c^\dagger_{\boldsymbol{k}} d^\dagger_{-\boldsymbol{k}} d_{cv} + h.c.\right) \end{aligned} \tag{2.27}$$

where, $\mathcal{E}^e_{\boldsymbol{k}} = E_{\boldsymbol{k}1}$ $\left(\mathcal{E}^h_{\boldsymbol{k}} = -E_{\boldsymbol{k}2}\right)$ is the single-particle kinetic energy of an electron (hole), respectively.

In the electron-hole Hamiltonian H_{e-h} Eq. (2.28), I include only those Coulomb interaction processes that converse particle number in each band. In other words, inter-

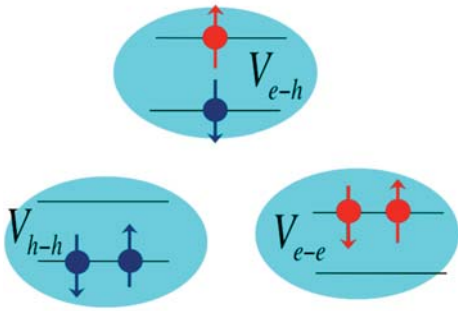

Figure 2.2: The Coulomb interactions between electrons $(e-e)$, between holes $(h-h)$, and between electron and hole $(e-h)$

band Coulomb processes in which, e.g., one electron and one hole are annihilated and two electrons are created are not taken into account due to the relatively large energy gap between both bands. It ensures that the system is charge neutral. In which, I have included the exchange interaction as well as the Coulomb attractive interaction between an electron and a hole are taken into account. This can be understood by considering the various interactions in the electron-hole system. There are three kinds of interaction in an e-h system: the repulsive interactions between electrons $(e-e)$ and between holes $(h-h)$, and the attractive interactions between electron and hole $(e-h)$ (see Fig. 2.2).

The $e-h$ interaction is attractive interaction represented by

$$V_{e-h} = -\sum_{\boldsymbol{kpq}} \mathcal{V}_{\boldsymbol{q}} c^{\dagger}_{\boldsymbol{k+q}} d^{\dagger}_{\boldsymbol{p\text{-}q}} d_{\boldsymbol{p}} c_{\boldsymbol{k}} \tag{2.28}$$

Here the factor of 2 is added because the interaction comes both from electrons and holes. In which the e-h interaction inside exciton is represented by

$$-\sum_{\boldsymbol{kpq}} \mathcal{V}_{\boldsymbol{q}} c^{\dagger}_{\boldsymbol{k+q}} d^{\dagger}_{\boldsymbol{-k\text{-}q}} d_{\boldsymbol{-k}} c_{\boldsymbol{k}} \tag{2.29}$$

where the electron and hole have the opposite momentum because they are excited by photons. The repulsive interactions are e-e and h-h interactions defined by

$$V_{e-e} = -\frac{1}{2}\sum_{\boldsymbol{kpq}} \mathcal{V}_{\boldsymbol{q}} c^{\dagger}_{\boldsymbol{k+q}} c^{\dagger}_{\boldsymbol{p\text{-}q}} c_{\boldsymbol{p}} c_{\boldsymbol{k}} \tag{2.30}$$

$$V_{h-h} = -\frac{1}{2}\sum_{\boldsymbol{kpq}} \mathcal{V}_{\boldsymbol{q}} d^{\dagger}_{\boldsymbol{k+q}} d^{\dagger}_{\boldsymbol{p\text{-}q}} d_{\boldsymbol{p}} d_{\boldsymbol{k}} \tag{2.31}$$

respectively. These Coulomb interactions will be discussed in detail in the later sections when the plasma screening and Coulomb-hole effect are taken into account.

2.2 BCS-like Mean Field Approximation

A many-body system such that the $e-h$ system in semiconductor with interactions is generally very difficult to solve exactly except the very simple cases such as 1D Ising model. It is shown in experiments that a single-particle description forms a surprisingly good approximation in many different systems, for example, metals, atoms, and nuclei. Hence a natural approach to solve a many-body problem is to retain the single-particle picture with choosing a good external field. This is the main idea of the mean field theory (MFT also known as self-consistent theory).

Based on the BCS-like mean field theory, I introduce the mean-fields $\chi^{\mu}_{\boldsymbol{k}}$ ($\mu = 0, 1, \cdots, 3$), with mean-field Hamiltonian

$$H_m = \sum_{\boldsymbol{k}} \chi^{\mu}_{\boldsymbol{k}} \left(c^{\dagger}_{\boldsymbol{k}} \tau^{\mu} c_{\boldsymbol{k}} \right) \tag{2.32}$$

Then e-h Hamiltonian H_{e-h} defined in Eq. (2.20) is decomposed into two parts,

$$H_{e-h} = H^{'}_0 + H^{'}_1 \tag{2.33}$$

where,

$$H^{'}_0 = \sum_{\boldsymbol{k}} \left(\mathcal{E}^{\mu}_{\boldsymbol{k}} + \chi^{\mu}_{\boldsymbol{k}} \right) \left(c^{\dagger}_{\boldsymbol{k}} \tau^{\mu} c_{\boldsymbol{k}} \right) \tag{2.34}$$

$$H^{'}_1 = \frac{1}{2}\sum_{ab}\sum_{\boldsymbol{kpq}} \mathcal{V}_{\boldsymbol{k}a} c^{\dagger}_{\boldsymbol{k+q}a} c^{\dagger}_{\boldsymbol{p\text{-}q}b} c_{\boldsymbol{p}b} c_{\boldsymbol{k}a} - \sum_{\boldsymbol{k}} \chi^{\mu}_{\boldsymbol{k}} \left(c^{\dagger}_{\boldsymbol{k}} \tau^{\mu} c_{\boldsymbol{k}} \right) \tag{2.35}$$

Here $\left(c^{\dagger}_{\boldsymbol{k}} \tau^{\mu} c_{\boldsymbol{k}} \right)$ is defined by $\left(c^{\dagger}_{\boldsymbol{k}} \tau^{\mu} c_{\boldsymbol{k}} \right) \equiv c^{\dagger}_{\boldsymbol{k}a} \left(\tau^{\mu} \right)_{ab} c_{\boldsymbol{k}a}$.

In this approximation, the original Coulomb potential has been replaced by the potential defined in Eq. (2.36) and assuming that each particle in the e-h system moves in a single-particle potential that comes from its average interaction with all of the other particles. To employ the mean-field approximation in the calculation, we need to determine the mean-field $\chi_{\boldsymbol{k}}^{\mu}$ by solving the BCS-like gap equation that is obtained by a variational method. For this purpose, in the following section I will introduce Bogoliubov transformation, which is often accompanied with the mean field theory.

2.3 Bogoliubov transformation

The present study aims at investigating the exciton Mott transition in a bulk semiconductor for various e-h pair densities. To simultaneously incorporate the particle density which becomes relevant in high density states and the interband polarization which plays an essential role in low density states, I employ the BCS-like pairing theory. The solutions of BCS theory in a homogeneous system are found using a Bogoliubov transformation. In theoretical physics, the Bogoliubov transformation is a unitary transformation often used to diagonalize Hamiltonians, which yields the steady-state solutions of the corresponding Schrodinger equation. In this approach, I introduce the Bogoliubov transformation

$$\begin{aligned} c_{\boldsymbol{k}} &= u_{\boldsymbol{k}}\alpha_{\boldsymbol{k}} + v_{\boldsymbol{k}}\beta_{-\boldsymbol{k}}^{\dagger}, \\ d_{-\boldsymbol{k}} &= u_{\boldsymbol{k}}\beta_{-\boldsymbol{k}} - v_{\boldsymbol{k}}\alpha_{\boldsymbol{k}}^{\dagger} \end{aligned} \tag{2.36}$$

where $\alpha_{\boldsymbol{k}}$ and $\beta_{-\boldsymbol{k}}$ are the annihilation operators of Bogoliubov quasiparticles, $u_{\boldsymbol{k}}$ and $v_{\boldsymbol{k}}$ are Bogoliubov parameters.

Bogoliubov transformation is generated by the operator $U = U_3U_2$, where U_j is defined by

$$U_j = exp\left[i\sum_{\boldsymbol{k}}\theta_{\boldsymbol{k}}^{j}\left(c_{\boldsymbol{k}}^{\dagger}\tau^{j}c_{\boldsymbol{k}}\right)\right], j = 2, 3 \tag{2.37}$$

where $c_{\boldsymbol{k}a}$ the annihilation operator of fermions in the band $a(a = 1, 2)$. The Bogoliubov

parameters $u_{\boldsymbol{k}}$ and $v_{\boldsymbol{k}}$ are subject to the condition $u_{\boldsymbol{k}}^2 + v_{\boldsymbol{k}}^2 = 1$ to ensure the unitary condition. In the present study, the Bogoliubov parameters $u_{\boldsymbol{k}}$ and $v_{\boldsymbol{k}}$ are determined based on the BCS-like mean-field theory by choosing the real parameter $\theta_{\boldsymbol{k}}^j$ diagonalize Hamiltonian $H_0^{'}$. The parameters $\theta_{\boldsymbol{k}}^j$ are chosen to be satisfied

$$\begin{aligned} cos\left(2\theta_{\boldsymbol{k}}^3\right) &= \frac{\chi_{\boldsymbol{k}}^1}{\sqrt{\left(\chi_{\boldsymbol{k}}^1\right)^2 + \left(\chi_{\boldsymbol{k}}^2\right)^2}} \\ &= \frac{\chi_{\boldsymbol{k}}^1}{E_{\boldsymbol{k}}^{'}} \\ sin\left(2\theta_{\boldsymbol{k}}^3\right) &= -\frac{\chi_{\boldsymbol{k}}^2}{\sqrt{\left(\chi_{\boldsymbol{k}}^1\right)^2 + \left(\chi_{\boldsymbol{k}}^2\right)^2}} \\ &= -\frac{\chi_{\boldsymbol{k}}^2}{E_{\boldsymbol{k}}^{'}} \end{aligned} \tag{2.38}$$

and

$$\begin{aligned} cos\left(2\theta_{\boldsymbol{k}}^2\right) &= \frac{\mathcal{E}_{\boldsymbol{k}}^3 + \chi_{\boldsymbol{k}}^3}{\sqrt{\left(E_{\boldsymbol{k}}^3 + \chi_{\boldsymbol{k}}^3\right)^2 + \left(\chi_{\boldsymbol{k}}^1\right)^2 + \left(\chi_{\boldsymbol{k}}^2\right)^2}} \\ &= \frac{\mathcal{E}_{\boldsymbol{k}}^3 + \chi_{\boldsymbol{k}}^3}{E_{\boldsymbol{k}}^{''}} \\ sin\left(2\theta_{\boldsymbol{k}}^2\right) &= -\frac{\sqrt{\left(\chi_{\boldsymbol{k}}^1\right)^2 + \left(\chi_{\boldsymbol{k}}^2\right)^2}}{\sqrt{\left(E_{\boldsymbol{k}}^3 + \chi_{\boldsymbol{k}}^3\right)^2 + \left(\chi_{\boldsymbol{k}}^1\right)^2 + \left(\chi_{\boldsymbol{k}}^2\right)^2}} \\ &= -\frac{E_{\boldsymbol{k}}^{'}}{E_{\boldsymbol{k}}^{''}} \end{aligned} \tag{2.39}$$

From the calculation above we have the Bogoliubov parameters $u_{\boldsymbol{k}}$ and $v_{\boldsymbol{k}}$ expressed as

$$\begin{aligned} u_{\boldsymbol{k}}^2 - v_{\boldsymbol{k}}^2 &= \frac{\mathcal{E}_{\boldsymbol{k}}^3 + \chi_{\boldsymbol{k}}^3}{E_{\boldsymbol{k}}^{''}} \\ 2u_{\boldsymbol{k}}v_{\boldsymbol{k}} &= -\frac{|\chi_{\boldsymbol{k}}^1 + i\chi_{\boldsymbol{k}}^2|}{E_{\boldsymbol{k}}^{''}} \end{aligned} \tag{2.40}$$

where,

$$\begin{aligned} E_{\boldsymbol{k}}^{'} &= \sqrt{\left(\chi_{\boldsymbol{k}}^1\right)^2 + \left(\chi_{\boldsymbol{k}}^2\right)^2} \\ E_{\boldsymbol{k}}^{''} &= \sqrt{\left(E_{\boldsymbol{k}}^3 + \chi_{\boldsymbol{k}}^3\right)^2 + \left(\chi_{\boldsymbol{k}}^1\right)^2 + \left(\chi_{\boldsymbol{k}}^2\right)^2} \end{aligned} \tag{2.41}$$

The physical meaning of $E''_{\boldsymbol{k}}$ is a half of the excitation energy of a Bogoliubov quasi-particle pair.

For the convenience in the subsequent formulations, I introduce here the quantities as the one-particle energy of the Bogoliubov quasiparticle defined by

$$E^{(\pm)}_{\boldsymbol{k}} = \mathcal{E}^0_{\boldsymbol{k}} + \chi^0_{\boldsymbol{k}} \pm E''_{\boldsymbol{k}} \tag{2.42}$$

And using $E^{(\pm)}_{\boldsymbol{k}}$, the distribution functions of the Bogoliubov quasi-particles are defined as

$$f^{(\pm)}_{\boldsymbol{k}} = \frac{1}{\left[exp\left(E^{(\pm)}_{\boldsymbol{k}}/T\right)+1\right]} \tag{2.43}$$

and the functions

$$\begin{aligned} F^0_{\boldsymbol{k}} &\equiv F^{(+)}_{\boldsymbol{k}} = f^{(+)}_{\boldsymbol{k}} + f^{(-)}_{\boldsymbol{k}} \\ F^3_{\boldsymbol{k}} &\equiv F^{(-)}_{\boldsymbol{k}} = f^{(+)}_{\boldsymbol{k}} - f^{(-)}_{\boldsymbol{k}} \end{aligned} \tag{2.44}$$

where $F^{(-)}_{\boldsymbol{k}}$ is Pauli blocking factor.

2.4 BCS-like gap equation

Using the Bogoliubov transformation the mean-fields $\chi^{\mu}_{\boldsymbol{k}}$ are determined by the stationary condition of the functional,

$$\mathcal{F} = -T\ln\mathrm{Tr}\left(e^{-H'_0/T}\right) + \left\langle\left\langle H'_1\right\rangle\right\rangle + \lambda\sum_{\boldsymbol{k}}\left[\left\langle\left\langle\left(c^{\dagger}_{\boldsymbol{k}}\tau^0 c_{\boldsymbol{k}}\right)-1\right\rangle\right\rangle\right] \tag{2.45}$$

where $\langle\langle\cdots\rangle\rangle$ denotes the statistical average defined by the Hamiltonian $H_0^{'}$. The Lagrange multiplier λ is introduced to impose the charge neutrality condition,

$$\begin{aligned}\sum_{\boldsymbol{k}}\left[\left\langle\left\langle\left(c_{\boldsymbol{k}}^{\dagger}\tau^{0}c_{\boldsymbol{k}}\right)-1\right\rangle\right\rangle\right] &= \sum_{\boldsymbol{k}}\left[\left\langle\left\langle\left(c_{\boldsymbol{k}1}^{\dagger}c_{\boldsymbol{k}1}-c_{\boldsymbol{k}2}^{\dagger}c_{\boldsymbol{k}2}\right)\right\rangle\right\rangle\right] \\ &= 0 \end{aligned} \tag{2.46}$$

Based on the BCS-like mean-field theory, let us calculate the expectation value of $c_{\boldsymbol{p}a}^{\dagger}c_{\boldsymbol{p}b}$ whose diagonal (off-diagonal) components correspond to the distribution (pair) function.

Applying the Bogoliubov transformation the diagonalized Hamiltonian $H_0^{'}$ becomes,

$$U^{\dagger}H_0^{'}U=\sum_{\boldsymbol{k}}\left[E_{\boldsymbol{k}}^{(+)}c_{\boldsymbol{k}1}^{\dagger}c_{\boldsymbol{k}1}+E_{\boldsymbol{k}}^{(-)}c_{\boldsymbol{k}2}^{\dagger}c_{\boldsymbol{k}2}\right] \tag{2.47}$$

And the quantum statistical average of $H_1^{'}$ yields,

$$\begin{aligned}\left\langle\left\langle H_1^{'}\right\rangle\right\rangle &= -\frac{1}{4}\sum_{\boldsymbol{kp}}\sum_{\mu=0}^{3}\mathcal{V}_{\boldsymbol{k\text{-}p}}\widetilde{F}_{\boldsymbol{k}}^{\mu}\widetilde{F}_{\boldsymbol{p}}^{\mu}-\sum_{\boldsymbol{kp}}\sum_{\mu=0}^{3}\chi_{\boldsymbol{k}}^{\mu}\widetilde{F}_{\boldsymbol{k}}^{\mu} \\ &= -\frac{1}{4}\sum_{\boldsymbol{kp}}\sum_{j=1}^{3}\mathcal{V}_{\boldsymbol{k\text{-}p}}F_{\boldsymbol{k}}^{3}F_{\boldsymbol{p}}^{3}\frac{\left(\mathcal{E}_{\boldsymbol{k}}^{j}+\chi_{\boldsymbol{k}}^{j}\right)}{E_{\boldsymbol{k}}^{''}}\frac{\left(\mathcal{E}_{\boldsymbol{p}}^{j}+\chi_{\boldsymbol{p}}^{j}\right)}{E_{\boldsymbol{p}}^{''}}-\frac{1}{4}\sum_{\boldsymbol{kp}}\mathcal{V}_{\boldsymbol{k\text{-}p}}F_{\boldsymbol{k}}^{0}F_{\boldsymbol{p}}^{0} \\ &\quad -\sum_{\boldsymbol{k}}\sum_{j=1}^{3}\chi_{\boldsymbol{k}}^{j}F_{\boldsymbol{k}}^{3}\frac{\left(\mathcal{E}_{\boldsymbol{k}}^{j}+\chi_{\boldsymbol{k}}^{j}\right)}{E_{\boldsymbol{k}}^{''}}-\sum_{\boldsymbol{k}}\chi_{\boldsymbol{k}}^{0}F_{\boldsymbol{k}}^{0}\end{aligned} \tag{2.48}$$

The functional F defined in Eq. (2.46) can be calculated straightforwardly and resulted in

$$\begin{aligned}\mathcal{F} &= -T\sum_{\boldsymbol{k}}\ln\left[1+\exp\left(-\frac{E_{\boldsymbol{k}}^{(+)}}{T}\right)\right]-T\sum_{\boldsymbol{k}}\ln\left[1+\exp\left(-\frac{E_{\boldsymbol{k}}^{(-)}}{T}\right)\right] \\ &\quad -\frac{1}{4}\sum_{\boldsymbol{kp}}\sum_{j=1}^{3}\mathcal{V}_{\boldsymbol{k\text{-}p}}F_{\boldsymbol{k}}^{3}F_{\boldsymbol{p}}^{3}\frac{\left(\mathcal{E}_{\boldsymbol{k}}^{j}+\chi_{\boldsymbol{k}}^{j}\right)}{E_{\boldsymbol{k}}^{''}}\frac{\left(\mathcal{E}_{\boldsymbol{p}}^{j}+\chi_{\boldsymbol{p}}^{j}\right)}{E_{\boldsymbol{p}}^{''}}-\frac{1}{4}\sum_{\boldsymbol{kp}}\mathcal{V}_{\boldsymbol{k\text{-}p}}F_{\boldsymbol{k}}^{0}F_{\boldsymbol{p}}^{0} \\ &\quad -\sum_{\boldsymbol{k}}\sum_{j=1}^{3}\chi_{\boldsymbol{k}}^{j}F_{\boldsymbol{k}}^{3}\frac{\left(\mathcal{E}_{\boldsymbol{k}}^{j}+\chi_{\boldsymbol{k}}^{j}\right)}{E_{\boldsymbol{k}}^{''}}-\sum_{\boldsymbol{k}}\chi_{\boldsymbol{k}}^{0}F_{\boldsymbol{k}}^{0}+\lambda\sum_{\boldsymbol{k}}\left(F_{\boldsymbol{k}}^{0}-1\right)\end{aligned} \tag{2.49}$$

The stationary conditions $\delta\mathcal{F}/\delta\chi_{\boldsymbol{k}}^{\mu}=0$ $(\mu=0,1,\cdots,3)$ gives the following self-consistent

equations for the Hartree-Fock self-energies $\chi^{\mu}_{\boldsymbol{k}}$ ($\mu = 0, 1, \cdots, 3$),

$$\begin{aligned}
\chi^{0}_{\boldsymbol{k}} &= -\frac{1}{2}\sum_{\boldsymbol{p}} \mathcal{V}_{\boldsymbol{k}\text{-}\boldsymbol{p}} \left[F^{0}_{\boldsymbol{p}} - 1\right] \\
\chi^{1}_{\boldsymbol{k}} + i\chi^{2}_{\boldsymbol{k}} &= -\frac{1}{2}\sum_{\boldsymbol{p}} \mathcal{V}_{\boldsymbol{k}\text{-}\boldsymbol{p}} F^{3}_{\boldsymbol{p}} \left[\frac{\chi^{1}_{\boldsymbol{p}} + i\chi^{2}_{\boldsymbol{p}}}{E''_{\boldsymbol{p}}}\right] \\
\chi^{3}_{\boldsymbol{k}} &= -\frac{1}{2}\sum_{\boldsymbol{p}} \mathcal{V}_{\boldsymbol{k}\text{-}\boldsymbol{p}} F^{3}_{\boldsymbol{p}} \frac{\left(\mathcal{E}^{3}_{\boldsymbol{k}} + \chi^{3}_{\boldsymbol{p}}\right)}{E''_{\boldsymbol{p}}}
\end{aligned} \tag{2.50}$$

where the physical meaning of $\chi^{0}_{\boldsymbol{k}} + \chi^{3}_{\boldsymbol{k}}$ ($\chi^{0}_{\boldsymbol{k}} - \chi^{3}_{\boldsymbol{k}}$) is the Hartree-Fock self-energy of conduction (valence) band electrons, $\chi^{1}_{\boldsymbol{k}} + i\chi^{2}_{\boldsymbol{k}}$ is the order parameter of the $e-h$ BCS state. Whereas I investigate the system at $T > T_c$, where T_c is the critical temperature of the BCS-BEC crossover in $e-h$ system in semiconductors, I have self-consistently calculate $\chi^{1,2}_{k}$ in the numerical analysis.

In Eqs. (2.51-2.53), $\chi^{\mu}_{\boldsymbol{k}}$ depends on $\mu_e \pm \mu_h$ through the one-particle energy of the Bogoliubov quasiparticle defined

$$E^{(\pm)}_{\boldsymbol{k}} = \frac{1}{2}\left[\frac{\boldsymbol{k}^2}{2}\left(\frac{1}{m_e} - \frac{1}{m_h}\right) + E_g - \mu_e + \mu_h\right] \pm E''_{\boldsymbol{k}} \tag{2.51}$$

In the following analysis, it is convenience to introduce the two-component operator in Nambu presentation, the Nambu pseudo spinors, defined by

$$\phi_{\boldsymbol{k}} = \begin{pmatrix} \alpha^{\dagger}_{\boldsymbol{k}} \\ \beta_{-\boldsymbol{k}} \end{pmatrix}, \quad \phi^{\dagger}_{\boldsymbol{k}} = \begin{pmatrix} \alpha_{\boldsymbol{k}} & \beta^{\dagger}_{-\boldsymbol{k}} \end{pmatrix} \tag{2.52}$$

Introducing the coherence factors $C^{(\mu)}_{\boldsymbol{k},\boldsymbol{p}}$ ($\mu = 0, 1, \cdots, 3$) given by

$$\begin{aligned}
C^{(0)}_{\boldsymbol{k},\boldsymbol{p}} &= u_{\boldsymbol{k}} u_{\boldsymbol{p}} + v_{\boldsymbol{k}} v_{\boldsymbol{p}} \\
C^{(1)}_{\boldsymbol{k},\boldsymbol{p}} &= u_{\boldsymbol{k}} v_{\boldsymbol{p}} + v_{\boldsymbol{k}} u_{\boldsymbol{p}} \\
C^{(2)}_{\boldsymbol{k},\boldsymbol{p}} &= u_{\boldsymbol{k}} u_{\boldsymbol{p}} - v_{\boldsymbol{k}} v_{\boldsymbol{p}} \\
C^{(3)}_{\boldsymbol{k},\boldsymbol{p}} &= u_{\boldsymbol{k}} v_{\boldsymbol{p}} - v_{\boldsymbol{k}} u_{\boldsymbol{p}}
\end{aligned} \tag{2.53}$$

In order to obtain physical insight into 2.53, it is convenient to rewrite them using the

identities,

$$\begin{aligned}
\left\langle \phi_{\boldsymbol{k}}^{\dagger}\tau^{0}\phi_{\boldsymbol{k}}\right\rangle &= F_{\boldsymbol{k}}^{0} \\
\left\langle \phi_{\boldsymbol{k}}^{\dagger}\tau^{j}\phi_{\boldsymbol{k}}\right\rangle &= F_{\boldsymbol{k}}^{3}\frac{\chi_{\boldsymbol{k}}^{j}}{E_{\boldsymbol{k}}''}, \quad j=1,2 \\
\left\langle \phi_{\boldsymbol{k}}^{\dagger}\tau^{3}\phi_{\boldsymbol{k}}\right\rangle &= \left(\frac{\widetilde{E}_{\boldsymbol{k}}^{3}+\chi_{\boldsymbol{k}}^{3}}{E_{\boldsymbol{k}}''}\right)
\end{aligned} \tag{2.54}$$

Introducing wave function $\psi_{\boldsymbol{k}}$ of the relative motion of an electron-hole pair with

$$\psi_{\boldsymbol{k}}^{\dagger}=\left\langle \phi_{\boldsymbol{k}}^{\dagger}\left(\tau^{1}+i\tau^{2}\right)\phi_{\boldsymbol{k}}\right\rangle =\left(\frac{\chi_{\boldsymbol{k}}^{1}+i\chi_{\boldsymbol{k}}^{2}}{E_{\boldsymbol{k}}''}\right)F_{\boldsymbol{k}}^{3} \tag{2.55}$$

the self-consistent Eqs. (15b) and (15c) are equivalent to the following equations

$$2\left(\widetilde{E}_{\boldsymbol{k}}^{3}+\chi_{\boldsymbol{k}}^{3}\right)\psi_{\boldsymbol{k}}+\left\langle \phi_{\boldsymbol{k}}^{\dagger}\tau^{3}\phi_{\boldsymbol{k}}\right\rangle \sum_{\boldsymbol{p}}\mathcal{V}_{\boldsymbol{k}\text{-}\boldsymbol{p}}\psi_{\boldsymbol{p}}=0 \tag{2.56}$$

Considering the fact that $\left(\left\langle \phi_{\boldsymbol{k}}^{\dagger}\tau^{3}\phi_{\boldsymbol{k}}\right\rangle +1\right)/2$ is the distribution function of electron-hole pairs, Eq.(2.56) is equivalent to the Wannier equation in the limit of low carrier density. [54-56] The BCS-like pair theory can properly describe the relative motion of exciton in low-density case as well as the BCS-like state in high-density case.

Chapter 3

Transverse Dielectric Function

The aim of this thesis is to investigate the THz absorption spectra of the e-h system in optically excited semiconductors for various carrier densities. The present analysis is based on solving the equation-of-motion of the transverse dielectric function. For this purpose, the derivation of the formulation to calculate the THz absorption spectra is presented in this chapter.

In my calculation of the THz response of semiconductors, the internal intraband transitions between the excitonic eigenstates are the source for THz signals emitted. To consider these transitions, we will need to consider the intraband transverse dielectric function of the e-h system. To obtain these quantities we will need several correlation functions composed of field operators. These correlation functions can be obtained by numerically solving the equations-of-motion of current-current correlation function or Bethe-Salpeter equations (BSEs).

This chapter is organized as follows. In Sec. 3.1, I derive the transverse dielectric function based on the linear response theory. The intraband transverse dieletric function is analyzed in Sec. 3.2 and the equation-of-motion of current-current correlation function, the Bethe-Salpeter equations are obtained. In Sec. 3.3, I investigate the screening effect with employing a longitudinal dielectric function given by the static single-plasmon-pole approximation (SPPA). Finally, Sec. 3.4 is brief discussion and summary for this chapter.

3.1 Transverse Dielectric Function

In this section, I will derive the transverse dielectric function based on the linear response theory.

Start from the Maxwell's equations, the polarization density $\mathcal{P}$ yields the electric displacement field D via

$$D^{\lambda}(\boldsymbol{q},t) = E^{\lambda}(\boldsymbol{q},t) + 4\pi\mathcal{P}^{\lambda}(\boldsymbol{q},t) \tag{3.1}$$

When the polarization density changes with time, the time-dependent bound-charge density creates a polarization current density of

$$J^{\lambda}(\boldsymbol{q},t) = \frac{\partial\mathcal{P}^{\lambda}(\boldsymbol{q},t)}{\partial t} \tag{3.2}$$

The Fourier transform of the displacement field $D^{\lambda}(\boldsymbol{q},\omega)$ can be expressed in terms of the Fourier transform of the electric field $E^{\lambda}(\boldsymbol{q},\omega)$ through the transverse dielectric function $\epsilon_{\boldsymbol{q}}(\omega)$,

$$D^{\lambda}(\boldsymbol{q},\omega) = \epsilon_{\boldsymbol{q}}(\omega)E^{\lambda}(\boldsymbol{q},\omega) \tag{3.3}$$

Then the equation for the transverse dielectric function yields,

$$\left[\epsilon_{\boldsymbol{q}}(\omega) - 1\right] E^{\lambda}(\boldsymbol{q},\omega) = -\frac{4\pi}{\omega^2}\int_{-\infty}^{+\infty} dt e^{i\omega t}\frac{\partial J^{\lambda}(\boldsymbol{q},t)}{\partial t} \tag{3.4}$$

where the current operator $J^{\lambda}(\boldsymbol{q},t)$ is determined in Eq. (2.12). Regarding the radiation-matter interaction Hamiltonian $H_1(t) + H_2(t)$ (see Eqs. 2.8 and 2.9) as the perturbation, then the transverse dielectric function can be calculated using the linear response theory,

and the result is

$$\epsilon^{\lambda\lambda'}(\omega) = \delta^{\lambda\lambda'}\left[1 - \frac{4\pi e^2}{m_0\omega^2}\right]\sum_a\sum_{\boldsymbol{k}}\left\langle c^\dagger_{\boldsymbol{k}a}c_{\boldsymbol{k}b}\right\rangle + \frac{4\pi e^2}{m_0^2\omega^2}G^{\lambda\lambda'}(\omega) + \frac{4\pi e^2}{\omega^2}\mathcal{G}^{\lambda\lambda'}(\omega) \tag{3.5}$$

where $G^{\lambda\lambda'}(\omega)$ and $\mathcal{G}^{\lambda\lambda'}(\omega)$ are defined by the Fourier transform of

$$G^{\lambda\lambda'}(t) = -i\theta(t)\left\langle\left[X^\lambda_{\boldsymbol{q}}(t), X^{\lambda'}_{-\boldsymbol{q}}(0)\right]\right\rangle \tag{3.6}$$

$$\mathcal{G}^{\lambda\lambda'}(t) = -i\theta(t)\left\langle\left[j^\lambda_{\boldsymbol{q}}(t), j^{\lambda'}_{-\boldsymbol{q}}(0)\right]\right\rangle \tag{3.7}$$

where $j^\lambda_{\boldsymbol{q}}$ and $X^\lambda_{\boldsymbol{q}}$are defined in Eq. (2.11) and (2.12), respectively. Here $\langle\cdots\rangle$ stands for the quantum statistical average with the density operator

$$\rho = \frac{\exp\left[-\beta\mathcal{K}\right]}{Z} \tag{3.8}$$

where $Z \equiv \mathrm{Tr}\,\exp\left[-\beta\mathcal{K}\right]$ with $\mathcal{K} \equiv H_0 + H_{int} - \sum_{\boldsymbol{k}}\sum_a \mu_a c^\dagger_{\boldsymbol{k}a}c_{\boldsymbol{k}}$. The time development of operators is governed by the Hamiltonian $H_0 + H_{int}$. For the sake of convenience, I write in this thesis ω in place of $\omega + i\delta$ where δ is the positive infinitesimal.

Following the analysis given in Ref. [66], I investigate the zero-frequency limit of $G^{\lambda\lambda'}(\omega)/\omega^2$, and will show that this term contributes to the mass renormalization as well as the interband transitions. In contrast with Ref. [66], the independent-particle approximation is invalid in the present case because the Coulomb interaction between carriers plays an essential role in exciton systems. To circumvent this difficulty, I introduce the spectral representation of $G^{\lambda\lambda'}(\omega)$:

$$G^{\lambda\lambda'}(\omega) = \sum_{ab}\sum_{\boldsymbol{k}} p^\lambda_{ab}(\boldsymbol{k})\, p^{\lambda'}_{ab}(\boldsymbol{k}) \int_{-\infty}^{+\infty}\frac{dz}{2\pi i}\frac{B^{ab}(\boldsymbol{k}, z)}{\omega - z} \tag{3.9}$$

where $p^\lambda_{ab}(\boldsymbol{k}) \equiv (1 - \delta_{ab})\left[e^\lambda_{\boldsymbol{q}} \cdot P_{ab}(\boldsymbol{k})\right]$. Here the spectral function $B^{ab}(\boldsymbol{k}, z)$ is the Fourier transform of

$$B^{ab}(\boldsymbol{k}, t) = -i\left\langle\left[c^\dagger_{\boldsymbol{k}a}(t)c_{\boldsymbol{k}b}(t), c^\dagger_{\boldsymbol{k}b}(0)c_{\boldsymbol{k}a}(0)\right]\right\rangle \tag{3.10}$$

and the fulfills sum rule

$$\int_{-\infty}^{+\infty} \frac{dz}{2\pi i} B^{ab}(\boldsymbol{k}, z) = -\left\langle c^{\dagger}_{\boldsymbol{k}a} c_{\boldsymbol{k}a} \right\rangle + \left\langle c^{\dagger}_{\boldsymbol{k}b} c_{\boldsymbol{k}b} \right\rangle \tag{3.11}$$

and

$$\sum_{ab} \sum_{\boldsymbol{k}} p^{\lambda}_{ab}(\boldsymbol{k})\, p^{\lambda'}_{ab}(\boldsymbol{k}) \int_{-\infty}^{+\infty} \frac{dz}{2\pi i} \frac{B^{ab}(\boldsymbol{k}, z)}{z^2} = 0 \tag{3.12}$$

Equation (3.12) is shown using the time-reversal symmetry, $B^{ab}(\boldsymbol{k}, t) = -B^{ba}(-\boldsymbol{k}, -t)$ and $p^{\lambda}_{ab}(-\boldsymbol{k}) = -p^{\lambda}_{ab}(\boldsymbol{k})$. Using the spectral representation, I obtain the following expression for the transverse dielectric function

$$\begin{aligned}
\epsilon^{\lambda\lambda'}(\omega) = \delta^{\lambda\lambda'} &\left[1 - \frac{4\pi e^2}{m_0 \omega^2} \sum_a \sum_{\boldsymbol{k}} \frac{1}{m_a} \left\langle c^{\dagger}_{\boldsymbol{k}a} c_{\boldsymbol{k}b} \right\rangle \right] \\
&- \frac{4\pi e^2}{m_0^2 \omega^2} \sum_a \sum_{\boldsymbol{k}} p^{\lambda}_{ab}(\boldsymbol{k})\, p^{\lambda'}_{ba}(\boldsymbol{k}) \int_{-\infty}^{+\infty} \frac{dz}{2\pi i} \frac{B^{ab}(\boldsymbol{k}, z)}{E_{\boldsymbol{k}a} - E_{\boldsymbol{k}b}} (z + E_{\boldsymbol{k}a} - E_{\boldsymbol{k}b}) \\
&- \frac{4\pi e^2}{m_0^2 \omega} \sum_a \sum_{\boldsymbol{k}} p^{\lambda}_{ab}(\boldsymbol{k})\, p^{\lambda'}_{ba}(\boldsymbol{k}) \int_{-\infty}^{+\infty} \frac{dz}{2\pi i} \frac{B^{ab}(\boldsymbol{k}, z)}{z^2} \\
&+ \frac{4\pi e^2}{m_0^2} \sum_a \sum_{\boldsymbol{k}} p^{\lambda}_{ab}(\boldsymbol{k})\, p^{\lambda'}_{ba}(\boldsymbol{k}) \int_{-\infty}^{+\infty} \frac{dz}{2\pi i} \frac{B^{ab}(\boldsymbol{k}, z)}{z^2(\omega - z)} \\
&- \frac{4\pi e^2}{\omega^2} \mathcal{G}^{\lambda\lambda'}(\omega)
\end{aligned} \tag{3.13}$$

where the third term on the RHS vanishes because of Eq. (3.12). When deriving Eq. (3.13), I have used Eq. (3.11) and the following expression for the inverse effective mass

$$\frac{1}{m_a} = \frac{\delta^{\lambda\lambda'}}{m_0} - \sum_b \frac{p^{\lambda}_{ab}(\boldsymbol{k})\, p^{\lambda'}_{ba}(\boldsymbol{k}) + p^{\lambda'}_{ab}(\boldsymbol{k})\, p^{\lambda}_{ba}(\boldsymbol{k})}{m_0 (E_{\boldsymbol{k}a} - E_{\boldsymbol{k}b})} \tag{3.14}$$

Here I have assumed that the system is isotropic.

The first term on the RHS of Eq. (3.13) gives the Drude response. In this thesis, I have investigated the two-band model, and the annihilation operators of electrons and holes are defined by $c_{\boldsymbol{k}} \equiv c_{\boldsymbol{k}1}$ and $d_{-\boldsymbol{k})} \equiv c^{\dagger}_{\boldsymbol{k}2}$, respectively. In this case, introducing the

reduced mass m, this term is rewritten as

$$\delta^{\lambda\lambda'}\left[1-\frac{2\pi e^2}{m\omega^2}\sum_{\boldsymbol{k}}\left\langle c_{\boldsymbol{k}}^{\dagger}c_{\boldsymbol{k}}+d_{\boldsymbol{k}}^{\dagger}d_{\boldsymbol{k}}\right\rangle\right] \tag{3.15}$$

where I have used the charge neutrality condition

$$\sum_{\boldsymbol{k}}\left\langle c_{\boldsymbol{k}}^{\dagger}c_{\boldsymbol{k}}-d_{\boldsymbol{k}}^{\dagger}d_{\boldsymbol{k}}\right\rangle=0 \tag{3.16}$$

and the relationship [66]

$$\sum_{\boldsymbol{k}}\frac{1}{m_h}=-\sum_{\boldsymbol{k}}\frac{\partial^2 E_{2\boldsymbol{k}}}{\partial\boldsymbol{k}^2}=0 \tag{3.17}$$

The second term on the RHS of Eq. (3.13) also contributes to the Drude response, even though it vanishes in the absence of the Coulomb interaction between carriers because the spectral weight $B^a b(\boldsymbol{k},z)$ is proportional to $\delta(z+E_{\boldsymbol{k}a}-E_{\boldsymbol{k}b})$. In the two-band model, $p_{ab}^{\lambda}(\boldsymbol{k})$ can be eliminated using Eq. (3.14), and this term reduces to

$$\frac{2\pi e^2}{m\omega^2}\sum_{\boldsymbol{k}}\int_{-\infty}^{+\infty}\frac{dz}{2\pi i}\left(1-\frac{E_{\boldsymbol{k}1}-E_{\boldsymbol{k}2}}{z}\right)B^{12}(\boldsymbol{k},z) \tag{3.18}$$

This result indicates that this term is a correction to Eq. (3.11) and

$$\mathcal{N}_{free}\equiv\frac{1}{2}\sum_{\boldsymbol{k}}\left\langle c_{\boldsymbol{k}}^{\dagger}c_{\boldsymbol{k}}+d_{\boldsymbol{k}}^{\dagger}d_{\boldsymbol{k}}\right\rangle-\sum_{\boldsymbol{k}}\int_{-\infty}^{+\infty}\frac{dz}{4\pi i}\left(1-\frac{E_{\boldsymbol{k}1}-E_{\boldsymbol{k}2}}{z}\right)B^{12}(\boldsymbol{k},z) \tag{3.19}$$

is the density of the ionized plasma. In the present theory, I have evaluated $\mathcal{N}_{free}$ based on BCS-like pairing theory as in the case of $\mathcal{G}^{\lambda\lambda'}(\omega)$.

The forth (fifth) term arises from the interband (intraexciton) transitions. Furthermore, since $[j_{\boldsymbol{q}}^{\lambda}(t),c_{\boldsymbol{k}a}^{\dagger}c_{\boldsymbol{k}a}]=0,\mathcal{G}^{\lambda\lambda'}(\omega)$ vanishes when the total carrier density is greater than that of the exciton Mott transition.

3.2 The Bethe-Salpeter Equations

Because the main aim of this thesis is to investigate the THz absorption spectra in optically excited semiconductors; then in this study I just focus on examining the excitonic intraband transitions. From the transverse dielectric function derived in the section 3.1, we have the intraband transverse dielectric function expressed as

$$\epsilon_{\boldsymbol{q}}(\omega) = 1 - \frac{4\pi e^2}{m\omega^2}\mathcal{N}_{free} + \frac{4\pi i e^2}{\omega^2}\mathcal{G}_{\boldsymbol{q}}(\omega) \tag{3.20}$$

where $\mathcal{N}_{free}$ is the density of the ionized plasma, $m = m_1 m_2/(m_1 + m_2)$ is the reduced mass of an $e-h$ pair, and $\mathcal{G}_{\boldsymbol{q}}(\omega)$ is the Fourier transform of the retarded current-current correlation function

$$\mathcal{G}_{\boldsymbol{q}}(t) = -i\theta(t)\left\langle \left[e^{iHt} j^{\lambda}_{\boldsymbol{q}} e^{-iHt}, (j^{\lambda}_{\boldsymbol{q}})^{\dagger} \right] \right\rangle \tag{3.21}$$

where $\theta(t)$ is the step function and $\langle \cdots \rangle$ denotes the quantum statistical average given by the Hamiltonian H.

The reason why not the total $e-h$ pair density $\mathcal{N}$ but $\mathcal{N}_{free}$ appears in Eq. (3.19) is because bound $e-h$ pairs do not contribute to the electrical current. I have supposed that the incident THz field propagates in the q-direction. Furthermore, the $|\boldsymbol{q}|$ dependence of the transverse paramagnetic current operator $j^{\lambda}_{\boldsymbol{q}}$ with polarization λ is neglected because of the long wavelength of the THz field. In the following, paramagnetic current operator $j^{\lambda}_{\boldsymbol{q}}$ is approximated by

$$j^{\lambda}_{\boldsymbol{q}} \simeq -\frac{e}{V}\sum_{a}\sum_{\boldsymbol{p}} \frac{1}{m_a}\left(e^{\lambda}_{\boldsymbol{q}} \cdot \boldsymbol{p}\right) c^{\dagger}_{\boldsymbol{p}\text{-}\boldsymbol{q}a} c_{\boldsymbol{p}a} \tag{3.22}$$

Based on the BCS-like pairing theory, I consider not only the electron (hole) distribution function $f^{e}_{\boldsymbol{k}} \equiv c^{\dagger}_{\boldsymbol{k}1} c_{\boldsymbol{k}1}$ ($f^{h}_{\boldsymbol{k}} \equiv c^{\dagger}_{\boldsymbol{k}2} c_{\boldsymbol{k}2}$) but also the interband polarization $\psi_{\boldsymbol{k}} \equiv c_{\boldsymbol{k}2} c_{\boldsymbol{k}1}$ which obeys the generalized Wannier equation for finite temperatures and densities, [54,73,72]

$$\left[\frac{\boldsymbol{k}^2}{2m} + E_g - \mu - \sum_{\boldsymbol{p}} V_{\boldsymbol{k}\text{-}\boldsymbol{p}}\left(f^{e}_{\boldsymbol{p}} + f^{h}_{\boldsymbol{p}}\right)\right]\psi_{\boldsymbol{k}} - \left(1 - f^{e}_{\boldsymbol{k}} - f^{h}_{\boldsymbol{k}}\right)\sum_{\boldsymbol{p}} V_{\boldsymbol{k}\text{-}\boldsymbol{p}}\psi_{\boldsymbol{p}} = 0 \tag{3.23}$$

where $V_{\boldsymbol{q}}$ is the screened Coulomb energy with the longitudinal static dielectric function $\epsilon_{\boldsymbol{q}}$; they will be defined and discussed later in Sec. 3.3.

The current-current correlation function $\mathcal{G}_{\boldsymbol{q}}(t)$

Next, let us consider the 2×2 matrix correlation function $\mathcal{G}_{\boldsymbol{q}}(t)$ defined by Eq. (3.20). Applying Bogoliubov transformation, the current-current correlation function $\mathcal{G}_{\boldsymbol{q}}(t)$ becomes

$$\mathcal{G}_{\boldsymbol{q}}(t) = \sum_{\mu=0}^{3}\sum_{\nu=0}^{3}\sum_{\boldsymbol{k},\boldsymbol{p}} \left(k\cdot e_{\boldsymbol{q}}^{\lambda}\right)\left(\boldsymbol{p}\cdot e_{\boldsymbol{q}}^{\lambda}\right) K_{\boldsymbol{k}}^{\mu}\Pi_{\boldsymbol{k},\boldsymbol{p}}^{\mu\nu}(t)K_{\boldsymbol{p}}^{\nu} \tag{3.24}$$

where the four-component vector, $K_{\boldsymbol{k}}^{\mu}$, is expresses with respect to the electron (hole) effective mass m_e (m_h) as

$$\begin{aligned} K_{\boldsymbol{k}}^{0} &\equiv \frac{1}{m_e}-\frac{1}{m_h}; \quad K_{\boldsymbol{k}}^{1} \equiv \frac{2u_{\boldsymbol{k}}v_{\boldsymbol{k}}}{m}; \\ K_{\boldsymbol{k}}^{2} &\equiv 0; \qquad\quad K_{\boldsymbol{k}}^{3} \equiv \frac{(u_{\boldsymbol{k}}^2+v_{\boldsymbol{k}}^2)}{m} \end{aligned} \tag{3.25}$$

where $1/m = 1/m_e + 1/m_h$ is the inverse reduced mass of an $e-h$ pair.

Furthermore, the 4×4 matrix correlation function $\Pi_{\boldsymbol{k},\boldsymbol{p}}^{\mu\nu}(t)$ is

$$\Pi_{\boldsymbol{k},\boldsymbol{p}}^{\mu\nu} \equiv -i\theta(t)\left\langle\left[e^{iHt}\left(\phi_{\boldsymbol{k}}^{\dagger}\tau^{\mu}\phi_{\boldsymbol{k}}\right)e^{-iHt},\left(\phi_{\boldsymbol{p}}^{\dagger}\tau^{\nu}\phi_{\boldsymbol{p}}\right)\right]\right\rangle \tag{3.26}$$

where $\phi_{\boldsymbol{k}}$ and $\phi_{\boldsymbol{k}}^{\dagger}$ are the two-component operators in Nambu presentation, the Nambu pseudo spinors.

Obtaining a group of closed equations

In the present analysis, I evaluate $\Pi_{\boldsymbol{k},\boldsymbol{p}}^{\mu\nu}(t)$ with solving its equation-of-motion. To overcome hierarchy problem originating from the commutation relation between Coulomb

interaction Hamiltonian and $\left(\phi_{\boldsymbol{k}}^{\dagger}\tau^{\mu}\phi_{\boldsymbol{k}}\right)$, one needs to introduce some approximations to obtain a closed set of equations. Truncation has widely been used for this purpose, and, up to this time, many truncation schemes have been proposed. Whereas the perturbative expansion with respect to the radiation field [31] is the simplest approximation, it cannot be applied to investigate the spectral position in THz absorption spectra as a function of exciton density or pump-light intensity. More intricate truncation methods, such as the cluster expansions [45-47] and the dynamic truncation scheme [67] make it possible to investigate coherences up to arbitrary order. However, resulting dynamical equations are hard to deal with even with the newest computer systems. In the present theory, I use the simple time-dependent Hartree-Fock approximation (TDHFA), in which I assume that two particles propagate independently. In particular, I employ the following approximation

$$\begin{aligned}
&\left\langle\left[\phi_{\boldsymbol{k}}^{\dagger}\phi_{\boldsymbol{p}}^{\dagger}\phi_{\boldsymbol{q}}\phi_{\boldsymbol{r}},\phi_{\boldsymbol{s}}^{\dagger}\phi_{\boldsymbol{t}}\right]\right\rangle \\
&\qquad\simeq\left\langle\phi_{\boldsymbol{k}}^{\dagger}\phi_{\boldsymbol{r}}\right\rangle\left\langle\left[\phi_{\boldsymbol{p}}^{\dagger}\phi_{\boldsymbol{q}},\phi_{\boldsymbol{s}}^{\dagger}\phi_{\boldsymbol{t}}\right]\right\rangle-\left\langle\phi_{\boldsymbol{k}}^{\dagger}\phi_{\boldsymbol{q}}\right\rangle\left\langle\left[\phi_{\boldsymbol{p}}^{\dagger}\phi_{\boldsymbol{r}},\phi_{\boldsymbol{s}}^{\dagger}\phi_{\boldsymbol{t}}\right]\right\rangle \\
&\qquad\quad+\left\langle\phi_{\boldsymbol{p}}^{\dagger}\phi_{\boldsymbol{q}}\right\rangle\left\langle\left[\phi_{\boldsymbol{k}}^{\dagger}\phi_{\boldsymbol{r}},\phi_{\boldsymbol{s}}^{\dagger}\phi_{\boldsymbol{t}}\right]\right\rangle-\left\langle\phi_{\boldsymbol{p}}^{\dagger}\phi_{\boldsymbol{r}}\right\rangle\left\langle\left[\phi_{\boldsymbol{k}}^{\dagger}\phi_{\boldsymbol{q}},\phi_{\boldsymbol{s}}^{\dagger}\phi_{\boldsymbol{t}}\right]\right\rangle
\end{aligned}\tag{3.27}$$

where the operator ϕ schematically denotes the Nambu pseudo spinor, and the expectation value $\left\langle\phi^{\dagger}\phi\right\rangle$ is evaluated using the mean-field approximation. Essentially the same approximation has been used in Ref. [52] to study photoluminescence spectra as a function of carrier density at $T=0$, and the resulting density dependence of the spectral profiles qualitatively agrees with experiment particularly for the wide bandgap semiconductors such as CuCl and ZnO. Furthermore, considering the fact that TDHFA is known to be equivalent to the random phase approximation (RPA) on which the semiconductor Bloch equation (SBE) is based, and the fact that the SBE can successfully describe the optical properties of semiconductors at least qualitatively, it is worthwhile to investigate THz absorption spectra within this approximation.

Within the TDHFA, it is found that $\left(\phi_{\boldsymbol{k}}^{\dagger}\tau^{\mu}\phi_{\boldsymbol{k}}\right)$ for $\mu=0$ and 3 are constants-of-

motion:

$$\left[\left(\phi_{\boldsymbol{k}}^{\dagger}\tau^{\mu}\phi_{\boldsymbol{k}}\right), H\right] \simeq 0 \quad (\mu = 0, 3) \tag{3.28}$$

This property considerably simplifies Eq. (3.18), because

$$\Pi_{\boldsymbol{k},\boldsymbol{p}}^{0\mu}(t) = \Pi_{\boldsymbol{k},\boldsymbol{p}}^{\mu 0}(t) = \Pi_{\boldsymbol{k},\boldsymbol{p}}^{\mu\mu}(t) = 0 \tag{3.29}$$

$$\Pi_{\boldsymbol{k},\boldsymbol{p}}^{31}(t) = -\Pi_{\boldsymbol{k},\boldsymbol{p}}^{13}(t) = 2\delta_{\boldsymbol{k},\boldsymbol{p}}\theta(t)\left\langle\phi_{\boldsymbol{k}}^{\dagger}\tau^{2}\phi_{\boldsymbol{k}}\right\rangle \tag{3.30}$$

$$\Pi_{\boldsymbol{k},\boldsymbol{p}}^{23}(t) = -\Pi_{\boldsymbol{k},\boldsymbol{p}}^{32}(t) = 2\delta_{\boldsymbol{k},\boldsymbol{p}}\theta(t)\left\langle\phi_{\boldsymbol{k}}^{\dagger}\tau^{1}\phi_{\boldsymbol{k}}\right\rangle \tag{3.31}$$

where $\mu = 0, \cdots, 3$. We therefore arrive at the expression for the correlation function

$$\mathcal{G}_{\boldsymbol{q}}(t) = \sum_{\boldsymbol{k}}\left(\boldsymbol{k}\cdot e_{\boldsymbol{q}}^{\lambda}\right)u_{\boldsymbol{k}}v_{\boldsymbol{k}}\Psi_{\boldsymbol{k}}^{1}(t) \tag{3.32}$$

For convenience, I have introduced the auxiliary functions,

$$\Psi_{\boldsymbol{k}}^{\mu}(t) = 2\sum_{\boldsymbol{p}}\left(\boldsymbol{p}\cdot e_{\boldsymbol{q}}^{\lambda}\right)u_{\boldsymbol{p}}v_{\boldsymbol{p}}\Pi_{\boldsymbol{k},\boldsymbol{p}}^{\mu 1}(t) \tag{3.33}$$

with $\mu = 1, 2$. The equations-of-motion of the auxiliary functions can be obtained by TDHFA, Eq. (3.26). Here the screening effect is already considered with replacing the bare Coulomb energy $V_{\boldsymbol{q}}$ by the screened Coulomb energy $V_{\boldsymbol{q}}$, where ϵ_0 stands for the longitudinal dielectric constant of the unexcited crystal. After some straightforward algebra, the equations-of-motion turn out to be

$$\begin{aligned}
\frac{\partial\Psi_{\boldsymbol{k}}^{1}(t)}{\partial t} + 2iE_{\boldsymbol{k}}''\Psi_{\boldsymbol{k}}^{2}(t) &= -iF_{\boldsymbol{k}}^{(-)}\sum_{j=1,2}\sum_{\boldsymbol{p}}V_{\boldsymbol{k}\text{-}\boldsymbol{p}}C_{\boldsymbol{k},\boldsymbol{p}}^{2}\Psi_{\boldsymbol{p}}^{2}(t) \\
\frac{\partial\Psi_{\boldsymbol{k}}^{2}(t)}{\partial t} - 2iE_{\boldsymbol{k}}''\Psi_{\boldsymbol{k}}^{1}(t) &= -iF_{\boldsymbol{k}}^{(-)}\sum_{j=1,2}\sum_{\boldsymbol{p}}V_{\boldsymbol{k}\text{-}\boldsymbol{p}}C_{\boldsymbol{k},\boldsymbol{p}}^{1}\Psi_{\boldsymbol{p}}^{1}(t) \\
&\quad -4\theta(t)u_{\boldsymbol{k}}v_{\boldsymbol{k}}\left\langle\phi_{\boldsymbol{k}}^{\dagger}\tau^{3}\phi_{\boldsymbol{k}}\right\rangle\left(\boldsymbol{k}\cdot e_{\boldsymbol{q}}^{\lambda}\right)
\end{aligned} \tag{3.34}$$

where $2E_{\boldsymbol{k}}''$, $F_{\boldsymbol{k}}^{(-)}$, and $C_{\boldsymbol{k},\boldsymbol{p}}^{i}$ $(i = 1, 2)$ are the excitation energy of a Bogoliubov quasi-particle pair, the Pauli blocking factor, and the coherence factors, respectively.

The Fourier transform of $\Psi^j_{\boldsymbol{k}}(t)$ satisfies the following Bethe-Salpeter equations,

$$\begin{aligned} -i\omega\Psi^1_{\boldsymbol{k}}(\omega) + 2iE''_{\boldsymbol{k}}\Psi^2_{\boldsymbol{k}}(\omega) &= -iF^{(-)}_{\boldsymbol{k}} \sum_{j=1,2}\sum_{\boldsymbol{p}} V_{\boldsymbol{k}\text{-}\boldsymbol{p}} C^2_{\boldsymbol{k},\boldsymbol{p}} \Psi^2_{\boldsymbol{p}}(\omega) \\ i\omega\Psi^2_{\boldsymbol{k}}(\omega) + 2iE''_{\boldsymbol{k}}\Psi^1_{\boldsymbol{k}}(\omega) &= -iF^{(-)}_{\boldsymbol{k}} \sum_{j=1,2}\sum_{\boldsymbol{p}} V_{\boldsymbol{k}\text{-}\boldsymbol{p}} C^1_{\boldsymbol{k},\boldsymbol{p}} \Psi^1_{\boldsymbol{p}}(\omega) \\ &\quad + 4u_{\boldsymbol{k}} v_{\boldsymbol{k}} \left\langle \phi^\dagger_{\boldsymbol{k}} \tau^3 \phi_{\boldsymbol{k}} \right\rangle \left(\boldsymbol{k} \cdot e^\lambda_{\boldsymbol{q}} \right) \end{aligned} \tag{3.35}$$

If we appropriately choose the gauge, we can set $\chi^2_{\boldsymbol{k}} = 0$. With this choice, the coherence factors $C^i_{\boldsymbol{k},\boldsymbol{p}} (i = 1, 2)$ in Eq. (3.34) are expressed as

$$\begin{aligned} C^1_{\boldsymbol{k},\boldsymbol{p}} &= \mathrm{sgn}(\chi^1_{\boldsymbol{k}})\mathrm{sgn}(\chi^1_{\boldsymbol{p}}) \left(\frac{\mathcal{E}_k + \chi^3_{\boldsymbol{k}}}{E_{\boldsymbol{k}}} \right) \left(\frac{\mathcal{E}_{\boldsymbol{p}} + \chi^3_{\boldsymbol{p}}}{E_{\boldsymbol{p}}} \right) + \left(\frac{\chi^3_{\boldsymbol{k}}}{E_{\boldsymbol{k}}} \right) \left(\frac{\chi^3_{\boldsymbol{p}}}{E_{\boldsymbol{p}}} \right) \\ C^2_{\boldsymbol{k},\boldsymbol{p}} &= \mathrm{sgn}\left(\chi^1_{\boldsymbol{k}} \right) \mathrm{sgn}\left(\chi^1_{\boldsymbol{p}} \right) \end{aligned} \tag{3.36}$$

where $\mathrm{sgn}(x) \equiv x/|x|$ is the sign function.

3.3 Screening Effect

In a semiconductor where a finite density of electrons (holes) has been excited in the conduction (valence) band, one of the most important effects of the many-body interactions among the excited carriers is that they screen the Coulomb interaction among the carriers in the same band as well as between the electrons and holes in different bands. Here the plasma screening effect refers to the reduction of the range of the Coulomb potential of a charge in the presence of other charges.

To discuss plasma screening, the unscreened Coulomb potential $\mathcal{V}_{\boldsymbol{q}}$ in the Hamiltonian is replaced by the effective potential $V_{eff}(q)$, which is considered the effect of the presence of the other charges in the plasma. The redistribution of electrons may be expressed as the effect of decreasing (screening) the effective potential energy of the charge.

And I find the effective of screened potential $V_s(q,\omega)$ as,

$$V_{eff}(\boldsymbol{q}) \equiv V_s(\boldsymbol{q},\omega) = \frac{\mathcal{V}_{\boldsymbol{q}}}{\epsilon(\boldsymbol{q},\omega)} \tag{3.37}$$

The dynamic dielectric function $\epsilon(\boldsymbol{q},\omega)$ is given by the Lindhard (or RPA) formula for the longitudinal dielectric function,

$$\epsilon(\boldsymbol{q},\omega) = 1 - \mathcal{V}_{\boldsymbol{q}} \sum_{\boldsymbol{k}} \frac{f_{\boldsymbol{k}\text{-}\boldsymbol{q}} - f_{\boldsymbol{k}}}{\hbar\left(\omega + i\delta + \epsilon_{\boldsymbol{k}\text{-}\boldsymbol{q}} - \epsilon_{\boldsymbol{k}}\right)} \tag{3.38}$$

where $f_{\boldsymbol{k}}$ is the Fermi-Dirac distribution function. In the static limit, the statistically screened potential is expressed as,

$$V_s(\boldsymbol{q},\omega) = \frac{\mathcal{V}_{\boldsymbol{q}}}{\epsilon(\boldsymbol{q},0)} = \frac{4\pi e^2}{\epsilon_0 V} \frac{1}{\boldsymbol{q}^2 + \kappa^2} \tag{3.39}$$

where κ is the inverse screening length or the screening wave number with two limiting cases of i) Thomas-Fermi screening wavenumber k_{TF} and ii) Debye-Hückel screening wavenumber k_{DH}.

In this analysis, I consider the screening effect in the static long wavelength limit with the static Single-Plasmon Pole Approximation (SPPA), [68-72] in which the inverse static longitudinal dielectric function is approximated by

$$\frac{1}{\epsilon_{\boldsymbol{q}}} \simeq \frac{1}{\epsilon_0}\left(1 - \frac{\omega_{\rm pl}^2}{\Omega_{\boldsymbol{q}}^2}\right) \tag{3.40}$$

Here $\omega_{\rm pl} \equiv [4\pi e^2 \mathcal{N}_{free}/(\epsilon_0 m)]^{1/2}$ is the plasma frequency. As long as we know, there are several versions of SPPA depending on the way to approximate the dispersion of the effective plasmon mode, $\Omega_{\boldsymbol{q}}$. Among them, I employ the version due to Zimmermann, [71] because it has no fit parameters, in which $\Omega_{\boldsymbol{q}}$ is approximated by

$$\Omega_{\boldsymbol{q}}^2 = \omega_{\rm pl}^2\left(1 + \frac{\boldsymbol{q}^2}{k_{\rm TF}^2}\right) + \left(\frac{\boldsymbol{q}^2}{4m}\right)^2 + G_{eff}^2 \tag{3.41}$$

Here $k_{TF} = \{16me^2/\pi\epsilon_0\}\,(6\pi\mathcal{N}_{free}^2)^{1/3})$ is the Thomas-Fermi wavenumber, and G_{eff} is

the effective gap defined by the lowest excitation energy of a Bogoliubov quasi-particle pair,

$$G_{eff} \equiv 2\min_{k} E_k \tag{3.42}$$

The effective gap is the self-consistently determined in the numerical computation.

The second term on the right-hand side of Eq. (3.34) approximately considers the contribution of the e-h pair continuum. The non-metallic screening of the exciton gases is taken into account with introducing the effective gap G_{eff}, which is in contrast with the original SPPA introduced by Lundqvist. [68,69] Furthermore, one of the most distinctive advantages of the Zimmermann's version is that there are no fitting parameters. Owing to the effective gap, the long wavelength limit of the static polarizability becomes finite in low-density states. As shown in Sec. 3.1, we cannot explain the density dependence of the transition energy from $1s$ to $2pp$ exciton states in three-dimensional systems without the effective gap. On the other hand, in high-density states where the effective gap vanishes, the static polarizability diverges in the long wavelength limit, and this behavior simulates the $e-h$ plasmas.

The screened Coulomb potential

Taking into account the screening effect with the SPPA introduced above, the unscreened Coulomb potential $\mathcal{V}_{\boldsymbol{q}}$ defined in Eq. (2.17) is replaced by screened Coulomb potential $V_{\boldsymbol{q}}$ expressed as

$$V_{\boldsymbol{q}} \equiv \frac{4\pi e^2}{\epsilon_{\boldsymbol{q}} \boldsymbol{q}^2 V} \tag{3.43}$$

with the longitudinal static dielectric function $\epsilon_{\boldsymbol{q}}$ is defined in Eq. (3.33).

BCS-like gap equations

In the BCS-like gap equation, I incorporate the screening effect with SPPA by replacing the unscreened Coulomb potential $\mathcal{V}_{\boldsymbol{q}}$ by the screened Coulomb potential $V_{\boldsymbol{q}}$. The self-consistent equations for $\chi^{\mu}_{\boldsymbol{k}}$ are then written as,

$$\chi^{0}_{\boldsymbol{k}} = -\frac{1}{2}\sum_{\boldsymbol{p}} V_{\boldsymbol{k}\text{-}\boldsymbol{p}}\left[F^{(+)}_{\boldsymbol{p}} - 1\right] \tag{3.44}$$

$$\chi^{1}_{\boldsymbol{k}} + i\chi^{2}_{\boldsymbol{k}} = -\frac{1}{2}\sum_{\boldsymbol{p}} V_{\boldsymbol{k}\text{-}\boldsymbol{p}} F^{(-)}_{\boldsymbol{p}}\left[\frac{\chi^{1}_{\boldsymbol{p}} + i\chi^{2}_{\boldsymbol{p}}}{E''_{\boldsymbol{p}}}\right] \tag{3.45}$$

$$\chi^{3}_{\boldsymbol{k}} = -\frac{1}{2}\sum_{\boldsymbol{p}} V_{\boldsymbol{k}\text{-}\boldsymbol{p}} F^{(-)}_{\boldsymbol{p}}\left[1 + \frac{\widetilde{E}^{3}_{\boldsymbol{p}} + \chi^{3}_{\boldsymbol{p}}}{E''_{\boldsymbol{p}}}\right] + \frac{1}{4}\sum_{\boldsymbol{p}}\left[V_{\boldsymbol{p}} - \mathcal{V}_{\boldsymbol{p}}\right] \tag{3.46}$$

The second-term on the right-hand side of Eq. (3.39) represents the Coulomb-hole self-energy.

The Coulomb-hole is the situation the equally charged fermions repulse each other because of the Coulomb repulsive interaction. The Coulomb-hole self-energy results in the bandgap reduction or bandgap renomalization. This effect plays an important role in several optical phenomena in high-density $e-h$ systems in semiconductors. In the present analysis, when I numerically solve Eqs. (3.37)-(3.39), the chemical potential of electrons μ_e (holes μ_h), is tuned to control the electron (hole) density. Since my interest is the charge-neutral systems, $\mu_e - \mu_h$ is self-consistently determined to obey charge neutrality, while $\mu_e + \mu_h$ is tuned to control the e-h pair density $\mathcal{N}$.

3.4 Discussion and Summary of Chapter 3

The equation-of-motion method based on BCS-like pair theory with TDHFA getting a closed set of BSE has been developed in this work. These formulae can be proper for description of the relative motion of exciton in low-density case as well as the BCS-like state in high carrier density. The many-body effects, screening and state-filling effects, are taken into account. This approach calculates the current-current correlation

function based on the linear response theory that provides an accessible way to study THz intraexcitonic transition with reasonable numerical computations.

Based on the equation-of-motion of dielectric function and the set of equations derived we have developed a numerical computation programs to numerically solve and calculate THz absorption. The numerical results will be presented and discussed in the next section.

Chapter 4

Numerical Analysis with Mean-Field Approximation

The THz absorption spectra for various e-h pair densities of a two-band e-h system in bulk semiconductor are examined in this chapter to investigate the exciton Mott transition. I present numerical results that are obtained using the BSEs developed in Chapter 3. The main results include the THz conductivity spectra for various carrier densities (Sec. 4.2), and the ionization ratio and quasi-chemical potential (Sec. 4.3). One important feature observed in the THz absorption spectra is that the $1s-2p$ transition energy stays nearly unchanged in low density regime.

In this thesis, to theoretically investigate the exciton Mott transition (the density ionization) I study the exciton Mott transition based on the THz absorption spectra that constitutes a fundamentally different approach from the visible or near-infrared absorption. Furthermore, I also study the density dependences of the ionization ratio and the quasi-chemical potential of the $e-h$ pairs.

This chapter is organized as follows. Firstly, I show the results obtained from the equations-of-motion of the current-current correlation functions BSEs, the THz conductivity spectra for various $e-h$ pair densities in Sec. 4.2. The density dependence of the THz absorption spectra is examined to investigate the exciton Mott transition. I

then move to discuss the density dependence of the ionization ratio and the $e-h$ quasi-chemical potential of the $e-h$ pairs in Sec. 4.3. To summarize the results of our numerical analysis, I show the THz spectra with Drude component in the Sec. 4.4. Finally in Sec. 4.5, I present a brief summary for this chapter.

4.1 Parameters in numerical analysis

I investigate in the present work the two-band model of a direct bandgap semiconductor in quasi-equilibrium state and normalize all the formulae using the Bohr radius a_0 and the Rydberg energy E_0 of bulk exciton. Material parameters such as the effective masses and the static dielectric constants of the unexcited materials are taken into account through these quantities. In calculating THz absorption for direct bandgap semiconductors I have used 4 material parameters: effective masses of electron (m_e) and hole (m_h), exciton Bohr radius (a_0), and exciton Rydberg energy (E_0). By changing these parameters, I obtain the THz absorption spectra for various semiconductor materials. In the numerical analysis, to calculate the exciton density I have used the exciton Bohr radius a_0 for 1s paraexcitons of yellow series in Cu_2O, while the present analysis does not restrict to Cu_2O. The material parameters of Cu_2O used in the numerical analysis are shown in the Tab. 4.1.

In the numerical analysis I have chosen the semiconductor cuprous dioxide (Cu_2O). [74] Cu_2O has a direct bandgap. The lowest conduction band and highest valence band are formed out of Cu 4s and 3d orbitals, respectively. The yellow excitonic series results from the transition between these two bands. To calculate the exciton density, I have used the exciton Bohr radius a_0 for 1s paraexcitons of yellow series in Cu_2O, while the present analysis does not restrict to Cu_2O. The 1s paraexciton has the extraordinary long lifetime ($\approx$ 1ms) originating from the parity-forbidden band structure and the pure spin singlet nature. The other parameters of Cu_2O used in the numerical calculation are shown in the Tab. 4.1.

Since the present analysis is based on the BCS-like pairing theory, we can investigate

Table 4.1: Parameter of Cu_2O used in the numerical analysis.

Parameter	Cu_2O
m_e	0.99 m_0
m_h	0.58 m_0
a_0	0.74 nm
E_0	172 meV

Here m_0 is free electron mass.

the THz absorption in macroscopic quantum states of semiconductors, i.e., the Bose-Einstein condensate of excitons in low-density state and excitonic phase and high-density state. However, the present study focuses on the case where the carrier temperature is T is set to 0.077 E_0, which is sufficiently higher than the transition temperature T_c and satisfying $E_0 > T > T_c$, where T_c is the critical temperature of the macroscopic quantum state of the $e-h$ system, i.e., the exciton Bose-Einstein condensation (BEC) in low density states and the $e-h$ BCS state at high density states. In Cu_2O, this temperature T corresponds to 130 K.

4.2 Spectral Approach

This section is devoted to theoretically analyze the exciton Mott transition based on the spectral approach. I numerically solve the equation-of-motion for the current-current correlation function BSEs and calculate THz absorption spectra for various densities. Figure 4.1 shows the calculated conductivity spectra,

$$\Delta\sigma(\omega) = -\frac{1}{\omega}\mathrm{Im}\left[\mathcal{G}_q(\omega + i\delta)\right]_{q=0} \tag{4.1}$$

for various total $e-h$ pair densities N. For convenience, I only investigate spectral components originating from the intraexciton transition; the Drude component which arises from the second term on the RHS of Eq. (3.26) has been subtracted. I have phenomenologically introduced the finite line width δ, and it is set to 0.005, which is

sufficiently small to resolve the higher-order intraexciton transitions.

Concentrating on the low-density case, I show in Fig. 4.1 (a) the THz conductivity spectrum in low-density state. The sharp peaked structures at energy $\omega \simeq 0.75$, 0.89, 0.96, 0.98 $\cdots$ associated with the broad absorption band at $\omega \gtrsim 1$ in the spectrum ($\mathcal{N} \simeq 2.0 \times 10^{16}$ cm^{-3}) are obtained. The spectral components are readily identified from their spectral positions,

$$\omega = E_0 \left(1 - \frac{1}{n^2}\right), \quad n = 2, 3, \cdots \infty \tag{4.2}$$

The sharp peaked structures originate from the THz absorption accompanied by the intraexciton transition from $1s$ to np (n = 2, 3, 4$\cdots$) states; the broad absorption band stems from the intraexciton transition from $1s$ to ionization continuum. The spectral components originating from $1s$ to $3p$, $4p$, and $5p$ states have experimentally been observed in Cu_2O [75] (see Fig. 4.1 (b)). Since the low-frequency conductivity is vanishingly small, the system is insulating.

The THz conductivity spectra without Drude component for various carrier densities are presented in Fig. 4.2. As shown in this figure, the sharp peaked structures originate from intraexcitonic transitions from $1s$ to np (n = 2, 3, $\cdots$) states. At low-density regime, the transition from $1s - 2p$ is almost unchanged while the transition energy from $1s$ to higher energy states ($3p$, $4p$, $\cdots$) and to continuum state increase with increasing carrier density. In the high-density regime, with increasing carrier density N the spectral components shifts towards lower energy. The sharp peaked structures due to the transitions from $1s$ to $4p$, and then to $3p$, and $2p$ states sequentially disappear when $e - h$ pair density increases. Above the critical density, the peaked structures originating from intraexcitonic transition disappear from the spectrum. In the spectral approach analysis, we define the exciton Mott transition as the disappearance of excitonic structures in the absorption spectra and the critical density at which all of excitonic structures disappear regarded as the exciton Mott density.

For further discussion, I now investigate spectral position of the $1s-2p$ transition line

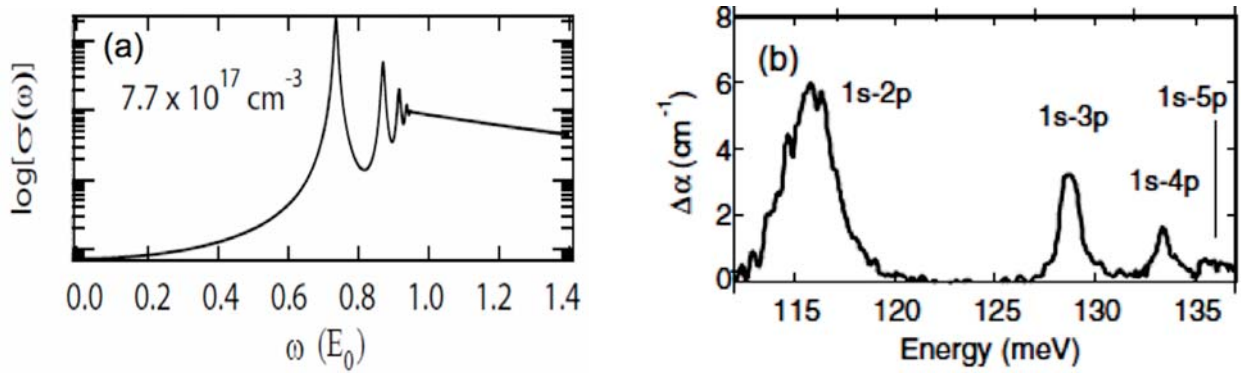

Figure 4.1: (a) Calculated THz conductivity spectrum at low-density state, where E_0 is exciton binding energy. (b) Induced THz absorption spectra of $1s$ exciton in Cu_2O from Ref. [75]

as a function of the total $e-h$ pair density $\mathcal{N}$. Recently, it is reported that the spectral position is almost independent of $\mathcal{N}$ in bulk Si [38, 64] (the open green triangle line in Fig. 4.3.(b)). This behavior is interesting because the screening effect predominates and the exciton binding energy is expected to reduce with increasing $\mathcal{N}$. In contrast with three dimensional case, energy dependence of the peak energy of the $1s-2p$ transition line is much complicated in quasi-two dimensional excitons; the spectral position of the $1s-2p$ transition line shifts towards longer wavelength with increasing $\mathcal{N}$ in GaAs/(AlGa)As QWs, [36,67] while it stays nearly unchanged in (InGa)As/GaAs QWs. [67]

I show in Fig. 4.3 (a) the calculated density dependence of the transition energy from the $1s$ to $2p$ states that, the black triangle line, corresponds to the spectral position of the $1s-2p$ line in Fig. 4.2. It is clearly found that the $1s-2p$ transition energy is almost independent of density for $\mathcal{N} \lesssim 2.0\times10^{19}$ cm^{-3}. Recently, the intraexciton $1s-2p$ transition energy has theoretically been studied in Refs. [49,50] based on the excitonic picture where the quasi-Boson operator corresponding to excitons is introduced by Usui transformation. In which the red shift of $1s-2p$ transition energy (the red dashed line in Fig. 4.3 (c)) has been shown. It shows that my theory is in good agreement with the experiments. This behavior arises because the density of ionized plasma $\mathcal{N}_{free}$, which considerably contributes to the screening effect, is almost independent of $\mathcal{N}$ as shown in Fig. 4.8; the $\mathcal{N}$ dependence of $\mathcal{N}_{free}$ and of the ionization ratio will be discussed in detail

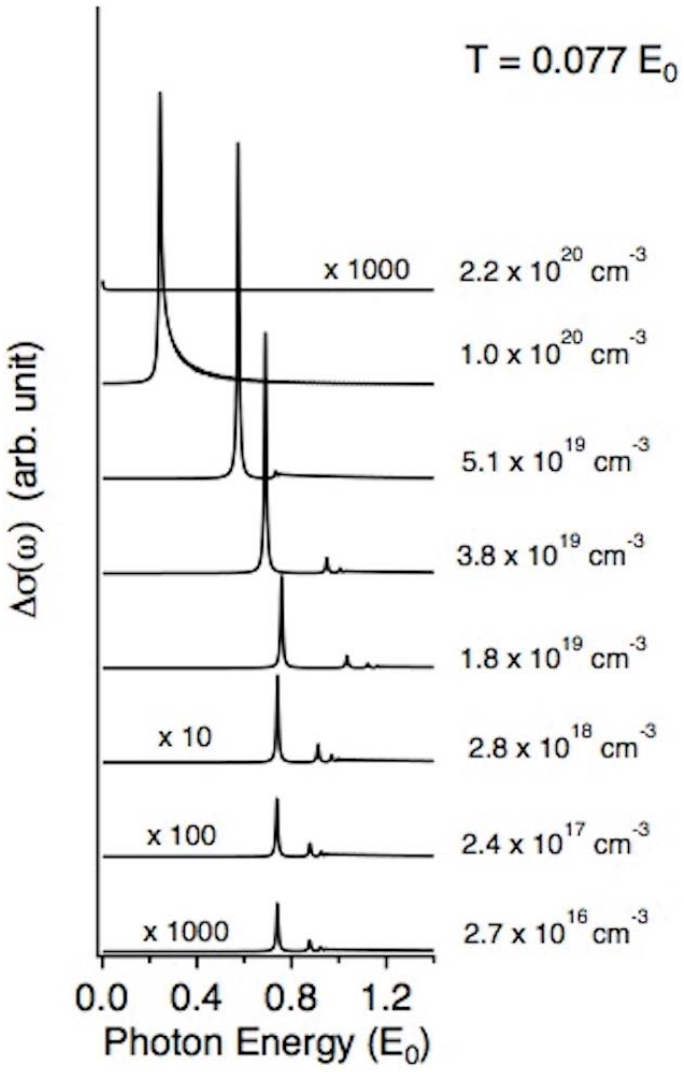

Figure 4.2: Conductivity spectra for various $e-h$ pair densities at $T = 0.077\ E_0$. Above $\mathcal{N} \simeq 1.8 \times 10^{20}$ cm^{-3} the exciton Mott transition occurs and $\Delta\delta(\omega)$ vanishes.

later in Sec. 4.3. Furthermore, I should remark that this phenomenon closely related to the long wavelength behavior of the static polarizability, which is finite in this density regime. In fact, I find that the transition energy depends on $\mathcal{N}$ if the third term on the RHS of Eq. (3.34) is neglected.

I also show in Fig. 4.4 the density dependences of the Fermi momentum and the Coulomb-hole self-energy (Debye shift). The Debye shift is defined by the deviation between the bare and screened Coulomb energies as

$$\mathcal{D} \equiv \frac{1}{2}\sum_{p} [\mathcal{V}_p - V_p] \tag{4.3}$$

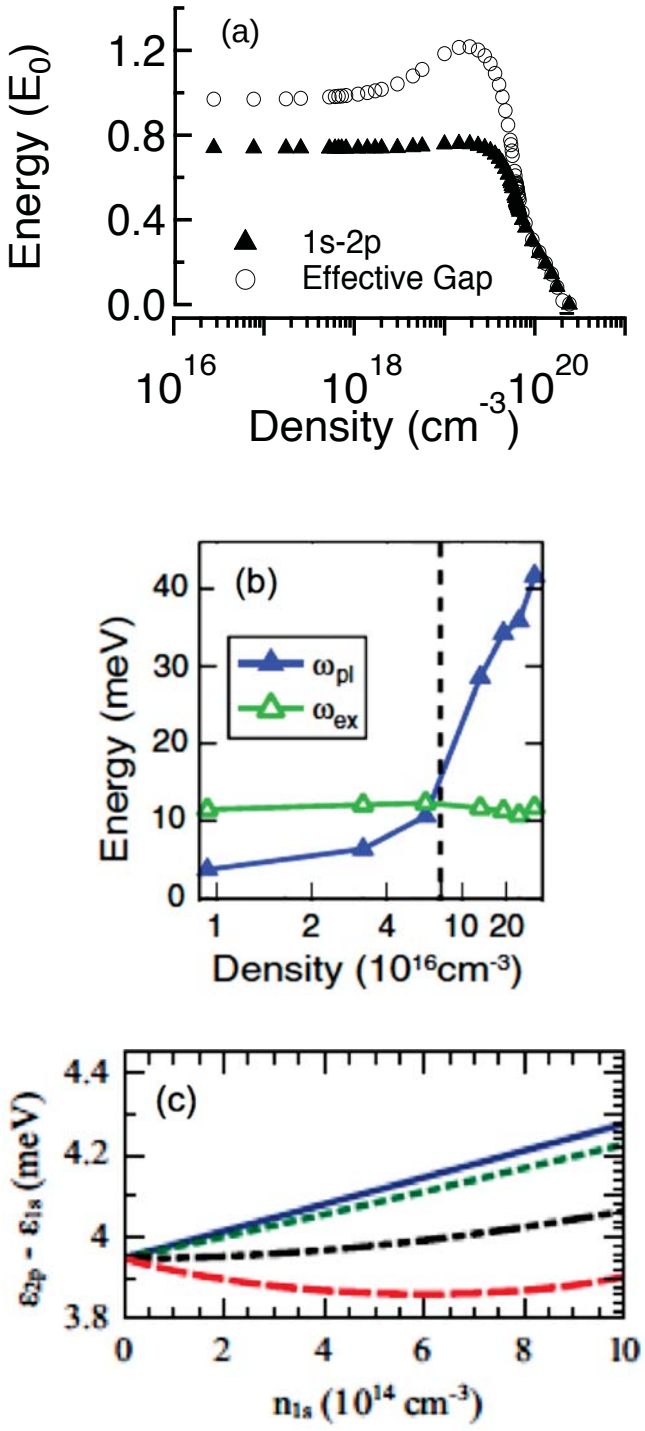

Figure 4.3: (a) Density dependences of the Coulomb-hole self-energy (Debye shift) (black triangle line) and Fermi momentum (open circle line). The temperature T is set to $0.077E_0$. To incorporate the screening effect, I have employed the SPPA where both the effective gap and the $e-h$ pair continuum are considered. (b) The green open triangle line is density dependence of $1s-2p$ transition energy in THz experiment for Si from Ref. [38]. (c) The red shift of $1s-2p$ transition energy (the red dashed line) in calculation from Ref. [50].

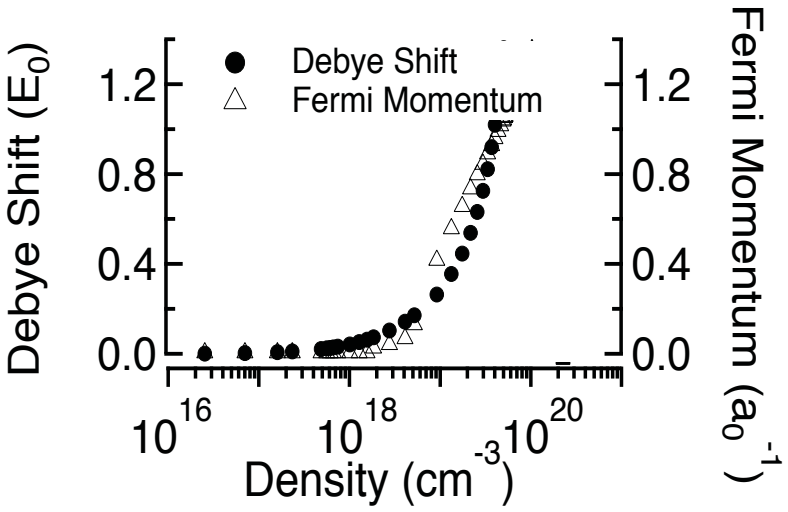

Figure 4.4: Density dependences of the $1s-2p$ transition energy (black triangle line) and the effective gap (open circle line). The carrier temperature T is set to $0.077E_0$. To incorporate the screening effect, I have employed the SPPA where both the effective gap and the $e-h$ pair continuum are considered.

where $\mathcal{V}_p$ (V_p) is the bare (screened) Coulomb energy. Because of their definitions, it is reasonable that the Fermi momentum is regarded as a measure of the state-filling effect, while the Coulomb-hole self-energy is a measure of the screening effect. I should remark that, even though the $1s-2p$ transition energy stays 0.75, which is the $1s-2p$ transition energy at the low density limit, neither the screening effect nor the state-filling effect cannot be neglected for $\mathcal{N} \gtrsim 1.0\times10^{18}$ cm^{-3}, because both the Coulomb-hole self-energy and the Fermi momentum are nonvanishing.

In contrast with $1s-2p$ transition energy, I find in Fig. 4.1 that the transition energies from 1s to 3p and to higher energy states increase with increasing density up to $\mathcal{N} \lesssim 2.0\times10^{19}$ cm^{-3}. The same behavior is found in Fig. 4.3(a), in which I show the density dependence of the effective gap that corresponds to the least transition energy from 1s to the ionization continuum. I think that this behavior originates from the state-filling effect which plays an essential role for $\mathcal{N} \gtrsim 2.0\times10^{18}$ cm^{-3}. To support this interpretation, I have also calculated the density dependences of the effective gap, the Fermi momentum and the Coulomb-hole self-energy, in which I neglect the second term on the right-hand side of Eq. (3.34). As shown in Fig. 4.5, the same behavior is found in transition energy from 1s to ionization continuum for $2.0\times10^{18} \lesssim \mathcal{N} \lesssim 2.0\times10^{19}$

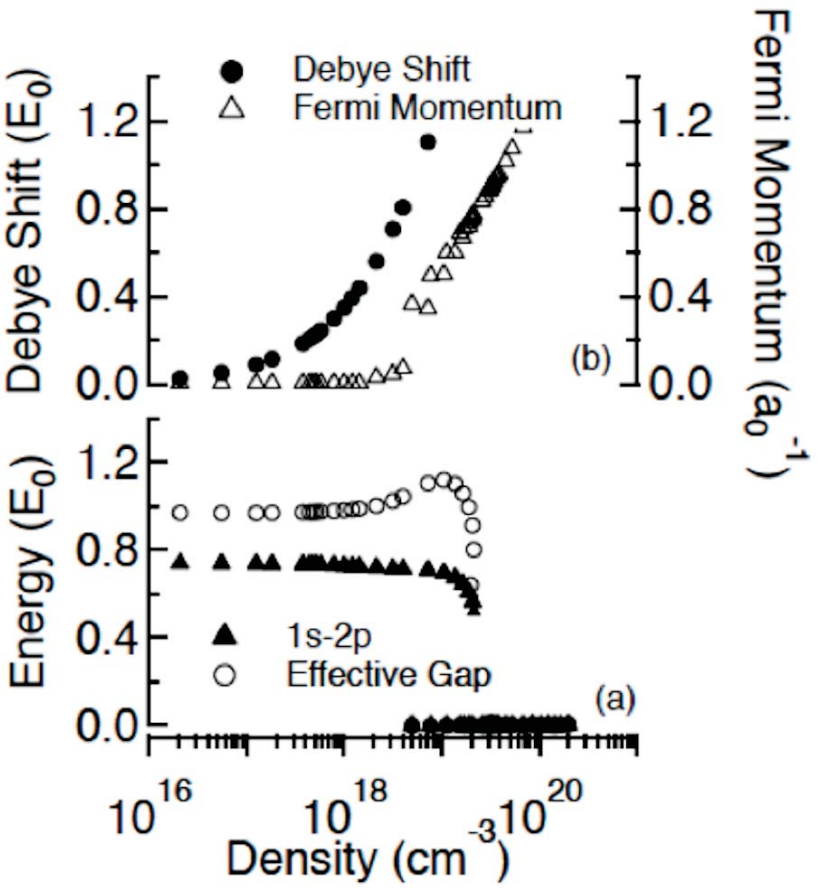

Figure 4.5: (a) Density dependences of the $1s-2p$ transition energy and the effective gap. (b) Density dependences of Coulomb-hole self-energy (Debye shift) and Fermi momentum. The temperature T is set to $0.077E_0$. To incorporate the screening effect, I have employed the SPPA where the effective gap is considered but the $e-h$ pair continuum is neglected. Since I have considered the effective gap, the $1s-2p$ transition energy is almost independent of density, as expected. I find a bistability behavior in $4.0\times10^{18} \lesssim \mathcal{N} \lesssim 2.0\times10^{19}$ cm^{-3} originating from the instability, $\partial\mu/\partial n \leq 0$, where μ is the quasi-chemical potential.

cm^{-3}, while the density above which the state-filling (screening) effect predominates is about 2.0×10^{18} (2.0×10^{16}) cm^{-3}. Considering the fact that the density above which this behavior becomes distinctive is about 2.0×10^{18} cm^{-3}, it stems from the state-filling effect.

I next analyze the conductivity spectra in high-density states ($\mathcal{N} \gtrsim 4.0\times10^{18}$ cm^{-3}). As shown in Fig. 4.2, all the spectral components shifts towards lower energy with increasing $\mathcal{N}$, because the screening effect predominates in this density regime. To support this interpretation, I find that in the Coulomb-hole self-energy becomes nonnegligible in this density regime in Fig. 4.4, and that the density of ionized excitons $\mathcal{N}_{free}$ that

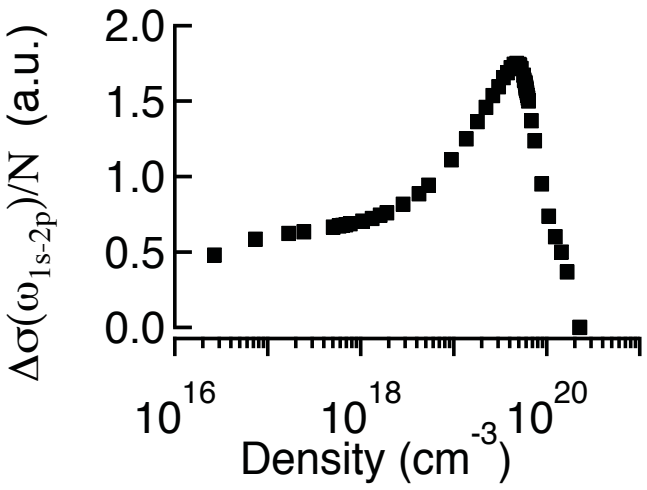

Figure 4.6: Density dependences of the absorption strength of the main absorption peak which corresponds to $1s-2p$ line in low density states. The temperature T is set to $0.077E_0$. To incorporate the screening effect, I have employed the SPPA where both the effective gap and the $e-h$ pair continuum are considered.

significantly contribute the screening abruptly increases with increasing $\mathcal{N}$ as shown in Fig. 4.7. The sharp peaked structures due to the transitions from $1s$ to $4p$, $3p$, and $2p$ states sequentially disappear, and the absorption strength of the main peaked structure decreases exponentially as shown in Fig. 4.6. Furthermore, I find a van der Waals loop for $4.0\times10^{19} \lesssim \mathcal{N} \lesssim 6.0\times10^{19}$ cm^{-3}; this behavior is also found in Fig. 4.5. The van der Waals loop is a region with an instability $\partial\mu/\partial n \leq 0$, where μ is the $e-h$ quasi-chemical potential. Eventually, the exciton Mott transition, i.e., disappearance of the excitonic structures in the THz absorption, occurs above $\mathcal{N} \simeq 1.8\times10^{20}$ cm^{-3}. As shown in Fig. 4.4, the absorption strength of the main peaked structure vanishes above the exciton Mott transition (density).

4.3 Thermodynamical approach

In this section, I investigate the exciton Mott transition with thermodynamical approach. For this purpose, I next investigate the density dependence of the ionization ratio and that of the $e-h$ quasi-chemical potential.

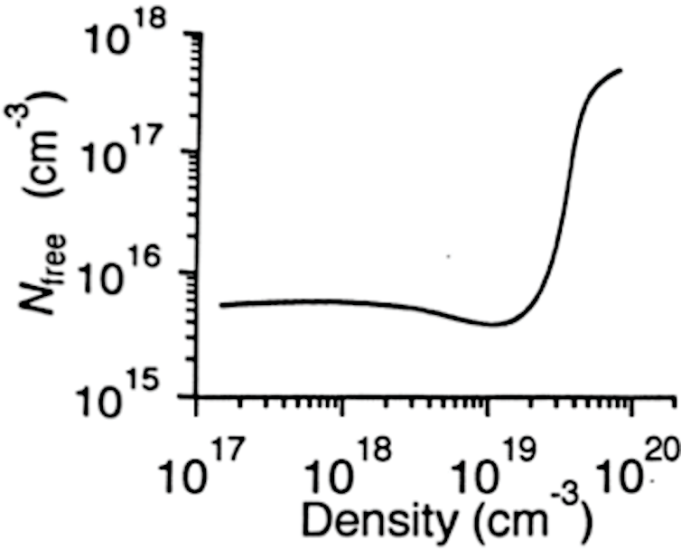

Figure 4.7: The ionized plasma density $\mathcal{N}_{free}$ as a function of the total $e-h$ pair density $\mathcal{N}$.

The ionization ratio is defined by the ratio between density of ionized plasma and total $e-h$ pair density as in the following expression

$$\alpha \equiv \frac{\mathcal{N}_{free}}{\mathcal{N}} \tag{4.4}$$

where, $\mathcal{N}_{free}$ and $\mathcal{N}$ are density of ionized plasma and total $e-h$ pair density, respectively. The density of ionized plasma $\mathcal{N}_{free}$ as a function of total $e-h$ pair density is calculated and shown in Fig. 4.7. It is clearly seen that the $\mathcal{N}_{free}$ is almost unchanged when carrier density increases up to density $\mathcal{N} \lesssim 2.0 \times 10^{19}$ cm^{-3}.

Figure 4.8 exhibits the density dependence of the ionization ratio and $e-h$ quasi-chemical potential. I find in Fig. 4.8 that α is novanishing either when $\mathcal{N} \lesssim 1.0 \times 10^{18}$ cm^{-3} or when $\mathcal{N} \gtrsim 5.0 \times 10^{19}$ cm^{-3}. In the intermediate density regime ($1.0 \times 10^{18} \lesssim \mathcal{N} \lesssim 5.0 \times 10^{19}$ cm^{-3}), the α nearly equals to zero. It is also found that the quasi-chemical potential of $e-h$ pairs nearly equals -1.0 when $\mathcal{N} \lesssim 5.0 \times 10^{19}$ cm^{-3}. Above the density 5.0×10^{19} cm^{-3}, the quasi-chemical potential and the ionization ratio increase sharply.

The nonvanishing α in low-density regime ($\mathcal{N} \lesssim 1.0 \times 10^{18}$ cm^{-3}) is due to the entropy dissociation, [56] and the system is regarded as the classical gases consisting of electrons, holes, and excitons with the lowest energy eigenvalue. This interpretation is supported by

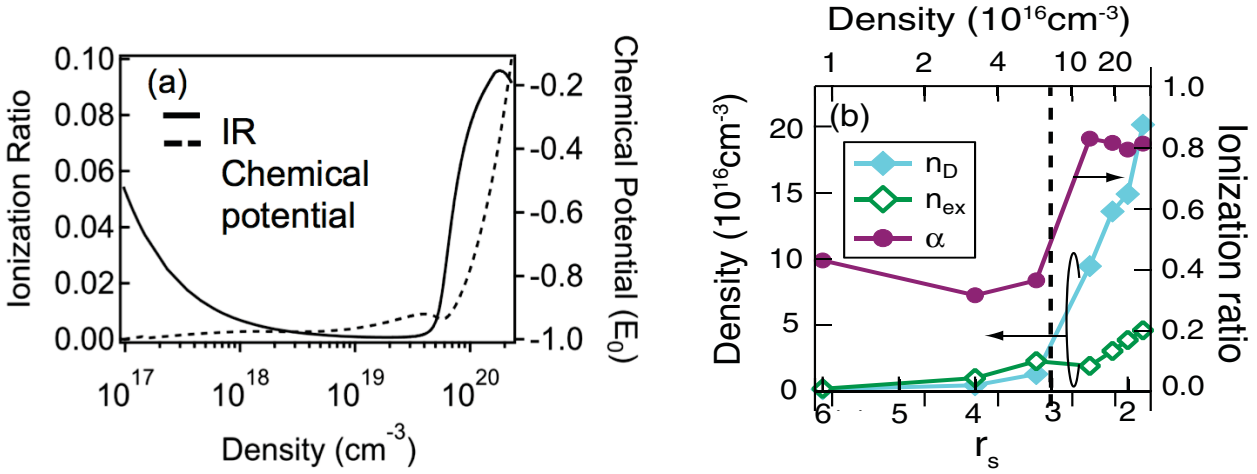

Figure 4.8: (a)Density dependence of the ionization ratio α (solid line) and the quasi-chemical potential of $e-h$ pairs (dashed line). It is found that the ionization ratio does not reach unity even if the exciton Mott transition occurs; this behavior suggests that the existence of the $e-h$ pair correlations above the exciton Mott transition. I find a bistability behavior in $4.0\times10^{18}\lesssim\mathcal{N}\lesssim2.0\times10^{19}$ cm^{-3} originating from the instability, $\partial\mu/\partial n\leq0$, where μ is the quasi-chemical potential. (b) Purple line is density dependence of the ionization ratio in experimental result in Si from Ref. [38].

the fact that either the state-filling effect or the screening effect is irrelevant in this density regime as shown in Fig. 4.4. The ionization ratio α is monotonically decreasing function in this density regime because the density of ionized plasma is almost independent of $\mathcal{N}$ as shown in Fig. 4.7.

In comparison experiment, it shows that the behavior of density dependence of ionization ratio in my theory is in good agreement with density dependence of ionization ratio experimentally reported in Si in Fig. 4.7(b). I should remark that, while this behavior is qualitatively well described by the Saha equation, the present theory predicts the larger ionization ratio comparing with the Saha equation especially in low densities.

This point is readily confirmed with Fig. 4.9 in which I show density $\mathcal{N}$ dependence of $f(\mathcal{N},T)\equiv\mathcal{N}\alpha^2/(1-\alpha)$; if α agrees with the Saha prediction, $f(\mathcal{N},T)$ only depends on the carrier temperature T, and its value corresponding to $T=0.077E_0$ is shown as the dashed line in Fig. 3 (c). This behavior is in contrasts with the quasi-two-dimensional case in which the two dimensional version of the Saha equation successfully explains the

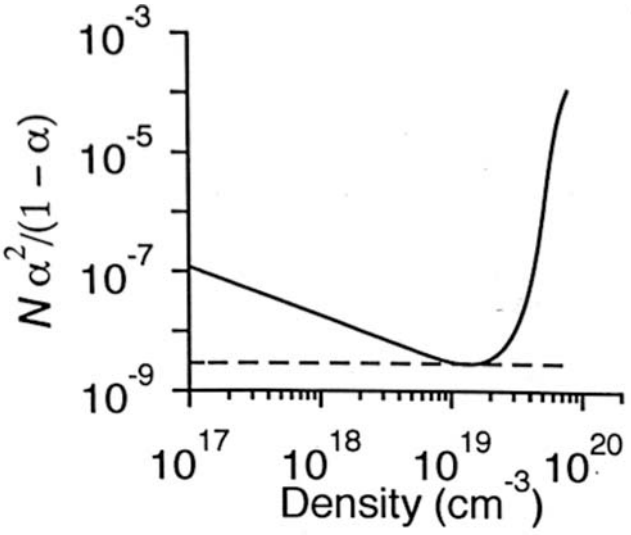

Figure 4.9: $\mathcal{N}\alpha^2/(1-\alpha)$ as a function of $\mathcal{N}$. The solid line corresponds to the present theory while the Saha equation predicts the dashed line.

experimental results. [36] I think that the discrepancy in bulk systems arises because the present theory is based on the mean-field analysis, and more intricate analysis based on the self-consistent T-matrix theory can successfully explain the $\mathcal{N}$ dependence of the ionization ratio in low-density regime. As shown in Fig. 4.7, the quasi-chemical potential of $e-h$ pairs nearly equals -1.0. This result indicates that only an exciton with lowest energy eigenvalue is generated in this density regime if I add an $e-h$ pair in the system; this interpretation is consistent with $\mathcal{N}$ dependence of $\mathcal{N}_{free}$ which is shown in Fig. 4.8.

Just below the exciton Mott transition point at which all of spectral components originating from the intraexcitonic transitions disappear, I find a drastic increase in the ionization ratio; this increase has absolutely different nature from the entropy dissociation. This increase originates from the quantum dissociation, [76] in which density of the ionized plasma abruptly increases with increasing $\mathcal{N}$ as shown in Fig. 4.8. Since the ionized plasmas significantly contribute to screening, reduction of the exciton binding energy and of the THz absorption strength are found as shown in Fig. 4.2 and 4.4, respectively. Since degenerate ionized plasmas are effectively generated, I also find an abrupt increase in the $e-h$ quasi-chemical potential in this density regime. These abrupt increases in the quasi-chemical potential and in the ionization ratio can be regarded as the precursors of the exciton Mott transition. Furthermore, I should remark that the

ionization ratio does not reach unity even if $\mathcal{N}$ is above the exciton Mott density; this behavior suggests that the $e-h$ correlation remains in this density regime. The issue of the $e-h$ pair correlation above the exciton Mott transition is interesting because it is closely related to the BCS-like pair correlation in the excitonic phase and because the correlation has experimentally been observed in bulk Si [64] while it is absent in the GaAs/AlGaAs quantum-well systems.

4.4 THz spectra with Drude component

To summarize the results of our numerical analysis, I show in Fig. 4.10(a) the calculated conductivity spectra with the Drude component. Here the phenomenological line width is set to 0.1, which is moderate for comparison with experiments. I also show in Fig. 4.10(b) the experimental results from Shimano's group [38] as a reference. For convenience, I also use, as a measure of density, the r_s parameter defined by

$$r_s = \left[\frac{3}{(4\pi\mathcal{N}a_0^3)}\right]^{1/3} \tag{4.5}$$

that is the mean inter-pair distance normalized by the exciton Bohr radius a_0.

At sufficiently low densities ($\mathcal{N} \lesssim 2.0 \times 10^{19}$ cm^{-3}, $r_s \gtrsim 50$), only the Drude component is found in the calculated spectra, since the absorption strength of the spectral components originating from the intraexciton transition is too weak. This result is reasonable because, owing to the entropy dissociation that predominates in the low-density limit, fraction of exciton is too small comparing with that of ionized plasma. As shown in Fig. 4.7, nonnegligible fraction of excitons coexists with ionized plasmas with increasing $\mathcal{N}$. Therefore the conductivity spectra around $\mathcal{N} \simeq 2.7 \times 10^{16}$ cm^{-3} ($r_s \simeq 28$) consist of two parts: the Drude component and the one originating from the intraexciton transitions. With further increasing $\mathcal{N}$, the ionization ratio α monotonically decreases and the absorption strength of Drude component gradually decreases comparing with that of the component arising from the intraexciton transition. In fact, the Drude compo-

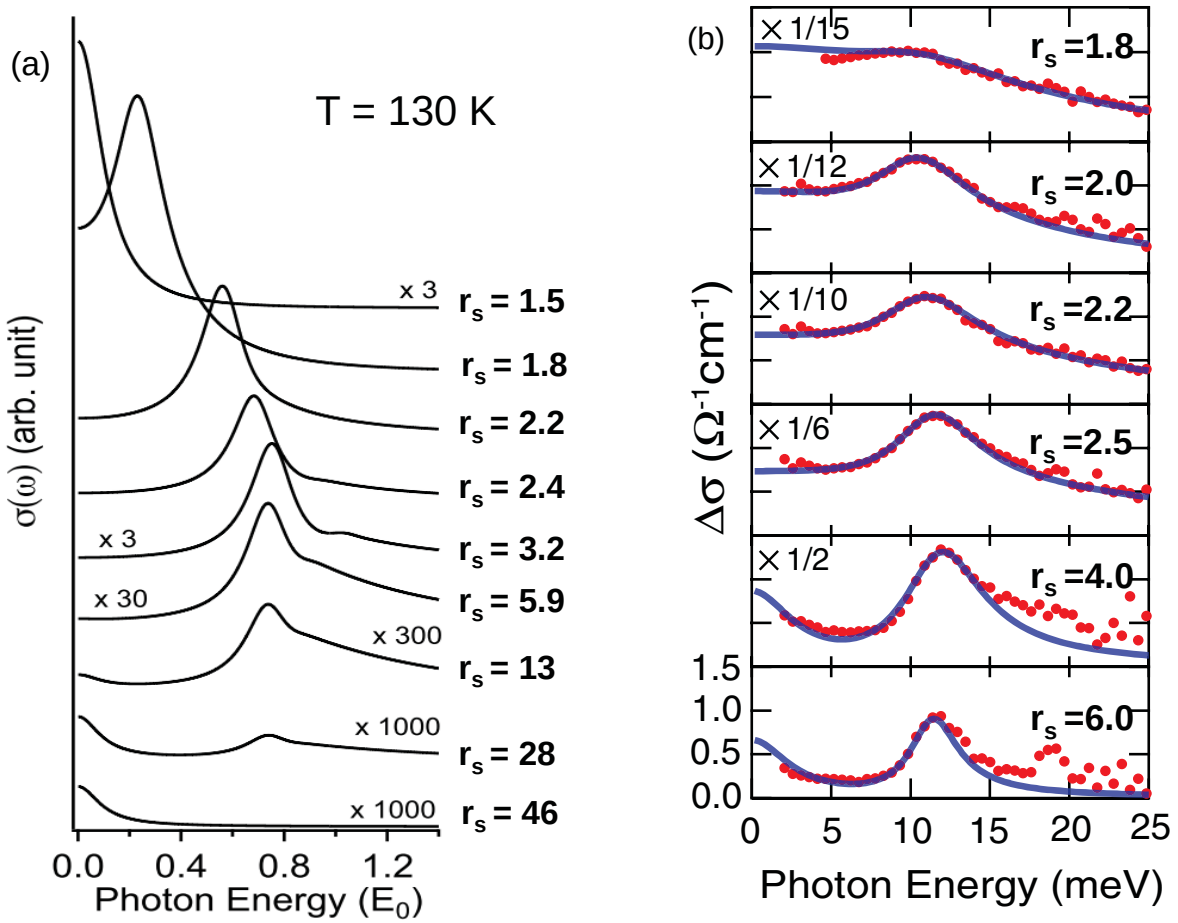

Figure 4.10: (a) Conductivity spectra for various $e-h$ pair densities at $T = 0.077E_0$. Above $\mathcal{N} \gtrsim 1.8 \times 10^{20}$ cm^{-3} , the exciton Mott transition occurs and only the Drude component survives. (b) THz conductivity spectra from experiment for Si at lattice temperature $T = 30K$ from Ref. [38].

nent is absent in Fig. 4.10(a) for $2.0 \times 10^{18} \lesssim \mathcal{N} \lesssim 5.0 \times 10^{19}$ cm^{-3} ($6.7 \gtrsim r_s \gtrsim 2.2$). The line width of the component originating from the intraexciton transition increases because the transition energy from $1s$ to $3p$ and to higher exciton eigenstates increase, while the $1s - 2p$ transition energy stays nearly unchanged with increasing the $e - h$ pair density. At higher densities $5.0 \times 10^{19} \lesssim \mathcal{N} \lesssim 1.8 \times 10^{20}$ cm^{-3} ($2.2 \gtrsim r_s \gtrsim 1.5$), the Drude component as well as the one originating from the intraexciton transition is found in the spectrum, because the ionization ratio abruptly increases and excitons and the $e - h$ plasmas coexist. The system is this density regime is metallic because of the nonvanishing low-frequency conductivity. The line width of the component due to intraexciton transition decreases because spectral components originating from the 1s to 3p and to higher exciton eigenstates sequentially disappear because of the screening. For $\mathcal{N} \gtrsim 1.8 \times 10^{20}$ cm^{-3} ($r_s \lesssim 1.5$), the exciton Mott transition, i.e., density ionization, takes place and the component originating from the intraexciton transition disappears.

4.5 Discussion

In this chapter, I have presented the THz absorption spectra for various carrier densities obtained by numerically solving equation-of-motion of dielectric function. The density dependence of the THz absorption spectra has been reproduced and well analyzed. Comparing with the experimental result for Si [51], it shows that the present theory qualitatively explains the density dependence of the THz absorption spectra. With analyzing density dependence of THz absorption spectra in spectral approach, the exciton Mott transition is defined as the disappearance of the excitonic structures in the spectra. On the other hand, I also investigate exciton Mott transition with thermodynamical approach by calculate density dependence of ionization ratio and quasi-chemical potential of $e - h$ pair. It shows that around the exciton Mott density both ionization ratio and quasi-chemical potential abruptly increase.

4.6 Summary of Chapter 4

In this chapter, I initially analyze the THz absorption spectra in optically excited bulk semiconductor with spectral approach in Sec. 4.2 and with thermodynamical approach in Sec 4.3. The THz absorption spectra with Drude component have shown in Sec. 4.4, which is moderate in comparison with experiments. I have reproduced the density dependence of the THz absorption spectra. I have also found the independence of the spectral position of the component originating from the $1s$ to $2p$ intraexciton transition, which is in agreement with experimental results. I have obtained the density dependence of ionization ratio and $e-h$ quasi-chemical potential, which are useful to investigate the exciton Mott transition.

With analyzing THz absorption spectra in optically excited semiconductors, I have shown that the exciton Mott transition can clearly be studied.

Chapter 5

Concluding Remarks

In conclusion, we have analyzed the density dependence of the THz absorption spectra in optically excited bulk semiconductors, and have shown that the exciton Mott transition (density ionization) can clearly be studied with analyzing the THz absorption. Comparing with the experimental result for Si [51], we can conclude that the present theory qualitatively explains the density dependence of the THz absorption spectra. In particular, the theory reproduces the density independence of the spectral position of the component originating from the $1s$ to $2p$ intraexciton transition for a wide range of $e-h$ pair densities, the disappearance of the Drude component in the intermediate density regime, and the density dependence of the broadening of the spectral component originating from the intraexciton transitions in the intermediate density regime. While the theory predicts the lower density at which the Drude component disappears in the intermediate density regime comparing with the experimental finding, we believe that this discrepancy is attributed to the band degeneracy of Si. Just below the exciton Mott transition point, the theory predicts the redshift of the spectral component originating from intraexciton transitions, whereas in the experiment such a redshift has not been observed. Furthermore, while considerable increase in the line width has been observed in experiment near the exciton Mott transition point, the present theory cannot explain such behavior because we have phenomelogically introduced the constant line width. These points will be studied in a forthcoming paper based on the more intricate theory.

To focus on the density dependence of the THz absorption spectra, we have not analyzed the temperature dependence of the spectra, which is important to determine the phase diagram of the Coulomb interacting $e-h$ systems. This problem is particularly interesting not only in device applications but also in fundamental physics because the crossover between the exciton BEC and the BCS-like $e-h$ pairing state has theoretically been predicted at low temperatures, [44, 56] and because the exciton BEC has recently been realized in Cu_2O [57, 58] To investigate these phenomena in a unified framework, a more intricate approach based on the self-consistent T-matrix theory will be developed in the future work.

Bibliography

[1] D. Saeekia, Handbook of Terehertz Technology for Imaging, Sensing and Communications (Woodhead Publishing, Cambridge, UK, 2013).

[2] X. Yin, B. W. H. Ng, and D. Abbott, Terahertz Imaging for Biomedical Applications: Pattern Recognition and Tomographic Reconstruction (Springer, New York, 2012).

[3] E. Hendry, F. Wang, J. Shan, T. F. Heinz, and M. Bonn, Phys. Rev. B **69**, 081101 (2004).

[4] R. A. Kaindl, M. A. Carnahan, D, Hägele, R. Lövenich, and D. S. Chemla, Nature **423**, 734 (2003).

[5] P. H. Siegel, IEEE Trans. Microwave Theory Tech. **52**, 2438 (2004).

[6] M. Vanexter, C. Fattinger, and D. Grischkowsky, Opt. Lett. **14**, 1128 (1989).

[7] H. Hirori, M. Nagai, and K. Tanaka, Phys. Rev. B **81**, 081305 (2010).

[8] H. Hirori, A. Doi, F. Blanchard, and K. Tanaka, Appl. Phys. Lett. **98**, 091106 (2011).

[9] J. A. Fülöp, L. Pálfalvi, M. C. Hoffmann, and J. Hebling, Optics Express **19**, 15090 (2011).

[10] H. Hirori, K. Shinokita, M. Shirai, S. Tani, Y. Kadoya, and K. Tanaka, Nature Commun. **2**, 594 (2011).

[11] K. L. Ishikawa, Phys. Rev. B **82**, 201402 (2010).

[12] S. A. Moskalenko and D. W. Snoke, Bose-Einstein Condensation of Excitons (Cambridge University Press, Cambridge, England, 2000).

[13] A. Griffin, D. W. Snoke, and S. Stringari, Bose-Einstein Condensation (Cambridge University Press, Cambridge, England, 1995).

[14] D. W. Snoke, J. P. Wolfe, and A. Mysyrowicz, Phys. Rev. B **41**, 11171 (1990).

[15] J. L. Lin and J. P. Wolfe, Phys. Rev. Lett. **71**, 1222 (1993).

[16] K. E. O'Hara, L. O. Súilleabháin, and J. P. Wolfe, Phys. Rev. B **60**, 10565 (1999).

[17] K. Johnsen and G. M. Kavoulakis, Phys. Rev. Lett. **86**, 858 (2001).

[18] H. Haken, Fortsch. Phys. **38**, 271 (1958).

[19] S. Nikitine, J. Phys. Chem. Solids **45**, 949 (1984).

[20] M. Jörger, E. Tsitsishvili, T. Flek, and C. Klingshirn, Phys. Stat. Sol. B **238**, 470 (2003).

[21] M. Jörger, T. Flek, and C. Klingshirn, J. Lumin. 112, 21 (2005).

[22] M. Kira, W. Hoyer, T. Stroucken, and S. W. Koch, Phys. Rev. Lett. **87**, 176401 (2001)

[23] M. Kira, and S. W. Koch, Euro. Phys. J. D. **36**, 143 (2005).

[24] R. A. Kaindl, D. Hägele, M. A. Carnahan, R. Lövenich, and D. S. Chemla, Phys. Stat. Sol. B **238**, 451 (2003).

[25] M. Kira, F. Jahnke, and S. W, Koch, Phys. Rev. Lett. **81**, 3263 (1998).

[26] N. F. Mott, Philos. Mag. **6**, 287 (1961).

[27] N. F. Mott, Metal-Insulator Transitions (Taylor and Francis, London, UK, 1974).

[28] Y. Hayamizu, M. Yoshita, Y. Takahashi, H. Akiyama, C. Z. Ning, L. N. Pfeifer, and K. W. West, Phys. Rev. Lett. **99**, 167403 (2007).

[29] T. Yoshioka and K. Asano, Phys. Rev. Lett. **107**, 256403 (2011).

[30] T. Yoshioka and K. Asano, Phys. Rev. B **86**, 115314 (2012).

[31] H. Haug and S. W. Koch, Quantum Theory of the Optical and Electronic Properties of Semiconductors, 5th ed. (World Scientific, Singapore, 2009)

[32] J. Shah, Ultrafast Spectroscopy of Semiconductors and Semiconductor Nanostructures (Springer, 1996).

[33] I. Galbraith, et al., Phys. Rev. B **71**, 073302 (2005).

[34] C. F. Klingshirn, Semiconductor Optics (Springer, New York, 2006).

[35] S. W. Koch, M. Kira, G. Khitrova , and H. M. Gibbs, Nature Matter. **5**, 523 (2006).

[36] R. Huber, R. A. Kaindl, B. A. Schmid, and D. S. Chemla, Phys. Rev. B **72**, 161314 (2005).

[37] R. A. Kaindl, D. Hägele, M. A. Carnahan, and D. S. Chemla, Phys. Rev. B **79**, 045320 (2009).

[38] T. Suzuki and R. Shimano, Phys. Rev. Lett. **103**, 057401 (2009).

[39] R. Huber, B. A. Schmid, Y. R. Chen, D. S. Chemla, and R. A. Kaindl, Phys. Rev. Lett. **96**, 017402 (2006).

[40] S. Leinss, T. Kampfrath, K. von Volkmann, M. Wolf, J. T. Steiner, M. Kira, S. W. Koch, A. Leitenstorfer, and R. Huber, Phys. Rev. Lett. **101**, 246401 (2008).

[41] D. Wang, M. Hawton, and M. M. Dignam, Phys. Rev. B **76**, 115311 (2007).

[42] V. M. Axt and T. Kuhn, Rep. Prog. Phys. **67**, 433 (2004).

[43] H. C. Schneider, W. W. Chow, and S. W. Koch, Phys. Rev. B **70**, 235308 (2004).

[44] N. Peyghambarian, S. W. Koch, and A. Mysyrowicz, Introduction to Semiconductor Optics (1993).

[45] H. W. Wyld and B. D. Fried, Ann. Phys. **23**, 374 (1963).

[46] J. Fricke, Ann. Phys. **252**, 479 (1996).

[47] M. Kira and S. W. Koch, Prog. Quantum Electron. **30**, 155 (2006).

[48] M. Kira, W. Hoyer, and S. W. Koch, Phys. Status Solidi B **238**, 443 (2003).

[49] D. Wang, X. Lei and Z. Wu, J. Phys. Cond. Mat. **23**, 345801 (2011).

[50] A. M. Parks, M. M. Dignam and D. Wang, Phys. Rev. B **87**, 205306 (2013).

[51] T. J. Inagaki, T. Iida, and M. Aihara, Phys. Rev. B **62**, 10852 (2000).

[52] T.J. Inagaki and M. Aihara, Phys. Rev. B **65**, 205204 (2002).

[53] T.J. Inagaki and M. Aihara, Phys. Rev. B **66**, 075204 (2002).

[54] L. V. Keldysh and A. N. Kozlov, Zh. Eksp. Teor. Fiz. **54**, 978 (1968), [Sov. Phys. JETP **27**, 521 (1968)].

[55] C. Comte and P. Nozières, J.Phys (Paris) **43**, 1069 (1982).

[56] P. Nozières and C. Comte, J. Phys. (Paris) **43**, 1083 (1982).

[57] C. Comte and G. Mahler, Phys. Rev. B **34**, 7164 (1986).

[58] S. Glutsch and R. Zimmermann, Phys. Rev. B **45** (1992).

[59] H. Chu and Y. C. Chang, Phys. Rev. B **54**, 5020 (1996).

[60] H. Chu and Y. C. Chang, Europhys. Lett. **35**, 535 (1996).

[61] P. Nozières and S. Schmitt-Rink, J. Low Temp. Phys. **59**, 195 (1985).

[62] H. Stolz and R. Zimmermann, Phys. Status Solidi B **94**, 135 (1979).

[63] R. Zimmermann and H. Stolz, Phys. Status Solidi B **131**, 151 (1985).

[64] T. Suzuki and R. Shimano, Phys. Rev. Lett. **109**, 046402 (2012).

[65] N. H. Kwong, G. Rupper, and R. Binder, Phys. Rev. B **79**, 155205 (2009).

[66] J. E. Sipe, and Ed Ghahramani, Phys. Rev. B **48**, 11705 (1993).

[67] T.Grunwald, T.Jung, D.Köler, S.W.Koch, G.Khitrova, H. M. Gibbs, R. Hey, and S. Chatterjee, Phys. Status Solidi C **6**, 500 (2009).

[68] B. I. Lundqvist, Phys. Konden. Mat. **6**, 193 (1967).

[69] B. I. Lundqvist, Phys. Konden. Mat. **6**, 206 (1967).

[70] J. C. Inkson, J. Phys. C **5**, 2599 (1972).

[71] R. Zimmermann, Phys. Status Solidi B **76**, 191 (1976).

[72] H. Haug and S. Schmitt-Rink, Prog. Quantum Electron. **9**, 3 (1984).

[73] S. Schmitt-Rink, D. S. Chemla, and H. Haug, Phys. Rev. B **37**, 941 (1988).

[74] T. Ohyama, T. Ogawa, and H. Nakata, Phys. Rev. B **56**, 3871 (1997).

[75] T. Tayagaki, A. Mysyrowicz, and M. Kuwata-Gonokami, J. Phys. Soc. Jpn. **74**, 1423 (2005).

[76] M. Combescot, Phys. Status Solidi B **86**, 349 (1978).

[77] D. Kremp, D. Semkat, and K. Henneberger, Phys. Rev. B **78**, 125315 (2008).

[78] K. Yoshioka, E. Chae, and M. Kuwata-Gonokami, Nature Commun. **2**, 328 (2011).

[79] H. Stolz, R. Schwartz, F. Kieseling, S. Som, M. Kaupsch, S. Sobkowiak, D. Semkat, N. Naka, T. Koch, and H. Fehske, New J. Phys. **14**, 105007 (2012).

[80] R. Zimmermann, K. Kilimann, W. D. Kraeft, D. Kremp, and G. Röpke, Phys. Status Solidi B **90**, 175 (1978).

[81] D. Semkat, F. Richter, D. Kremp, G. Manzke, W.D. Kraeft, and K. Henneberger, Phys. Rev. B **80**, 155201 (2009).

[82] T. Kazimierczuk, D. Fröhlich, S. Scheel, H. Stolz, and M. Bayer, Nature **514**, 343-347 (2014).

Appendix A

FORTRAN PROGRAM FOR MAIN PROGRAM

```
!=================================================
!   Main Program
!
!   p00(i):         momentum abscissae
!   etilde(i,1):    e_tilde_0 at p00(i)
!   etilde(i,2):    e_tilde_1 at p00(i)
!   etilde(i,3):    e_tilde_3 at p00(i)
!   chi(i,1)        Hartree-Fock energy chi_0 at p00(i)
!   chi(i,2)        Hartree-Fock energy chi_1 at p00(i)
!   chi(i,3)        Hartree-Fock energy chi_3 at p00(i)
!=================================================
PROGRAM lyman
   USE param
   IMPLICIT NONE
!  INTEGER, PARAMETER:: maxloop = 300
   INTEGER, PARAMETER:: maxloop = 900
!  REAL(8), PARAMETER:: Epsa = 1.0d-5
!  REAL(8), PARAMETER:: Epsr = 1.0d-4
   REAL(8), PARAMETER:: Epsa = 1.0d-6
   REAL(8), PARAMETER:: Epsr = 1.0d-6
   REAL(8), DIMENSION(Ndiv):: p00
   REAL(8), DIMENSION(Ndiv,3):: etilde
   REAL(8), DIMENSION(Ndiv,3):: chi
   INTEGER:: i

   REAL(8):: p, e1, e2, e3, ee, f00, f03
   REAL(8), EXTERNAL:: myabs, f0, f3

   COMPLEX(8), DIMENSION(2*Ndiv):: e_val
   COMPLEX(8), DIMENSION(2*Ndiv, 2*Ndiv):: e_vec, inve_vec
   COMPLEX(8), DIMENSION(2*Ndiv):: hv, hv1

   REAL(8), PARAMETER:: Omega_max = 2.0d0
   REAL(8), PARAMETER:: Omega_min = 0.0d0
   INTEGER, PARAMETER:: Nomega    = 2**11
   REAL(8):: omega, w, dw, res
   COMPLEX(8):: zres
   INTEGER:: flag
   REAL(8), PARAMETER:: Omega_max2 = 4.0d0
   REAL(8), PARAMETER:: Omega_min2 = -4.0d0

! open files
   CALL open_files

! input parameters
   CALL read_param

! initialize momentum & energy
   CALL init_momentum_energy(p00, etilde)
!do i=1, Ndiv
!!  print *, etilde(i, 1)
!   print *, etilde(i, 2)
!end do
```

```
! calculate Hartree-Fock self-energy self-consistently
   CALL solve_gap(p00, etilde, epsa, epsr, maxloop, chi)

! calculate electron-hole pair density
   CALL calc_eh_density(p00, etilde, chi, density)

! output parameters
   CALL write_param
   WRITE(*,*) 'beta␣=', beta
   WRITE(*,*) 'omega_0␣=', omega_0
   WRITE(*,*) 'rabi␣=', rabi
   WRITE(*,*) 'mass_ratio␣=', mass_ratio

   WRITE(*,*) 'pi␣=', pi
   WRITE(*,*) 'Ndiv␣=', Ndiv
   WRITE(*,*) 'Max_momentum␣=', Max_Momentum
   WRITE(*,*) 'Eps␣␣=', Eps

   WRITE(*,*) 'density␣=', density
   WRITE(*,*) 'density␣(cm^{-3})␣=', density / (Ab**3)
   WRITE(*,*) 'r_s␣=', (3.0d0/(4.0d0*pi*density))**(1.0d0/3.0d0)
   WRITE(*,*) 'lambda␣=', lambda
   WRITE(*,*) 'Thomas-Fermi␣momentum␣␣=', SQRT(ptf)
   WRITE(*,*) 'Debye-Huckel␣momentum␣␣=', SQRT(pdh)
   WRITE(*,*) 'plasma␣frequency␣=', SQRT(wpl)
   WRITE(*,*) 'effective␣gap␣=', SQRT(del)
   WRITE(*,*) 'Fermi␣momentum␣=', pfermi
   WRITE(*,*) 'Debye␣shift␣=', ds

! output chi0, chi1, chi3, and quasi-particle energy
   WRITE(101,1)
   WRITE(102,2)
   WRITE(103,3)
   WRITE(104,4)
   WRITE(105,5)
   WRITE(106,6)
   WRITE(107,7)
   WRITE(108,8)
   WRITE(109,9)

   DO i=1, Ndiv
      p = p00(i)
      e1 = etilde(i, 1) + chi(i, 1)
      e2 = etilde(i, 2) + chi(i, 2)
      e3 = etilde(i, 3) + chi(i, 3)
      ee = myabs(e2, e3)
      f00 = f0(e1, ee)
      f03 = f3(e1, ee)
      WRITE(101, *) p, chi(i, 1), chi(i, 3)
      WRITE(102, *) p, chi(i, 2), ee
      WRITE(103, *) p, e1 + ee, e1 - ee
      WRITE(104, *) p, 0.5d0*(1.0d0 + f00 + f03*(e3/ee)),   &
                       0.5d0*(1.0d0 - f00 + f03*(e3/ee))
      WRITE(105, *) p, -0.5d0*f03*(e2/ee), f03*(e3/ee)
   END DO
   CLOSE(UNIT=101, STATUS='keep')
   CLOSE(UNIT=102, STATUS='keep')
   CLOSE(UNIT=103, STATUS='keep')
   CLOSE(UNIT=104, STATUS='keep')
   CLOSE(UNIT=105, STATUS='keep')

!!---------------<intraband response>-----------------
```

```
!! solve Bethe-Salpeter equation for THz absorption spectra
!   PRINT *, '... THz absorption spectra ...'
!   flag = 1
!   CALL solve_bs(flag, p00, etilde, chi, e_val, e_vec, inve_vec)
!
!! hv is the inhomogeneous term of the bs equation
!! for intraband dielectric function
!   CALL make_hv(p00, etilde, chi, hv)
!   hv  = MATMUL(inve_vec, hv)
!
!   dw  = (Omega_max - Omega_min)/REAL(Nomega, 8)
!   DO i=1, Nomega
!      omega = Omega_min + REAL(i, 8) * dw
!
!! calculate THz absorption spectrum
! CALL calc_spectra(omega, p00, etilde, chi,
!! e_val, e_vec, hv, zres)
!      WRITE(106, *) omega, omega*Ry, DIMAG(zres)*omega
!      WRITE(107, *) omega, omega*Ry, DIMAG(zres)
!!     WRITE(107, *) omega, omega*Ry, REAL(zres,8)
!   END DO
   CLOSE(UNIT=106, STATUS='keep')
   CLOSE(UNIT=107, STATUS='keep')

!!---------------<interband absorption>-----------------
!! solve Bethe-Salpeter equation for optical absorption spectra
!   PRINT *, '... interband absorption spectra ...'
!   flag = 0
!   CALL solve_bs(flag, p00, etilde, chi, e_val, e_vec, inve_vec)
!
!! hv1 is the inhomogeneous term of the bs equation
!! for interband dielectric function
!   CALL make_hv1(p00, etilde, chi, hv1)
!   hv1  = MATMUL(inve_vec, hv1)
!
!! calculate interband absorption
!   dw  = (Omega_max2 - Omega_min2)/REAL(Nomega, 8)
!   DO i=1, Nomega
!      omega = Omega_min2 + REAL(i, 8) * dw
!!     w = omega - omega_0
!!     w = omega - omega_0 + 0.5d0*ds   ! old_version
!      w = omega - omega_0 - 0.5d0*ds   ! ???
!      CALL calc_abs(w, p00, etilde, chi, e_val, e_vec, hv1, res)
!      WRITE(108, *) omega, omega*Ry, res
!   END DO
   CLOSE(UNIT=108, STATUS='keep')

!---------------<photoluminescence>-----------------
! hv3 is the inhomogeneous term of the bs equation
!! for photoluminescence
!  PRINT *, '... photoluminescence spectra ...'
!  CALL make_hv2(p00, etilde, chi, hv2)
!  hv2  = MATMUL(inve_vec, hv2)

! calculate photoluminescence
!  dw  = (Omega_max2 - Omega_min2)/REAL(Nomega, 8)
!  DO i=1, Nomega
!     omega = Omega_min2 + REAL(i, 8) * dw
! CALL calc_pl(omega, p00, etilde, chi, e_val, e_vec, hv2, res)
!     WRITE(109, *) omega, omega*Ry, res
!  END DO
   CLOSE(UNIT=109, STATUS='keep')

! output formats
 1 FORMAT('# p | chi_0 | chi_3')
```

```
 2 FORMAT('# p    | chi_1    |    E'' ')
 3 FORMAT('# p|quasi-particle energy1| quasi-particle energy2')
 4 FORMAT('# p    |    Ne(p)    |    Nh(e)')
 5 FORMAT('# p    |    Normalized e-h pair wave function | <X3>')
 6 FORMAT('# omega  |    omega (meV)    |    &
                  real part of conductivity')
 7 FORMAT('# omega  | omega (meV)    |    &
                  imaginary part of dielectric function')
 !7 FORMAT('# omega |   omega (meV)   |  &
               real part of dielectric function')
  8 FORMAT('# omega | omega (meV)   |  &
               interband absorption')
  9 FORMAT('# omega | omega (meV)   |   &
                photoluminescence')

END PROGRAM lyman
```

Appendix B

FORTRAN PROGRAM FOR MAIN SUBROUTINES

B1. Electron-hole pair density

```
!=================================================
! calculate electron-hole pair density
!
!   p00(i): momentum abscissae
!   etilde(i,1): e_tilde_0 at p00(i)
!   etilde(i,2): e_tilde_1 at p00(i)
!   etilde(i,3): e_tilde_3 at p00(i)
!   chi(i, j):   j-th self-energy at p00(i)
!   density:     density of e-h pair
!=================================================
SUBROUTINE calc_eh_density(p00, etilde, chi, density)
   USE param, ONLY: Ndiv, pi
   IMPLICIT NONE
   REAL(8), DIMENSION(Ndiv), INTENT(IN):: p00
   REAL(8), DIMENSION(Ndiv,3), INTENT(IN):: etilde
   REAL(8), DIMENSION(Ndiv,3), INTENT(IN):: chi
   REAL(8), INTENT(OUT):: density
   REAL(8), EXTERNAL:: integ_density
   REAL(8), DIMENSION(Ndiv):: integ
   INTEGER:: i, icon
   REAL(8):: p, e1, e2, e3, res

   DO i=1, Ndiv
      p   = p00(i)
      e1  = etilde(i, 1) + chi(i, 1)
      e2  = etilde(i, 2) + chi(i, 2)
      e3  = etilde(i, 3) + chi(i, 3)

      integ(i) = p*p*integ_density(e1, e2, e3)
   END DO

   CALL davint(p00, integ, Ndiv, p00(1), p00(Ndiv), res, icon)
   density = res/(4.0d0*pi*pi)

END SUBROUTINE calc_eh_density

!=================================================
! integ_density = 1.0d0 + f3(ee) * (e3/ee)
!=================================================
FUNCTION integ_density(e1, e2, e3) RESULT(res)
   USE param, ONLY: beta
   IMPLICIT NONE
   REAL(8), INTENT(IN):: e1, e2, e3
   REAL(8):: res
   REAL(8):: ee
   REAL(8), EXTERNAL:: f3, myabs, func

! check
```

```
!print *, 'integ_density: beta =', beta

   ee  = myabs(e2, e3)
   IF(e3 < 0.0d0) THEN
      res = 1.0d0 + f3(e1,ee)*(e3/ee)
   ELSE
       res = e2*e2/(ee*(ee + e3))            &
          + 2.0d0*(e3/ee)*fermi(2.0d0*ee)    &
          + (e3/ee)*TANH(beta*ee)*func(beta*e1, beta*ee)
!      res = e2*e2/(ee*(ee + e3))            &
!         + (e3/ee)*(1.0d0 - TANH(beta*ee)*func(beta*ee, beta*e1))
   END IF

CONTAINS

!=================================================
! fermi(x) = 1/(EXP(x) + 1)
!=================================================
FUNCTION fermi(x) RESULT(res1)
   REAL(8), INTENT(in):: x
   REAL(8):: res1
   REAL(8), PARAMETER:: cutoff = 5.0d0
   REAL(8):: y

! check
!print *, 'fermi: beta =', beta

   y = beta*x
   IF(y > cutoff) THEN
      res1 = EXP(-y)/(1.0d0 + EXP(-y))
   ELSE
      res1 = 1.0d0/(EXP(y) + 1.0d0)
   END IF
END FUNCTION fermi

END FUNCTION integ_density
```

B2. Coulomb potential

```
!=================================================
! bare Coulomb potential
!=================================================
FUNCTION dpot(k1, k2) RESULT(res)
   USE param, ONLY: pi
   IMPLICIT NONE
   REAL(8), INTENT(IN):: k1, k2
   REAL(8):: res

   IF(k1 == k2) then
      res = 0.0d0
   ELSE
      res = LOG(ABS(k1+k2)/ABS(k1-k2))/(k1*k2*pi)
   END IF

END FUNCTION dpot

!=================================================
! calculate Debye shift using static SPPA with q^4 term
!=================================================
FUNCTION calc_ds(ptf, wpl, del) RESULT(res)
   USE param, ONLY: pi
   IMPLICIT NONE
   REAL(8), INTENT(IN):: ptf, wpl, del
   REAL(8):: res
```

```
   REAL(8):: Bound = 0.0d0
   INTEGER, PARAMETER:: Inf = 1
   REAL(8), PARAMETER:: Epsa = 1.0d-6
   REAL(8), PARAMETER:: Epsr = 1.0d-6
   INTEGER, PARAMETER:: Lw = 2000
   INTEGER, PARAMETER:: Liw = 500
   REAL(8), DIMENSION(Lw):: w
   REAL(8), DIMENSION(Liw):: iw
   REAL(8):: aerr
   INTEGER:: ifail

! d01amf (NAG) calculates integral Sum_k (Vs(k) - V(k))
   ifail = 0
   CALL d01amf(f, Bound, Inf, Epsa, Epsr, res, aerr,   &
      w, Lw, iw, Liw, ifail)
   res = 4.0d0*res/pi

CONTAINS

FUNCTION f(x) RESULT(resf)
   REAL(8), INTENT(IN):: x
   REAL(8):: resf
   resf = -1.0d0/(1.0d0 + x*x/ptf + 0.25d0*(x**4)/wpl + del/wpl)
END FUNCTION f

END FUNCTION calc_ds

!=================================================
!  calculate s-wave interaction energy spot(i, j)
!  and following quantities
!
!  REAL(8):: pdh    ! (Debye-Huckel momentum)**2
!  REAL(8):: ptf    ! (Thomas-Fermi momentum)**2
!  REAL(8):: wpl    ! (plasma frequency)**2
!  REAL(8):: del    ! (effective gap)**2
!  REAL(8):: ds     ! Sum_p (spot(p) - dpot(p))
!  REAL(8):: pfermi ! fermi momentum
!  REAL(8):: beta   ! inverse temperature
!=================================================
SUBROUTINE calc_spot(p00, etilde, chi, spot)
   USE param, ONLY: pi, Ndiv, ptf, wpl, del, ds, pfermi,
                    pdh, beta, Screening
   IMPLICIT NONE
   REAL(8), DIMENSION(Ndiv), INTENT(IN):: p00
   REAL(8), DIMENSION(Ndiv, 3), INTENT(IN):: etilde
   REAL(8), DIMENSION(Ndiv, 3), INTENT(IN):: chi
   REAL(8), DIMENSION(Ndiv,Ndiv), INTENT(OUT):: spot
   REAL(8):: density
   REAL(8):: e2, e3, ee
   REAL(8):: p1, p2, pp, pm, coef1, coef2, coef3
   REAL(8):: det, tmp, del2
   INTEGER:: i, j
   REAL(8), EXTERNAL:: myabs, dpot, calc_ds

   CALL calc_eh_density(p00, etilde, chi, density)
   ptf = 16.0d0*(6.0d0*density/pi)**(1.0d0/3.0d0)
   wpl = 16.0d0*pi*density
   pdh = 8.0d0*pi*beta*density

   del = 9.9d9       ! arbitrary large number
   pfermi = -9.9d9   ! arbitrary number
   DO i=1, Ndiv
      e2 = etilde(i, 2) + chi(i, 2)
```

```
      e3 = etilde(i, 3) + chi(i, 3)
      ee = 2.0d0*myabs(e2, e3)
      IF(ee < del) then
         del = ee
         pfermi = p00(i)
      END IF
   END DO
   del = del**2
   IF(Screening == 0) THEN
      del2 = del
   ELSE IF(Screening == 1) THEN
      del2 = 0.0d0
   ELSE
      PRINT *, 'calc_spot: irregal value: Screening =', Screening
      STOP
   END IF
   ds = calc_ds(ptf, wpl, del2)

   coef1 = 4.0d0*wpl/ptf
   coef2 = 4.0d0*(wpl + del2)
   det = 0.25d0*(coef1**2) - coef2
   DO j=1, Ndiv
      DO i=1, Ndiv
         IF(i == j) THEN
            spot(i,j) = 0.0d0
         ELSE
            p1 = p00(i)
            p2 = p00(j)
            pp = ABS(p1 + p2)
            pm = ABS(p1 - p2)
            IF(det > 0.0d0) THEN
               coef3 = LOG(((pp**4) + coef1*(pp**2) + coef2)    &
                           /((pm**4) + coef1*(pm**2) + coef2))   &
                     - 2.0d0*LOG((pp**2 + 0.5d0*coef1 + SQRT(det))
&
                                 /(pm**2 + 0.5d0*coef1 + SQRT(det)))
               coef3 = 0.5d0*coef3/SQRT(det)
            ELSE
               coef3 = ATAN2(pp**2 + 0.5d0*coef1, SQRT(-det)) &
                     - ATAN2(pm**2 + 0.5d0*coef1, SQRT(-det))
               coef3 = coef3/SQRT(-det)
            END IF
            tmp = del2*LOG(pp/pm)                                    &
             + 0.25d0*wpl*LOG(((pp**4) + coef1*(pp**2) + coef2)   &
                              /((pm**4) + coef1*(pm**2) + coef2))  &
             + 0.25d0*wpl*coef1*coef3
            spot(i, j) =  tmp/(pi*p1*p2*(del2 + wpl))
         END IF
      END DO
   END DO

END SUBROUTINE calc_spot

!=================================================
!  calculate p-wave interaction energy ppot(i, j)
!  and following quantities
!
!  REAL(8):: pdh    ! (Debye-Huckel momentum)**2
!  REAL(8):: ptf    ! (Thomas-Fermi momentum)**2
!  REAL(8):: wpl    ! (plasma frequency)**2
!  REAL(8):: del    ! (effective gap)**2
!  REAL(8):: ds     ! Sum_p (spot(p) - dpot(p))
!  REAL(8):: pfermi ! fermi momentum
!  REAL(8):: beta   ! inverse temperature
```

```
!================================================
SUBROUTINE calc_ppot(p00, etilde, chi, ppot)
   USE param, ONLY: pi, Ndiv, ptf, wpl, del, pdh, beta, Screening
   IMPLICIT NONE
   REAL(8), DIMENSION(Ndiv), INTENT(IN):: p00
   REAL(8), DIMENSION(Ndiv, 3), INTENT(IN):: etilde
   REAL(8), DIMENSION(Ndiv, 3), INTENT(IN):: chi
   REAL(8), DIMENSION(Ndiv,Ndiv), INTENT(OUT):: ppot
   REAL(8):: density
   REAL(8):: e2, e3, ee
   REAL(8):: p1, p2, pp, pm, coef1, coef2, coef3
   REAL(8):: coef4, coef5, det, tmp, del2
   INTEGER:: i, j
   REAL(8), EXTERNAL:: myabs, dpot, calc_ds

   CALL calc_eh_density(p00, etilde, chi, density)
   ptf = 16.0d0*(6.0d0*density/pi)**(1.0d0/3.0d0)
   wpl = 16.0d0*pi*density
   pdh = 8.0d0*pi*beta*density

   del = 9.9d9       ! arbitrary large number
   DO i=1, Ndiv
      e2 = etilde(i, 2) + chi(i, 2)
      e3 = etilde(i, 3) + chi(i, 3)
      ee = 2.0d0*myabs(e2, e3)
      IF(ee < del) then
         del = ee
      END IF
   END DO
   del = del**2
   IF(Screening == 0) THEN
      del2 = del
   ELSE IF(Screening == 1) THEN
      del2 = 0.0d0
   ELSE
      PRINT *, 'calc_ppot:␣irregal␣value:␣Screening␣=', Screening
      STOP
   END IF

   coef1 = wpl/ptf            ! beta
   coef2 = wpl + del2         ! gamma
   det = coef1**2 - coef2
   DO j=1, Ndiv
      DO i=1, Ndiv
         IF(i == j) THEN
           ppot(i,j) = 0.0d0
         ELSE
           p1    = p00(i)
           p2    = p00(j)
           pp    = ABS(p1 + p2)
           pm    = ABS(p1 - p2)
           coef4 = (p1**2 + p2**2)/(p1**2)
           coef5 = 2.0d0 + (p1**2 + p2**2)/ptf
           IF(det > 0.0d0) THEN
             coef3 = LOG(((pp**4) + 4.0d0*coef1*(pp**2) + 4.0d0*coef2)
&
                         /((pm**4) + 4.0d0*coef1*(pm**2) + 4.0d0*coef2)) &
                   - 2.0d0*LOG((pp**2 + 2.0d0*coef1 + 2.0d0*SQRT(det))
&
                               /(pm**2 + 2.0d0*coef1 + 2.0d0*SQRT(det)))
             coef3 = 0.25d0*coef3/SQRT(det)
           ELSE
             coef3 = ATAN2(pp**2 + 2.0d0*coef1, 2.0d0*SQRT(-det)) &
                   - ATAN2(pm**2 + 2.0d0*coef1, 2.0d0*SQRT(-det))
```

```
            coef3 = 0.5d0*coef3/SQRT(-det)
          END IF
          tmp = - 2.0d0*(p2/p1)                          &
            +         (del2/coef2)*coef4*LOG(pp/pm)      &
            + 0.25d0*(wpl/coef2)*coef4                   &
               *LOG(((pp**4) + 4.0d0*coef1*(pp**2) + 4.0d0*coef2)
&
                    /((pm**4) + 4.0d0*coef1*(pm**2) + 4.0d0*coef2)) &
            + wpl*coef3*coef5/(p1**2)
          ppot(i, j) = tmp/pi
        END IF
      END DO
   END DO

END SUBROUTINE calc_ppot
```

B3. The gap equation

```
!=================================================
!   Solving the gap equation
!
!  --- input variables
!   p00(i):        momentum abscissae
!   etilde(i,1):   e_tilde_0 at p00(i)
!   etilde(i,2):   e_tilde_1 at p00(i)
!   etilde(i,3):   e_tilde_3 at p00(i)
!
!  --- output variables
!   chi(i,1)       Hartree-Fock energy chi_0 at p00(i)
!   chi(i,2)       Hartree-Fock energy chi_1 at p00(i)
!   chi(i,3)       Hartree-Fock energy chi_3 at p00(i)
!   lambda         Lagrange multiplier for charge neutrality
!=================================================
SUBROUTINE solve_gap(p00, etilde, epsa, epsr, maxloop, chi)
   USE param, ONLY: Ndiv, lambda, ds
   IMPLICIT NONE
   REAL(8), DIMENSION(Ndiv), INTENT(IN):: p00
   REAL(8), DIMENSION(Ndiv,3), INTENT(IN):: etilde
   REAL(8), INTENT(IN):: epsa, epsr
   INTEGER, INTENT(IN):: maxloop
   REAL(8), DIMENSION(Ndiv,3), INTENT(OUT):: chi

   REAL(8), DIMENSION(Ndiv,3):: old1_chi, old2_chi
   REAL(8):: old_lambda, new_lambda
   REAL(8):: abserr0, abserr1, abserr2
   REAL(8):: relerr0, relerr1, relerr2
   INTEGER:: i
   REAL(8), EXTERNAL:: g05caf

! initialize self-energies
! g05ccf (NAG) sets the seed of pseudo random-number generator
! g05caf (NAG) generates pseudo random-number
   CALL g05ccf
   old_lambda = g05caf(0.0d0)
   ds         = g05caf(0.0d0)
   DO i=1, Ndiv
      old1_chi(i, 1) = g05caf(0.0d0)
      old1_chi(i, 2) = g05caf(0.0d0)
      old1_chi(i, 3) = g05caf(0.0d0)
      old2_chi(i, 1) = g05caf(0.0d0)
      old2_chi(i, 2) = g05caf(0.0d0)
      old2_chi(i, 3) = g05caf(0.0d0)
```

```
   END DO

! initialize estimated errors
   abserr2 = g05caf(0.0d0)
   abserr1 = g05caf(0.0d0)

   relerr2 = g05caf(0.0d0)
   relerr1 = g05caf(0.0d0)

! consistency loop
   consistency: DO i=0, maxloop-1

      CALL calc_chi(old_lambda, p00, etilde, old1_chi, chi)
      CALL calc_lambda(p00, etilde, chi, new_lambda)
print *, 'lambda␣=', new_lambda, 'err_lambda␣=', new_lambda - old_lambda

      abserr0 = MAXVAL(ABS(chi - old1_chi))
      relerr0 = abserr0/MAX(MAXVAL(ABS(chi)), epsr)

      abserr0 = MAX(abserr0, ABS(new_lambda - old_lambda))

      WRITE(*,*) 'loop␣=', i+1
      WRITE(*,*) 'abserr␣=', abserr0, 'relerr␣=', relerr0

      IF((MAX(abserr0, abserr1, abserr2) < Epsa) .AND.   &
         (MAX(relerr0, relerr1, relerr2) < Epsr)) EXIT

      abserr2 = abserr1
      abserr1 = abserr0

      relerr2 = relerr1
      relerr1 = relerr0

      old2_chi(1:Ndiv, 1:3) = old1_chi(1:Ndiv, 1:3)
      old1_chi(1:Ndiv, 1:3) = chi(1:Ndiv, 1:3)

      old_lambda = new_lambda

   END DO consistency

   lambda = new_lambda
   chi(1:Ndiv, 1) = chi(1:Ndiv, 1) - lambda
!  chi(1:Ndiv, 3) = chi(1:Ndiv, 3) + 0.25d0*ds   ! ???

END SUBROUTINE solve_gap
```

B4. The Bethe-Salpeter equation

```
!=================================================
! Solving the Bethe-Salpeter equation   version 0
!
! --- input variables
!  flag:  flag = 1 for intraband,
!         flag = 0 for interband spectrum
!  p00(Ndiv):       momentum abscissae
!  etilde(Ndiv, 3): bare energy
!  chi(Ndiv, 3):    Hartree-Fock self-energy
!
! --- output variables
!  e_val(2*Ndiv):    eigenvalues of Hamiltonian
!  e_vec(2*Ndiv):    eigenvectors of Hamiltonian
!  inve_vec(2*Ndiv): inverse of e_vec
!
!  mat(2*Ndiv, 2*Ndiv): Hamiltonian
```

```
!  weight(Ndiv):: weight for numerical integration
!================================================
SUBROUTINE solve_bs(flag, p00, etilde, chi, e_val, e_vec, inve_vec)
   USE param, ONLY: Ndiv
   IMPLICIT NONE
   INTEGER, INTENT(IN):: flag
   REAL(8),    DIMENSION(Ndiv),    INTENT(IN):: p00
   REAL(8),    DIMENSION(Ndiv, 3), INTENT(IN):: etilde
   REAL(8),    DIMENSION(Ndiv, 3), INTENT(IN):: chi
   COMPLEX(8), DIMENSION(2*Ndiv),  INTENT(OUT):: e_val
   COMPLEX(8), DIMENSION(2*Ndiv, 2*Ndiv), INTENT(OUT):: e_vec, inve_vec

   REAL(8),    DIMENSION(Ndiv):: weight
   COMPLEX(8), DIMENSION(2*Ndiv, 2*Ndiv):: mat, mat2

   REAL(8),    DIMENSION(4*Ndiv):: rwork
   INTEGER,    PARAMETER:: lwork = 2*2*Ndiv
   COMPLEX(8), DIMENSION(lwork):: work
   INTEGER,    PARAMETER:: lwork2 = 2*Ndiv * 4
   COMPLEX(8), DIMENSION(lwork2):: work2
   INTEGER,    DIMENSION(2*Ndiv):: ipiv
   INTEGER:: ifail

 ! debugging use
   INTEGER:: i, j, k

   CALL make_weight(weight)

print *, 'solve_bs: flag =', flag
   IF(flag == 1) THEN                                    !intraband
      CALL make_matrix1(p00, etilde, chi, weight, mat)
   ELSE IF(flag == 0) THEN                               !interband
      CALL make_matrix0(p00, etilde, chi, weight, mat)
   ELSE
      PRINT *, 'solve_bs: irregal value of flag:', flag
      STOP
   ENDIF

! f02gbf (NAG) calculates eigenvalue and eigenvector
   mat2 = mat
   CALL f02gbf('V', 2*Ndiv, mat2, 2*Ndiv, e_val, e_vec, &
      2*Ndiv, rwork, work, lwork, ifail)
   PRINT *, 'solve_bs: f02gbf: ifail =', ifail

! f07arf (NAG) calculates the LU factorization of e_vec
   inve_vec = e_vec      ! because matrix is overwitten
   CALL f07arf(2*Ndiv, 2*Ndiv, inve_vec, 2*Ndiv, ipiv, ifail)
   PRINT *, 'solve_bs: f07arf: ifail =', ifail

! f07awf (NAG) calculates the inversion matrix of e_vec
   CALL f07awf(2*Ndiv, inve_vec, 2*Ndiv, ipiv, work2, lwork2, ifail)
   PRINT *, 'solve_bs: f07awf: ifail =', ifail

! check diagonalization
!  mat2 = matmul(inve_vec, matmul(mat, e_vec))
!  do i=1, 2*Ndiv
!     print *, 'i =',  i, mat2(i,i)
!     print *, 'i =',  i, mat2(i,mod(i+1, Ndiv))
!  end do

! check matrix inversion
!  mat2 = matmul(inve_vec, e_vec)
!  do i = 1, 2*Ndiv
!     print *, i, mat2(i, i)
!  end do
```

```
END SUBROUTINE solve_bs

!================================================
! Solving the Bethe-Salpeter equation   version 1
!
! --- input variables
!  flag:  flag = 1 for intraband,
!         flag = 0 for interband spectrum
!  p00(Ndiv):       momentum abscissae
!  etilde(Ndiv, 3): bare energy
!  chi(Ndiv, 3):    Hartree-Fock self-energy
!
! --- output variables
!  e_val(2*Ndiv):    eigenvalues of Hamiltonian
!  e_vec(2*Ndiv):    eigenvectors of Hamiltonian
!  inve_vec(2*Ndiv): inverse of e_vec
!
!  mat(2*Ndiv, 2*Ndiv): Hamiltonian
!  weight(Ndiv):: weight for numerical integration
!================================================
SUBROUTINE solve_bs0(flag, p00, etilde, chi, e_val, e_vec, inve_vec)
   USE param, ONLY: Ndiv
   IMPLICIT NONE
   INTEGER, INTENT(IN):: flag
   REAL(8), DIMENSION(Ndiv),    INTENT(IN):: p00
   REAL(8), DIMENSION(Ndiv, 3), INTENT(IN):: etilde
   REAL(8), DIMENSION(Ndiv, 3), INTENT(IN):: chi
   COMPLEX(8), DIMENSION(2*Ndiv),  INTENT(OUT):: e_val
   COMPLEX(8), DIMENSION(2*Ndiv, 2*Ndiv), INTENT(OUT):: e_vec, inve_vec

   REAL(8), DIMENSION(Ndiv):: weight
   REAL(8), DIMENSION(2*Ndiv, 2*Ndiv):: mat

 ! wr and wi are the real and imaginary
 !  part of eigenvalues, respectively
 ! vr and vi are the real and imaginary
 ! part of eigenvectors, respectively
   REAL(8), DIMENSION(2*Ndiv):: wr, wi
   REAL(8), DIMENSION(2*Ndiv,2*Ndiv):: vr, vi
   INTEGER, PARAMETER:: lwork = 4*2*Ndiv
   REAL(8), DIMENSION(lwork):: work

   INTEGER,    PARAMETER:: lwork2 = 4*2*Ndiv
   COMPLEX(8), DIMENSION(lwork2):: work2
   INTEGER,    DIMENSION(2*Ndiv):: ipiv
   INTEGER:: ifail

 ! debugging use
   INTEGER:: i, j, k

   CALL make_weight(weight)

print *, 'solve_bs: flag =', flag
   IF(flag == 0) THEN                                          ! interband
      CALL make_matrix0(p00, etilde, chi, weight, mat)
!   ELSE IF(flag == 1) THEN                                     ! intraband
!      CALL make_matrix1(p00, etilde, chi, weight, mat)
   ELSE
      PRINT *, 'solve_bs: irregal value of flag:', flag
      STOP
   ENDIF


! f02ebf (NAG) calculates eigenvalue and eigenvector
```

```
   CALL f02ebf('V', 2*Ndiv, mat, 2*Ndiv, wr, wi, vr, 2*Ndiv, vi, 2*Ndiv, &
           work, lwork, ifail)
   PRINT *, 'solve_bs: f02ebf: ifail =', ifail
   e_val = CMPLX(wr, wi, 8)
   e_vec = CMPLX(vr, vi, 8)

! f07arf (NAG) calculates the LU factorization of e_vec
   inve_vec = e_vec      ! because matrix is overwitten
   CALL f07arf(2*Ndiv, 2*Ndiv, inve_vec, 2*Ndiv, ipiv, ifail)
   PRINT *, 'solve_bs: f07arf: ifail =', ifail

! f07awf (NAG) calculates the inversion matrix of e_vec
   CALL f07awf(2*Ndiv, inve_vec, 2*Ndiv, ipiv, work2, lwork2, ifail)
   PRINT *, 'solve_bs: f07awf: ifail =', ifail

! check diagonalization
!  mat2 = matmul(inve_vec, matmul(mat, e_vec))
!  do i=1, 2*Ndiv
!     print *, 'i =',  i, mat2(i,i)
!     print *, 'i =',  i, mat2(i,mod(i+1, Ndiv))
!  end do

! check matrix inversion
!  mat2 = matmul(inve_vec, e_vec)
!  do i = 1, 2*Ndiv
!     print *, i, mat2(i, i)
!  end do

END SUBROUTINE solve_bs0

!=====================================================
!=====================================================
SUBROUTINE make_weight(weight)
   USE param, ONLY: dp, Ndiv
   IMPLICIT NONE
   REAL(8), DIMENSION(Ndiv), INTENT(OUT):: weight
   INTEGER:: i

print *, 'dp =', dp
!  Numerical Receipes in FORTRAN p. 128
   weight(1)        = (3.0d0/8.0d0)*dp
   weight(2)        = (7.0d0/6.0d0)*dp
   weight(3)        = (23.0d0/24.0d0)*dp
   weight(4:Ndiv-3) = dp
   weight(Ndiv-2)   = (23.0d0/24.0d0)*dp
   weight(Ndiv-1)   = (7.0d0/6.0d0)*dp
   weight(Ndiv)     = (3.0d0/8.0d0)*dp

! Sympson's rule
!  weight(1) = dp/3.0d0
!  weight(Ndiv) = dp/3.0d0
!  DO i=1, (Ndiv/2) - 1
!     weight(2*i) = (4.0d0/3.0d0)*dp
!     weight(2*i+1) = (2.0d0/3.0d0)*dp
!  END DO

! Trapezodical rule
!  weight(1) = 0.5d0*dp
!  weight(2:Ndiv-1) = dp
!  weight(Ndiv) = 0.5d0*dp

END SUBROUTINE make_weight
```